UNIVERSITY OF AMSTERDAM

UvA-DARE (Digital Academic Repository)

Search for production of vector-like quark pairs and of four top quarks in the lepton-plus-jets final state in pp collisions at √s = 8 TeV with the ATLAS detectors at sqrt s = 8 with the ATLAS detector

Aad, G.; et al., [Unknown]; Aben, R.; Angelozzi, I.; Beemster, L.J.; Bentvelsen, S.; Berge, D.; Bobbink, G.J.; Bos, K.; Brenner, L.; Butti, P.; Castelli, A.; Colijn, A.P.; de Jong, P.; de Nooij, L.; Deigaard, I.; Deluca, C.; Ferrari, P.; Gadatsch, S.; Geerts, D.A.A.; Hartjes, F.; Hessey, N.P.; Hod, N.; Igonkina, O.; Karastathis, N.; Kluit, P.; Koffeman, E.; Linde, F.; Mahlstedt, J.; Meyer, J.; Oussoren, K.P.; Sabato, G.; Salek, D.; Slawinska, M.; Valencic, N.; van den Wollenberg, W.; van der Deijl, P.C.; van der Geer, R.; van der Graaf, H.; van der Leeuw, R.; van Vulpen, I.; Verkerke, W.; Vermeulen, J.C.; Vreeswijk, M.; Weits, H.; Williams, S.

DOI
10.1007/JHEP08(2015)105

Publication date
2015

Document Version
Final published version

Published in
The Journal of High Energy Physics

Link to publication

Citation for published version (APA):
Aad, G., et al., U., Aben, R., Angelozzi, I., Beemster, L. J., Bentvelsen, S., Berge, D., Bobbink, G. J., Bos, K., Brenner, L., Butti, P., Castelli, A., Colijn, A. P., de Jong, P., de Nooij, L., Deigaard, I., Deluca, C., Ferrari, P., Gadatsch, S., ... Williams, S. (2015). Search for production of vector-like quark pairs and of four top quarks in the lepton-plus-jets final state in pp collisions at √s = 8 TeV with the ATLAS detectors at sqrt s = 8 with the ATLAS detector. *The Journal of High Energy Physics*, *2015*(8), Article 105. https://doi.org/10.1007/JHEP08(2015)105

General rights
It is not permitted to download or to forward/distribute the text or part of it without the consent of the author(s) and/or copyright holder(s), other than for strictly personal, individual use, unless the work is under an open content license (like Creative Commons).

UvA-DARE is a service provided by the library of the University of Amsterdam (https://dare.uva.nl)

Disclaimer/Complaints regulations
If you believe that digital publication of certain material infringes any of your rights or (privacy) interests, please let the Library know, stating your reasons. In case of a legitimate complaint, the Library will make the material inaccessible and/or remove it from the website. Please Ask the Library: https://uba.uva.nl/en/contact, or a letter to: Library of the University of Amsterdam, Secretariat, P.O. Box 19185, 1000 GD Amsterdam, The Netherlands. You will be contacted as soon as possible.

Download date:17 Oct 2026

Published for SISSA by Springer

Received: *May 19, 2015*
Accepted: *July 10, 2015*
Published: *August 20, 2015*

Search for production of vector-like quark pairs and of four top quarks in the lepton-plus-jets final state in pp collisions at $\sqrt{s} = 8$ TeV with the ATLAS detector

The ATLAS collaboration

E-mail: atlas.publications@cern.ch

Abstract: A search for pair production of vector-like quarks, both up-type (T) and down-type (B), as well as for four-top-quark production, is presented. The search is based on pp collisions at $\sqrt{s} = 8$ TeV recorded in 2012 with the ATLAS detector at the CERN Large Hadron Collider and corresponding to an integrated luminosity of 20.3 fb^{-1}. Data are analysed in the lepton-plus-jets final state, characterised by an isolated electron or muon with high transverse momentum, large missing transverse momentum and multiple jets. Dedicated analyses are performed targeting three cases: a T quark with significant branching ratio to a W boson and a b-quark ($T\bar{T} \to Wb$+X), and both a T quark and a B quark with significant branching ratio to a Higgs boson and a third-generation quark ($T\bar{T} \to Ht$+X and $B\bar{B} \to Hb$+X respectively). No significant excess of events above the Standard Model expectation is observed, and 95% CL lower limits are derived on the masses of the vector-like T and B quarks under several branching ratio hypotheses assuming contributions from $T \to Wb$, Zt, Ht and $B \to Wt$, Zb, Hb decays. The 95% CL observed lower limits on the T quark mass range between 715 GeV and 950 GeV for all possible values of the branching ratios into the three decay modes, and are the most stringent constraints to date. Additionally, the most restrictive upper bounds on four-top-quark production are set in a number of new physics scenarios.

Keywords: Hadron-Hadron Scattering

ArXiv ePrint: 1505.04306

Open Access, Copyright CERN,
for the benefit of the ATLAS Collaboration.
Article funded by SCOAP^3.

doi:10.1007/JHEP08(2015)105

Contents

1 Introduction **1**

2 ATLAS detector **3**

3 Object reconstruction **3**

4 Data sample and event preselection **5**

5 Signal modelling **6**
5.1 Vector-like quark pair production 6
5.2 Four-top-quark production 7

6 Background modelling **10**
6.1 $t\bar{t}$+jets background 11
6.2 W/Z+jets background 12
6.3 Other simulated background 12
6.4 Multijet background 13

7 Search for $T\bar{T} \to Wb$+X production **14**

8 Search for $T\bar{T} \to Ht$+X and $t\bar{t}t\bar{t}$ production **17**

9 Search for $B\bar{B} \to Hb$+X production **21**

10 Systematic uncertainties **29**
10.1 Luminosity 29
10.2 Reconstructed objects 31
10.2.1 Leptons 31
10.2.2 Jets and missing transverse momentum 31
10.2.3 Heavy- and light-flavour tagging 33
10.3 Background modelling 34
10.3.1 $t\bar{t}$+jets 34
10.3.2 W/Z+jets 35
10.3.3 Other simulated background 35
10.3.4 Multijet 36

11 Statistical analysis **36**

12 Results **37**
12.1 Likelihood fits to data 37
12.2 Limits on $T\bar{T}$ production 38
12.3 Limits on $B\bar{B}$ production 44
12.4 Limits on $t\bar{t}t\bar{t}$ production 45

JHEP08(2015)105

13 Conclusion **52**

A Post-fit event yields **54**

B Limits on $T\bar{T}$ production from individual searches **56**

The ATLAS collaboration **69**

1 Introduction

The discovery of a new particle consistent with the Standard Model (SM) Higgs boson by the ATLAS [1] and CMS [2] collaborations is a major milestone in high-energy physics. However, the underlying nature of electroweak symmetry breaking remains unknown. Naturalness arguments [3] require that quadratic divergences that arise from radiative corrections to the Higgs boson mass must be cancelled by some new mechanism in order to avoid fine-tuning. To that effect, several explanations have been proposed in theories beyond the SM (BSM). In supersymmetry, the cancellation comes from assigning superpartners to the SM bosons and fermions. Alternatively, Little Higgs [4, 5] and Composite Higgs [6, 7] models introduce a spontaneously broken global symmetry, with the Higgs boson emerging as a pseudo-Nambu-Goldstone boson [8]. Such models predict the existence of vector-like quarks, defined as colour-triplet spin-1/2 fermions whose left- and right-handed chiral components have the same transformation properties under the weak-isospin SU(2) gauge group [9, 10]. In these models vector-like quarks are expected to couple preferentially to third-generation quarks [9, 11] and they can have flavour-changing neutral current decays, in addition to the charged-current decays characteristic of chiral quarks. As a result, an up-type quark T with charge $+2/3$ can decay not only to a W boson and a b-quark, but also to a Higgs or Z boson and a top quark ($T \to Wb$, Zt, and Ht). Similarly, a down-type quark B with charge $-1/3$ can decay to a Higgs or Z boson and a b-quark, in addition to decaying to a W boson and a top quark ($B \to Wt$, Zb, and Hb). In order to be consistent with the results from the precision electroweak measurements, a small mass splitting between vector-like quarks belonging to the same SU(2) multiplet is required [12], which forbids cascade decays such as $T \to WB$ and leaves direct decays into SM particles as the only possibility. Couplings between the vector-like quarks and the first and second quark generations, although not favoured, are not excluded [13, 14]. This leads to a rich phenomenology at the LHC, which the experiments are investigating.

Early searches for the pair production of exotic heavy quarks published by the ATLAS and CMS collaborations focused on exclusive decay modes assuming a 100% branching ratio. These include searches for $T\bar{T} \to W^+bW^-\bar{b}$ [15–18], $B\bar{B} \to ZbZ\bar{b}$ [19–21], and $B\bar{B} \to W^+tW^-\bar{t}$ [20, 22, 23]. The limits derived from these searches cannot easily be applied to other branching ratio values, due to the potentially large expected signal contamination from mixed decay modes. A more general search strategy should consider simultaneously all three decay modes, providing a more extensive coverage of possible signal contributions. In absence of an excess, quasi-model-independent limits would be set in the plane defined by

JHEP08(2015)105

the branching ratios to two of the decay modes[1] as a function of the heavy-quark mass. The first search that considered all three decay modes in the interpretation of results, performed by the ATLAS Collaboration using pp collisions at $\sqrt{s} = 7$ TeV, primarily targeted the $T\bar{T} \to W^+bW^-\bar{b}$ process [24]. Using the full dataset collected at $\sqrt{s} = 8$ TeV, the ATLAS Collaboration has recently published searches for heavy quarks decaying to a Z boson and a third-generation quark [25], and searches for heavy quarks decaying predominantly to Wt in events with one lepton and jets [26] and in events with two leptons of the same charge or three leptons [27]. In the context of vector-like quarks, these searches are used to probe $T\bar{T}$ and $B\bar{B}$ production, and the three decay modes are considered in the interpretation of the results. The CMS Collaboration has published an inclusive search for $T\bar{T}$ production [28] resulting from the combination of several analyses in lepton-plus-jets and multilepton final states at $\sqrt{s} = 8$ TeV. This search set 95% confidence level (CL) lower limits on the T quark mass ranging between 690 GeV and 780 GeV for all possible values of the branching ratios into the three decay modes.

The results presented in this paper complete the program of searches for pair production of vector-like quarks decaying into third-generation quarks by the ATLAS Collaboration using the pp dataset collected at $\sqrt{s} = 8$ TeV. Three separate searches are presented, all of them focused on the pair production of vector-like quarks in final states involving one isolated electron or muon, high missing transverse momentum from the undetected neutrino and multiple jets. The first search, referred to as $T\bar{T} \to Wb$+X, is optimised for $T\bar{T}$ production with at least one $T \to Wb$ decay, where the resulting W boson acquires a high momentum from the large T quark mass. The second search, referred to as $T\bar{T} \to Ht$+X, targets $T\bar{T}$ production with at least one $T \to Ht$ decay, with $H \to b\bar{b}$, resulting in events with high jet multiplicity and a large number of jets tagged as originating from b-quarks. The third search, referred to as $B\bar{B} \to Hb$+X, is instead focused on $B\bar{B}$ production with at least one $B \to Hb$ decay and $H \to b\bar{b}$, in events with the same final-state signature probed by the $T\bar{T} \to Ht$+X search. In all three searches the isolated lepton and the high missing transverse momentum are provided by the leptonic decay of a W boson originating in the decay of a vector-like quark, a top quark, or a Higgs boson.

The large mass of the top quark makes it a prime candidate to help uncover the dynamics behind electroweak symmetry breaking and/or new physics at the electroweak scale. In many new physics models the top quark plays a prominent role, often participating in new interactions related to electroweak symmetry breaking, or preferentially coupling to new degrees of freedom. Such BSM scenarios usually predict an enhanced rate of events containing four top quarks ($t\bar{t}t\bar{t}$) in the final state, compared to the SM production via the strong interaction. Examples include top quark compositeness [29–31], Randall-Sundrum extra dimensions [32], models with coloured scalars [33–38], or universal extra dimensions [39–41]. The CMS Collaboration has performed a search for SM $t\bar{t}t\bar{t}$ production at $\sqrt{s} = 8$ TeV in the lepton-plus-jets final state [42], setting an observed (expected) 95% CL upper limit on the production cross section of 32 fb (32 fb). Using multilepton final states,

[1]The branching ratio to the third decay mode is fully determined by the requirement that the sum of branching ratios equals unity.

JHEP08(2015)105

the ATLAS Collaboration has also searched for SM $t\bar{t}t\bar{t}$ production at $\sqrt{s} = 8$ TeV, setting an observed (expected) 95% CL upper limit of 70 fb (27 fb) [27]. The observed limit is higher than the expected one owing to an excess of data above the background expectation with a significance of 2.5 standard deviations. In addition, the ATLAS multilepton search sensitively probes several of the above BSM scenarios giving rise to large enhancements in $t\bar{t}t\bar{t}$ production. Given its sensitivity to a wide range of models, the $T\bar{T} \to Ht$+X search presented in this paper is also used to search for a $t\bar{t}t\bar{t}$ signal, within the SM as well as in the same BSM scenarios as the ATLAS multilepton search, with comparable sensitivity.

2 ATLAS detector

The ATLAS detector [43] consists of the following main subsystems: an inner tracking system, electromagnetic and hadronic calorimeters, and a muon spectrometer. The inner detector provides tracking information from silicon pixel and microstrip detectors in the pseudorapidity[2] range $|\eta| < 2.5$ and from a straw-tube transition radiation tracker covering $|\eta| < 2.0$, all immersed in a 2 T axial magnetic field provided by a superconducting solenoid. The electromagnetic (EM) sampling calorimeter uses lead as the absorber material and liquid-argon (LAr) as the active medium, and is divided into barrel ($|\eta| < 1.475$) and end-cap ($1.375 < |\eta| < 3.2$) regions. Hadron calorimetry is also based on the sampling technique, with either scintillator tiles or LAr as the active medium, and with steel, copper, or tungsten as the absorber material. The calorimeters cover $|\eta| < 4.9$. The muon spectrometer measures the deflection of muons with $|\eta| < 2.7$ using multiple layers of high-precision tracking chambers located in a toroidal field of approximately 0.5 T and 1 T in the central and end-cap regions of ATLAS, respectively. The muon spectrometer is also instrumented with separate trigger chambers covering $|\eta| < 2.4$. A three-level trigger system [44] is used to select interesting events. The first-level trigger is implemented in custom electronics and uses a subset of detector information to reduce the event rate to at most 75 kHz. This is followed by two software-based trigger levels exploiting the full detector information and yielding a typical recorded event rate of 400 Hz during 2012.

3 Object reconstruction

The main reconstructed objects considered in this search are electrons, muons, jets, b-jets and missing transverse momentum.

Electron candidates [45] are reconstructed from energy deposits (clusters) in the EM calorimeter that are matched to reconstructed tracks in the inner detector. The candidates

[2] ATLAS uses a right-handed coordinate system with its origin at the nominal interaction point (IP) in the centre of the detector and the z-axis coinciding with the axis of the beam pipe. The x-axis points from the IP to the centre of the LHC ring, and the y-axis points upward. Cylindrical coordinates (r,ϕ) are used in the transverse plane, ϕ being the azimuthal angle around the beam pipe. The pseudorapidity is defined in terms of the polar angle θ as $\eta = -\ln\tan(\theta/2)$. For the purpose of the fiducial selection, this is calculated relative to the geometric centre of the detector; otherwise, it is relative to the reconstructed primary vertex of each event.

JHEP08(2015)105

are required to have a transverse energy[3] E_{T} greater than 25 GeV and $|\eta_{\mathrm{cluster}}| < 2.47$, where $|\eta_{\mathrm{cluster}}|$ is the pseudorapidity of the cluster associated with the electron candidate. Candidates in the EM calorimeter transition region $1.37 < |\eta_{\mathrm{cluster}}| < 1.52$ are excluded. Electrons are required to satisfy "tight" quality requirements [45], which include stringent selection requirements on calorimeter, tracking and combined variables that provide good separation between prompt electrons and jets. The longitudinal impact parameter of the electron track with respect to the event's primary vertex (see section 4), z_0, is required to be less than 2 mm. To reduce the background from non-prompt electrons resulting from semileptonic decays of b- or c-hadrons, and from jets with a high fraction of their energy deposited in the EM calorimeter, electron candidates must also satisfy calorimeter- and track-based isolation requirements. The calorimeter isolation variable is based on the energy sum of cells within a cone of radius $\Delta R = \sqrt{(\Delta\phi)^2 + (\Delta\eta)^2} = 0.2$ around the direction of each electron candidate, and an η-dependent requirement is made, giving an average efficiency of 90% for prompt electrons from Z boson decays. This energy sum excludes cells associated with the electron cluster and is corrected for leakage from the electron cluster itself and for energy deposits from additional pp interactions within the same bunch crossing ("pileup"). A further 90%-efficient isolation requirement is made on the track transverse momentum (p_{T}) sum around the electron in a cone of radius $\Delta R = 0.3$.

Muon candidates [46, 47] are reconstructed from track segments in the various layers of the muon spectrometer and matched with tracks found in the inner detector. The final candidates are refitted using the complete track information from both detector systems and are required to satisfy $p_{\mathrm{T}} > 25$ GeV and $|\eta| < 2.5$. Muons are required to have a hit pattern in the inner detector consistent with a well-reconstructed track to ensure good p_{T} resolution. The longitudinal impact parameter of the muon track with respect to the primary vertex, z_0, is required to be less than 2 mm. Muons are required to satisfy a p_{T}-dependent track-based isolation requirement: the scalar sum of the p_{T} of the tracks within a cone of variable radius $\Delta R = 10\ \mathrm{GeV}/p_{\mathrm{T}}^{\mu}$ around the muon (excluding the muon track itself) must be less than 5% of the muon p_{T} (p_{T}^{μ}). This requirement has good signal efficiency and background rejection even under high-pileup conditions, as well as in boosted configurations where the muon is close to a jet. For muons from W decays in simulated $t\bar{t}$ events the average efficiency of the isolation requirement is about 95%.

Jets are reconstructed with the anti-k_t algorithm [48–50] with a radius parameter $R = 0.4$ from calibrated topological clusters [51, 52] built from energy deposits in the calorimeters. Prior to jet finding, a local cluster calibration scheme [53] is applied to correct the topological cluster energies for the effects of non-compensating response of the calorimeter, dead material and out-of-cluster leakage. The corrections are obtained from simulations of charged and neutral particles. After energy calibration [54], jets are required to have $p_{\mathrm{T}} > 25$ GeV and $|\eta| < 2.5$. To reduce the contamination due to jets originating from pileup interactions, a requirement that the so-called "jet vertex fraction" (JVF) be above 0.5 is applied to jets with $p_{\mathrm{T}} < 50$ GeV and $|\eta| < 2.4$. This requirement ensures

[3]The electron transverse energy is defined as $E_{\mathrm{T}} = E_{\mathrm{cluster}}/\cosh\eta_{\mathrm{track}}$, where E_{cluster} is the energy of the cluster in the calorimeter and η_{track} is the pseudorapidity of its associated track.

JHEP08(2015)105

that at least 50% of the scalar sum of the p_{T} of the tracks matched to the jet comes from tracks originating from the primary vertex. During jet reconstruction, no distinction is made between identified electrons and jet energy deposits. Therefore, if any of the jets lie within $\Delta R = 0.2$ of a selected electron, the closest jet is discarded in order to avoid double-counting of electrons as jets. Finally, any electron or muon within $\Delta R = 0.4$ of a selected jet is discarded.

Jets are identified as originating from the hadronisation of a b-quark (b-tagged) via an algorithm [55] that uses multivariate techniques to combine information from the impact parameters of displaced tracks as well as topological properties of secondary and tertiary decay vertices reconstructed within the jet. For each jet, a value for the multivariate b-tagging discriminant is calculated, and is considered b-tagged if this value is above a given threshold. The threshold used in this search corresponds to 70% efficiency to tag a b-quark jet, with a light-jet rejection factor[4] of ∼130 and a charm-jet rejection factor of 5, as determined for jets with $p_{\mathrm{T}} > 20$ GeV and $|\eta| < 2.5$ in simulated $t\bar{t}$ events.

The missing transverse momentum ($E_{\mathrm{T}}^{\mathrm{miss}}$) is constructed [56] from the vector sum of all calorimeter energy deposits[5] contained in topological clusters. All topological cluster energies are corrected using the local cluster calibration scheme discussed above. Those topological clusters associated with a high-p_{T} object (e.g. jet or electron) are further calibrated using their respective energy corrections. In addition, contributions from the p_{T} of selected muons are included in the calculation of $E_{\mathrm{T}}^{\mathrm{miss}}$.

4 Data sample and event preselection

This search is based on pp collision data at $\sqrt{s} = 8$ TeV collected by the ATLAS experiment between April and December 2012. Only events recorded with a single-electron or single-muon trigger under stable beam conditions and for which all detector subsystems were operational are considered. The corresponding integrated luminosity is 20.3 ± 0.6 fb^{-1} [57]. Single-lepton triggers with different p_{T} thresholds are combined in a logical OR in order to increase the overall efficiency. The p_{T} thresholds are 24 or 60 GeV for the electron triggers and 24 or 36 GeV for the muon triggers. The triggers with the lower p_{T} threshold include isolation requirements on the candidate lepton, resulting in inefficiencies at high p_{T} that are recovered by the triggers with higher p_{T} threshold. Events satisfying the trigger selection are required to have at least one reconstructed vertex with at least five associated tracks with $p_{\mathrm{T}} > 400$ MeV, consistent with originating from the beam collision region in the x–y plane. The average number of pp interactions per bunch crossing is approximately 20, resulting in several vertices reconstructed per event. If more than one vertex is found, the hard-scatter primary vertex is taken to be the one which has the largest sum of the squared transverse momenta of its associated tracks. For the event topologies considered

[4]The rejection factor is defined as the reciprocal of the selection efficiency.

[5]Each cluster in the calorimeter is considered a massless object and is assigned the four-momentum $(E_{\mathrm{cluster}}, \vec{p}_{\mathrm{cluster}})$, where E_{cluster} is the measured energy and $\vec{p}_{\mathrm{cluster}}$ is a vector of magnitude E_{cluster} directed from $(x, y, z) = (0, 0, 0)$ to the centre of the cluster.

JHEP08(2015)105

in this paper, this requirement leads to a probability to reconstruct and select the correct hard-scatter primary vertex larger than 99%.

Events are required to have exactly one reconstructed electron or muon and at least four jets satisfying the quality and kinematic criteria discussed in section 3. The selected lepton is required to match, with $\Delta R < 0.15$, the lepton reconstructed by the trigger. The background from multijet production is suppressed by a requirement on $E_{\mathrm{T}}^{\mathrm{miss}}$ as well as on the transverse mass of the lepton and $E_{\mathrm{T}}^{\mathrm{miss}}$ (m_{T}^{W}).[6] For both lepton selections the requirements are $E_{\mathrm{T}}^{\mathrm{miss}} > 20$ GeV and $E_{\mathrm{T}}^{\mathrm{miss}} + m_{\mathrm{T}}^{W} > 60$ GeV. Further suppression of the background not including b-quark jets is achieved by requiring at least one b-tagged jet in the $T\bar{T} \to Wb$+X search, and at least two b-tagged jets in the $T\bar{T} \to Ht$+X and $B\bar{B} \to Hb$+X searches. In the following, events satisfying either the electron or muon selections are combined and treated as a single analysis channel.

5 Signal modelling

This section describes the different signal scenarios considered in the interpretation of the results, together with details of how they are modelled in the analysis.

5.1 Vector-like quark pair production

Vector-like quarks with mass below approximately 1 TeV are mostly produced in pairs via the strong interaction in pp collisions at $\sqrt{s} = 8$ TeV. For higher masses, single production mediated by the electroweak interaction can potentially dominate, depending on the strength of the interaction between the new quarks and the weak gauge bosons. The predicted pair-production cross section ranges from 5.3 pb for a quark mass of 350 GeV to 3.3 fb for a quark mass of 1000 GeV, with an uncertainty that increases from 8% to 14% over this mass range. This cross section is independent of the electroweak quantum numbers of the new heavy quark and just depends on its mass. It was computed using Top++ v2.0 [58] at next-to-next-to-leading order (NNLO) in QCD, including resummation of next-to-next-to-leading logarithmic (NNLL) soft gluon terms [59–63], and using the MSTW 2008 NNLO [64, 65] set of parton distribution functions (PDF). Theoretical uncertainties result from variations on the factorisation and renormalisation scales, as well as from uncertainties on the PDF and α_{S}. The latter two represent the largest contribution to the overall theoretical uncertainty on the cross section and were calculated using the PDF4LHC prescription [66] with the MSTW 2008 68% CL NNLO, CT10 NNLO [67, 68] and NNPDF2.3 5f FFN [69] PDF sets.

As discussed in section 1, vector-like quarks can couple preferentially to third-generation quarks, as the mixing between weak eigenstates of the same electric charge is proportional to the mass of the SM quark [9, 11], and thus present a rich phenomenology. In particular, a vector-like quark has neutral-current tree-level decays to a Z or H boson plus a SM quark, in addition to the charged-current decay mode to a W boson and a SM

[6] $m_{\mathrm{T}}^{W} = \sqrt{2p_{\mathrm{T}}^{\ell}E_{\mathrm{T}}^{\mathrm{miss}}(1-\cos\Delta\phi)}$, where p_{T}^{ℓ} is the transverse momentum (energy) of the muon (electron) and $\Delta\phi$ is the azimuthal angle separation between the lepton and the direction of the missing transverse momentum.

JHEP08(2015)105

quark, which is the only decay mode chiral quarks can have. Figure 1 depicts representative Feynman diagrams for the signals probed by the searches discussed in this paper. The branching ratios to each of these decay modes vary as a function of the heavy-quark mass and depend on its weak-isospin (SU(2)) quantum numbers [10]. Figure 2(a) shows the branching ratios as a function of T quark mass in the SU(2) singlet and doublet hypotheses.[7] In the case of a singlet, all three decay modes have sizeable branching ratios, while the charged-current decay mode $T \to Wb$ is absent in the doublet cases. The doublet prediction is valid for an (X,T) doublet, where the charge of the X quark is $+5/3$, as well as a (T,B) doublet when a mixing assumption of $|V_{Tb}| \ll |V_{tB}|$ is made, where V_{ij} are the elements of a generalised Cabibbo-Kobayashi-Maskawa matrix [10]. Since the T quark branching ratios are identical in both doublets, in the following no distinction between them is made when referring to the T quark doublet hypothesis. Similarly, figure 2(b) shows the branching ratios as a function of B quark mass in the singlet and doublet hypotheses. In the case of a (T,B) doublet with the mixing assumption $|V_{Tb}| \ll |V_{tB}|$, $\mathrm{BR}(B \to Wt) = 1$, while such a decay mode is absent for the (B,Y) doublet case, where the charge of the Y quark is $-4/3$. The Y quark is equivalent to a chiral quark since it only has charged-current decays, $Y \to W^- b$.

Simulated samples of $T\bar{T}$ and $B\bar{B}$ are generated with the leading-order (LO) generator Protos v2.2 [70] using the MSTW 2008 LO PDF set and passed to Pythia 6.426 [71] for parton showering and fragmentation. The AUET2B [72] set of optimised parameters for the underlying event (UE) description, referred to as the "UE tune", is used. The vector-like quarks are forced to decay with a branching ratio of 1/3 to each of the three modes (W,Z,H). Arbitrary sets of branching ratios consistent with the three decay modes summing to unity are obtained by reweighting the samples using particle-level information. Samples are generated assuming singlet couplings and for heavy-quark masses between 350 GeV and 1100 GeV in steps of 50 GeV. Additional samples are produced at two mass points (350 GeV and 600 GeV) assuming doublet couplings in order to confirm that kinematic differences arising from the different chirality of singlet and doublet couplings are negligible in this analysis. In all simulated samples (both signal and background) used in this search, the top quark and SM Higgs boson masses are set to 172.5 GeV and 125 GeV respectively. The samples are normalised using the Top++ cross section predictions discussed above.

5.2 Four-top-quark production

The production cross section for four-top-quark events in the SM is very small ($\sigma_{t\bar{t}t\bar{t}} \simeq 1\,\mathrm{fb}$ at $\sqrt{s} = 8$ TeV) [73, 74], but it can be significantly enhanced in several BSM scenarios. Figure 3 depicts representative LO Feynman diagrams for four-top-quark production within the SM and the different BSM scenarios considered in this paper. A class of models involving new heavy vector particles strongly coupled to the right-handed top quark, such as top quark compositeness [29–31] or Randall-Sundrum extra dimensions [32], can be de-

[7] The branching ratios in figure 2 are valid for small mixing between the new heavy quark and the third-generation quark [10–12].

JHEP08(2015)105

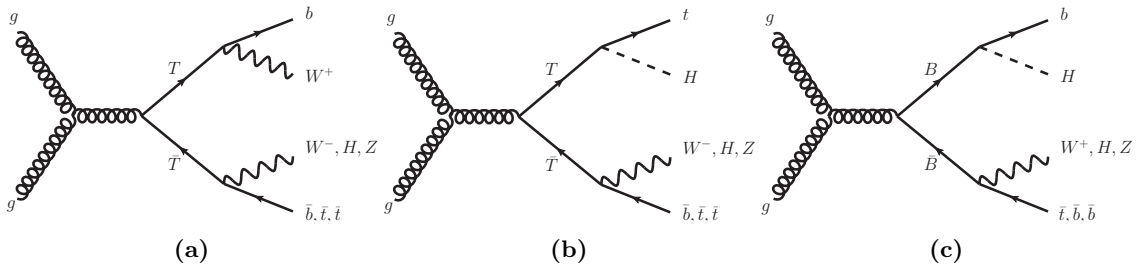

Figure 1. Representative leading-order Feynman diagrams for $T\bar{T}$ production probed by (a) the $T\bar{T} \to Wb$+X search and (b) the $T\bar{T} \to Ht$+X search, and (c) for $B\bar{B}$ production probed by the $B\bar{B} \to Hb$+X search.

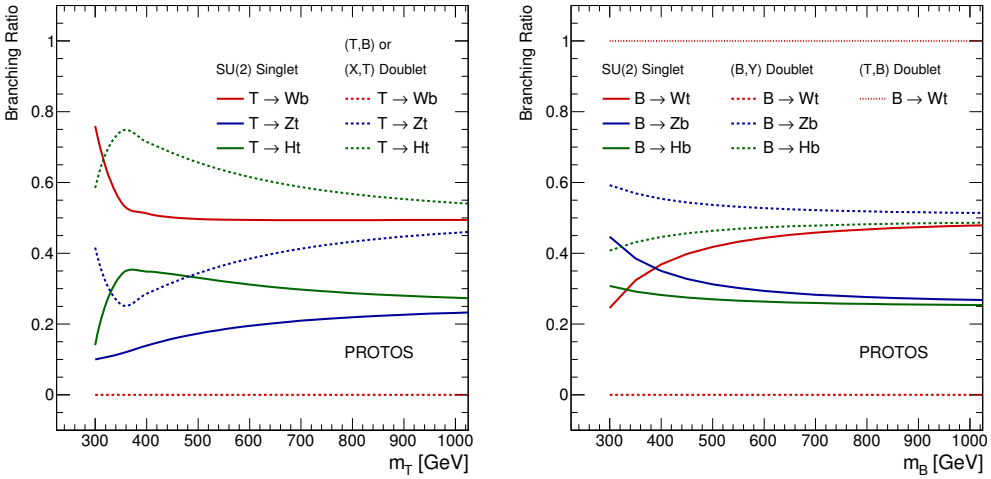

Figure 2. Branching ratios for the different decay modes as a function of heavy-quark mass in the case of (a) a vector-like T quark and (b) a vector-like B quark, as computed with Protos. In both cases the branching ratios are provided for an SU(2) singlet and two different SU(2) doublet scenarios.

scribed via an effective field theory (EFT) involving a four-fermion contact interaction [75] (figure 3(b)). The Lagrangian assumed is

$$\mathcal{L}_{4t} = \frac{|C_{4t}|}{\Lambda^2}(\bar{t}_{\mathrm{R}}\gamma^{\mu}t_{\mathrm{R}})(\bar{t}_{\mathrm{R}}\gamma_{\mu}t_{\mathrm{R}}), \tag{5.1}$$

where t_{R} is the right-handed top quark spinor, γ_{μ} are the Dirac matrices, C_{4t} is the coupling constant, and Λ is the energy scale of new physics. Only the contact interaction operator with right-handed top quarks is considered, since left-handed operators are already strongly constrained by the precision electroweak measurements [76].

In addition, two specific models are considered involving new heavy particles: scalar gluon (sgluon) pair production and a Universal Extra Dimensions (UED) model. Sgluons are colour-adjoint scalars, denoted by σ, that appear in several extensions of the SM, both

JHEP08(2015)105

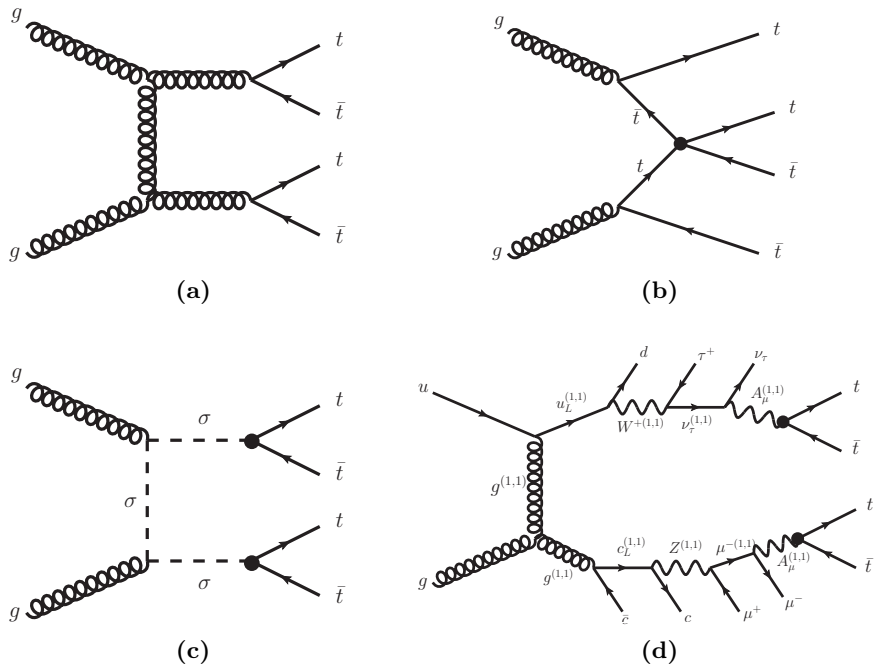

Figure 3. Representative leading-order Feynman diagrams for four-top-quark production within (a) the SM and several beyond-the-SM scenarios (see text for details): (b) via an effective four-top-quark interaction in an effective field theory model, (c) via scalar-gluon-pair production, and (d) via cascade decays from Kaluza-Klein excitations in a universal extra dimensions model with two extra dimensions compactified using the geometry of the real projective plane.

supersymmetric [33, 34] and non-supersymmetric [35–38]. The dominant production mode at the LHC is in pairs via the strong interaction, $gg \to \sigma\sigma$. For sgluon masses above twice the top quark mass, the dominant decay mode is into $t\bar{t}$, giving rise to a four-top-quark final state (figure 3(c)). The UED model considered has two extra dimensions that are compactified using the geometry of the real projective plane (2UED/RPP) [39], leading to a discretisation of the momenta along their directions. A tier of Kaluza-Klein towers is labelled by two integers, k and ℓ, referred to as "tier (k, ℓ)". Within a given tier, the squared masses of the particles are given at leading order by $m^2 = k^2/R_4^2 + \ell^2/R_5^2$, where πR_4 and πR_5 are the size of the two extra dimensions. The model is parameterised by R_4 and R_5 or, alternatively, by $m_{\mathrm{KK}} = 1/R_4$ and $\xi = R_4/R_5$. Four-top-quark production can arise from tier (1,1), where particles from this tier have to be pair produced because of symmetries of the model. Then they chain-decay to the lightest particle of this tier, the heavy photon $A^{(1,1)}$, by emitting SM particles (figure 3(d)). The branching ratios of $A^{(1,1)}$ into SM particles are not predicted by the model, although the decay into $t\bar{t}$ is expected to be dominant [40]. Four-top-quark events can also arise from tiers (2,0) and (0,2) via a similar mechanism. In this case the expected cross section for four-top-quark production is reduced compared to that from tier (1,1) since each state in tiers (2,0) and (0,2) can decay directly into a pair of SM particles or into a pair of states in tiers (1,0) or (0,1) via bulk

JHEP08(2015)105

interactions, resulting in smaller branching ratios for decay into $t\bar{t}$ [40]. In the following, when considering four-top-quark production from a given tier, it is assumed that the A photon in that tier decays with 100% branching ratio into $t\bar{t}$ while A photons from other tiers cannot decay into $t\bar{t}$. Within this model, observations of dark-matter relic abundance prefer values of m_{KK} between 600 GeV and 1200 GeV [41].

Simulated samples of four-top-quark production within the SM, within an EFT model, and within the 2UED/RPP model, are generated with the MADGRAPH5 1.3.33 [77] LO generator and the MSTW 2008 PDF set, interfaced to PYTHIA 8.1 [78] and the AU2 UE tune [79]. In the case of the 2UED/RPP model, samples are generated for four different values of m_{KK} (600, 800, 1000 and 1200 GeV) and the BRIDGE [80] generator is used to decay the pair-produced excitations from tier (1,1) generated by MADGRAPH5. Constraints for tiers (2,0) and (0,2) can be derived from those for tier (1,1) together with the theoretical cross sections. Samples of four-top-quark production via sgluon pairs are generated with PYTHIA 6.426 with the CTEQ6L1 [81] PDF set and the AUET2B UE tune, for seven different values of the sgluon mass between 350 GeV and 1250 GeV, and normalised to the NLO theoretical cross section [82].

Events from minimum-bias interactions are simulated with the PYTHIA 8.1 generator with the MSTW 2008 LO PDF set and the A2 tune [79]. They are overlaid on the simulated signal events according to the luminosity profile of the recorded data. The contributions from these pileup interactions are modelled both within the same bunch crossing as the hard-scattering process and in neighbouring bunch crossings. Finally, the generated samples are processed through a simulation [83] of the detector geometry and response using GEANT4 [84] with a fast simulation of the calorimeter response [83]. All samples are processed through the same reconstruction software as the data. Simulated events are corrected so that the object identification efficiencies, energy scales and energy resolutions match those determined from data control samples.

6 Background modelling

After event preselection, the main background is $t\bar{t}$+jets production, with the production of a W boson in association with jets (W+jets) and multijet events contributing to a lesser extent. Small contributions arise from single top quark, Z+jets and diboson (WW, WZ, ZZ) production, as well as from the associated production of a vector boson V ($V = W, Z$) or a Higgs boson and a $t\bar{t}$ pair ($t\bar{t}V$ and $t\bar{t}H$). Multijet events contribute to the selected sample via the misidentification of a jet or a photon as an electron or via the presence of a non-prompt lepton, e.g. from a semileptonic b- or c-hadron decay; the corresponding yield is estimated via data-driven methods. The rest of the background contributions are estimated from simulation and normalised to their theoretical cross sections. In the case of the $t\bar{t}$+jets and W/Z+jets background predictions, further corrections are applied to improve agreement between the data and simulation, as discussed in sections 6.1 and 6.2 respectively.

All simulated background samples utilise PHOTOS 2.15 [85] to simulate photon radiation and TAUOLA 1.20 [86] to simulate τ decays. Similarly to the signal samples, they also

JHEP08(2015)105

include a simulation of pileup interactions, and are processed through a full GEANT4 detector simulation and the same reconstruction software as the data. Further details about the modelling of each of the backgrounds are provided below.

6.1 $t\bar{t}$+jets background

Simulated samples of $t\bar{t}$+jets events are generated with the next-to-leading-order (NLO) generator POWHEG-BOX 2.0 [87–90] using the CT10 PDF set [67]. The nominal sample is interfaced to PYTHIA 6.425 [71] with the CTEQ6L1 PDF set and the Perugia2011C UE tune [91]. An alternative sample, used to study the uncertainty related to the fragmentation model, is interfaced to HERWIG v6.520 [92] with the CTEQ6L1 PDF set and JIMMY v4.31 [93] to simulate the UE. The $t\bar{t}$+jets samples are normalised to the theoretical cross section obtained with TOP++, performed at NNLO in QCD and including resummation of NNLL soft gluon terms.

The $t\bar{t}$+jets samples are generated inclusively, but events are categorised depending on the flavour content of additional particle jets in the event (i.e. jets not originating from the decay of the $t\bar{t}$ system). Particle jets are reconstructed with the anti-k_t algorithm with a radius parameter $R = 0.4$ and are required to have $p_{\mathrm{T}} > 15$ GeV and $|\eta| < 2.5$. Events where at least one such particle jet is matched within $\Delta R < 0.4$ to a b-hadron with $p_{\mathrm{T}} > 5$ GeV not originating from a top quark decay are labelled as $t\bar{t} + b\bar{b}$ events. Similarly, events where at least one such particle jet is matched within $\Delta R < 0.4$ to a c-hadron with $p_{\mathrm{T}} > 5$ GeV not originating from a W boson decay, that are not labelled already as $t\bar{t} + b\bar{b}$, are labelled as $t\bar{t} + c\bar{c}$ events. Events labelled as either $t\bar{t} + b\bar{b}$ or $t\bar{t} + c\bar{c}$ are generically referred to below as $t\bar{t}$+HF events, where HF stands for "heavy flavour". The remaining events are labelled as $t\bar{t}$+light-jet events, including those with no additional jets. In POWHEG+PYTHIA the modelling of $t\bar{t}$+HF is via the parton-shower evolution. To study uncertainties related to this simplified description, an alternative $t\bar{t}$+jets sample is generated with MADGRAPH5 1.5.11 using the CT10 PDF set. It includes tree-level diagrams with up to three additional partons (including b- and c-quarks) and is interfaced to PYTHIA 6.425.

Since the best possible modelling of the $t\bar{t}$+jets background is a key aspect of these searches, a correction is applied to simulated $t\bar{t}$ events in POWHEG+PYTHIA based on the ratio of the differential cross sections measured in data and simulation at $\sqrt{s} = 7$ TeV as a function of top quark p_{T} and $t\bar{t}$ system p_{T} [94]. The stability of the ratio between $\sqrt{s} = 7$ TeV and $\sqrt{s} = 8$ TeV was studied to support the usage of $\sqrt{s} = 7$ TeV data to correct the simulation at $\sqrt{s} = 8$ TeV. This correction significantly improves agreement between simulation and data in distributions such as the jet multiplicity and the p_{T} of decay products of the $t\bar{t}$ system. This correction is applied only to $t\bar{t}$+light-jets and $t\bar{t}+c\bar{c}$ events. The modelling of the $t\bar{t}+b\bar{b}$ background, particularly important for the Ht/Hb+X searches, is improved by reweighting the POWHEG+PYTHIA prediction to an NLO prediction of $t\bar{t}+b\bar{b}$ including parton showering [95], based on SHERPA+OPENLOOPS [96, 97] using the CT10 PDF set. This reweighting is performed for different topologies of $t\bar{t}+b\bar{b}$ in such a way that the inter-normalisation of each of the categories and the relevant kinematic distributions

JHEP08(2015)105

are at NLO accuracy. More details about the modelling of the $t\bar{t}$+jets background can be found in ref. [98].

6.2 W/Z+jets background

Samples of W/Z+jets events are generated with up to five additional partons using the ALPGEN v2.14 [99] LO generator and the CTEQ6L1 PDF set, interfaced to PYTHIA v6.426 for parton showering and fragmentation. To avoid double-counting of partonic configurations generated by both the matrix-element calculation and the parton shower, a parton-jet matching scheme ("MLM matching") [100] is employed. The W+jets samples are generated separately for W+light-jets, $Wb\bar{b}$+jets, $Wc\bar{c}$+jets, and Wc+jets. The Z+jets samples are generated separately for Z+light-jets, $Zb\bar{b}$+jets, and $Zc\bar{c}$+jets. Overlap between $VQ\bar{Q}$+jets ($V = W, Z$ and $Q = b, c$) events generated from the matrix-element calculation and those generated from parton-shower evolution in the W/Z+light-jets samples is avoided via an algorithm based on the angular separation between the extra heavy quarks: if $\Delta R(Q, \bar{Q}) > 0.4$, the matrix-element prediction is used, otherwise the parton-shower prediction is used. Both the W+jets and Z+jets background contributions are normalised to their inclusive NNLO theoretical cross sections [101]. Further corrections are applied to W/Z+jets events in order to better describe data in the preselected sample. Scale factors for each of the W+jets categories ($Wb\bar{b}$+jets, $Wc\bar{c}$+jets, Wc+jets and W+light-jets) are derived for events with one lepton and at least four jets by simultaneously analysing six different event categories, defined by the b-tag multiplicity (0, 1 and $\geq$2) and the sign of the lepton charge. The b-tag multiplicity provides information about the heavy-flavour composition of the W+jets background, while the lepton charge is used to determine the normalisation of each component, exploiting the expected charge asymmetry for W+jets production in pp collisions as predicted by ALPGEN. In the case of Z+jets events, a correction to the heavy-flavour fraction was derived to reproduce the relative rates of Z+2-jets events with zero and one b-tagged jets observed in data. In addition, the Z boson p_{T} spectrum was compared between data and the simulation in Z+2-jets events, and a reweighting function was derived in order to improve the modelling.

6.3 Other simulated background

Samples of single-top-quark backgrounds corresponding to the t-channel, s-channel and Wt production mechanisms are generated with POWHEG-BOX 2.0 [102, 103] using the CT10 PDF set and interfaced to PYTHIA 6.425 with the CTEQ6L1 PDF set and the Perugia2011C UE tune. Overlaps between the $t\bar{t}$ and Wt final states are removed using the "diagram removal" scheme [104]. The single-top-quark samples are normalised to the approximate NNLO theoretical cross sections [105–107] calculated using the MSTW 2008 NNLO PDF set.

The $WW/WZ/ZZ$+jets samples are generated with up to three additional partons using ALPGEN v2.13 and the CTEQ6L1 PDF set, interfaced to HERWIG v6.520 and JIMMY v4.31 for parton showering, fragmentation and UE modelling. The MLM parton-jet matching scheme is used. The WW+jets samples require at least one of the W bosons to decay leptonically, while the WZ/ZZ+jets samples require one Z boson to decay leptonically,

JHEP08(2015)105

with the other boson decaying inclusively. Additionally, WZ+jets samples requiring the W and Z bosons to decay leptonically and hadronically respectively, are generated with up to three additional partons (including massive b- and c-quarks) using Sherpa v1.4.1 and the CT10 PDF set. All diboson samples are normalised to their NLO theoretical cross sections [108]

Samples of $t\bar{t}V$ events, including $t\bar{t}WW$, are generated with up to two additional partons using Madgraph5 1.3.28 with the CTEQ6L1 PDF set, and interfaced to Pythia 6.425 with the AUET2B UE tune. A sample of $t\bar{t}H$ events is generated with the PowHel framework [109], which combines the Powheg-Box generator and NLO matrix elements obtained from the HELAC-Oneloop package [110]. The sample is generated using the CT10nlo PDF set [67]. Showering is performed with Pythia 8.1 using the CTEQ6L1 PDF set and the AU2 UE tune [72, 111]. Inclusive decays of the Higgs boson are assumed in the generation of the $t\bar{t}H$ sample. The $t\bar{t}V$ samples are normalised to the NLO cross section predictions [112]. The $t\bar{t}H$ sample is normalised using the NLO cross section [113–115] and the Higgs decay branching ratios [116–119] collected in ref. [120].

6.4 Multijet background

Multijet events can enter the selected data sample through several production and mis-reconstruction mechanisms. In the electron channel, the multijet background consists of non-prompt electrons as well as misidentified photons (e.g. with a conversion into an e^+e^- pair) or jets with a high fraction of their energy deposited in the EM calorimeter. In the muon channel, the background contributed by multijet events is predominantly due to final states with non-prompt muons, such as those from semileptonic b- or c-hadron decays.

The multijet background normalisation and shape are estimated directly from data by using the "matrix method" technique [121]. The matrix method exploits differences in lepton-identification-related properties between prompt, isolated leptons from W and Z boson decays (referred to as "real leptons" below) and those where the leptons are either non-isolated or result from the misidentification of photons or jets (referred to as "fake leptons" below). For this purpose, two samples are defined after imposing the final kinematic selection criteria, differing only in the lepton identification criteria: a "tight" sample and a "loose" sample, the former being a subset of the latter. The tight selection employs the complete set of lepton identification criteria used in the analysis. For the loose selection the lepton isolation requirements are omitted. The method assumes that the number of selected events in each sample (N^{loose} and N^{tight}) can be expressed as a linear combination of the numbers of events with real and fake leptons, so that the number of multijet events in the tight sample is given by

$$N_{\text{MJ}}^{\text{tight}} = \frac{\epsilon_{\text{fake}}}{\epsilon_{\text{real}} - \epsilon_{\text{fake}}}(\epsilon_{\text{real}} N^{\text{loose}} - N^{\text{tight}}), \tag{6.1}$$

where ϵ_{real} (ϵ_{fake}) represents the probability for a real (fake) lepton that satisfies the loose criteria to also satisfy the tight ones. Both probabilities are measured in data control samples. To measure ϵ_{real}, samples enriched in real leptons from W bosons decays are selected by requiring high $E_{\text{T}}^{\text{miss}}$ or m_{T}^{W}. The average ϵ_{real} is ∼0.75 (∼0.98) in the electron

JHEP08(2015)105

(muon) channel. To measure ϵ_{fake}, samples enriched in multijet background are selected by requiring either low $E_{\text{T}}^{\text{miss}}$ (electron channel) or high impact parameter significance for the lepton track (muon channel). The average ϵ_{fake} value is $\sim$0.35 ($\sim$0.20) in the electron (muon) channel. Dependencies of ϵ_{real} and ϵ_{fake} on quantities such as lepton p_{T} and η, ΔR between the lepton and the closest jet, or number of b-tagged jets, are parameterised in order to obtain a more accurate estimate.

7 Search for $T\bar{T} \to Wb$+X production

This search is sensitive to $T\bar{T}$ production where at least one of the T quarks decays into a W boson and a b-quark, although it is particularly optimised for $T\bar{T} \to W^+bW^-\bar{b}$ events. One of the W bosons present in the final state is then required to decay leptonically. After the preselection described in section 4, further background suppression is achieved by applying requirements aimed at exploiting the distinct kinematic features of the signal. The large T quark mass results in energetic W bosons and b-quarks in the final state with large angular separation between them, while the decay products from the boosted W bosons have small angular separation. The combination of these properties is very effective in distinguishing the dominant $t\bar{t}$ background since $t\bar{t}$ events with boosted W boson configurations are rare and are typically characterised by a small angular separation between the W boson and the b-quark from the top quark decay.

To take advantage of these properties, it is necessary to identify the hadronically decaying W boson (W_{had}) as well as the b-jets in the event. The candidate b-jets are defined as the two jets with the highest b-tag discriminant value, although only one of them is explicitly required to be b-tagged in the event selection. Two types of W_{had} candidates are defined, $W_{\text{had}}^{\text{type I}}$ and $W_{\text{had}}^{\text{type II}}$, depending on the angular separation between their decay products. $W_{\text{had}}^{\text{type I}}$ candidates correspond to boosted W bosons, where the quarks from the W-boson decay emerge with small angular separation and are reconstructed as a single jet. Alternatively, $W_{\text{had}}^{\text{type II}}$ candidates are characterised by two reconstructed jets. In the construction of both types of W_{had} candidates, the two candidate b-jets are not considered.

A $W_{\text{had}}^{\text{type I}}$ candidate is defined as a single jet with $p_{\text{T}} > 400$ GeV, which is the typical p_{T} above which the decay products from a W boson would have an angular separation $\Delta R \leq R_{\text{cone}} = 0.4$. A $W_{\text{had}}^{\text{type II}}$ candidate is defined as a dijet system with $p_{\text{T}} > 250$ GeV, angular separation $\Delta R(j,j) < 0.8$ and mass within the range of 60–120 GeV. The asymmetric window about the W-boson mass value is chosen in order to increase the acceptance for hadronically decaying Z bosons from $T\bar{T} \to WbZt$ events. Any jets satisfying the $W_{\text{had}}^{\text{type I}}$ requirements are excluded from consideration when forming $W_{\text{had}}^{\text{type II}}$ candidates. The leptonically decaying W boson (W_{lep}) is reconstructed using the lepton and $E_{\text{T}}^{\text{miss}}$, which is taken as a measurement of the neutrino p_{T}. Requiring that the invariant mass of the lepton-neutrino system equals the nominal W boson mass allows reconstruction of the longitudinal momentum of the neutrino up to a two-fold ambiguity. If two solutions exist, they are both considered. If no real solution exists, the pseudorapidity of the neutrino is set equal to that of the lepton, since in the kinematic regime of interest the decay products of the W boson tend to be collinear.

JHEP08(2015)105

Selection	Requirements
Preselection	Exactly one electron or muon $E_{\mathrm{T}}^{\mathrm{miss}} > 20$ GeV, $E_{\mathrm{T}}^{\mathrm{miss}} + m_{\mathrm{T}}^{W} > 60$ GeV $\geq$4 jets, $\geq$1 b-tagged jets
Loose selection	Preselection $\geq$1 W_{had} candidate (type I or type II) $H_{\mathrm{T}} > 800$ GeV $p_{\mathrm{T}}(b_1) > 160$ GeV, $p_{\mathrm{T}}(b_2) > 110$ GeV (type I) or $p_{\mathrm{T}}(b_2) > 80$ GeV (type II) $\Delta R(\ell, \nu) < 0.8$ (type I) or $\Delta R(\ell, \nu) < 1.2$ (type II)
Tight selection	Loose selection $\min(\Delta R(\ell, b_{1,2})) > 1.4$, $\min(\Delta R(W_{\mathrm{had}}, b_{1,2})) > 1.4$ $\Delta R(b_1, b_2) > 1.0$ (type I) or $\Delta R(b_1, b_2) > 0.8$ (type II) $\Delta m < 250$ GeV (type I) [see text for definition]

Table 1. Summary of event selection requirements for the $T\bar{T} \to Wb$+X analysis (see text for details).

Table 1 summarises the event selection requirements. Two selections, "loose" and "tight", are defined, with the latter being more restrictive than the former and representing the final selection. As discussed below, the loose selection is used to validate the background modelling in a kinematic regime close to the final selection. The loose selection considers preselected events with at least one $W_{\mathrm{had}}^{\mathrm{type\ I}}$ or $W_{\mathrm{had}}^{\mathrm{type\ II}}$ candidate. If multiple W_{had} candidates are found in a given event, the one with the highest p_{T} is chosen. Figure 4(a) shows the distribution of the number of W_{had} candidates after preselection. The events must satisfy $H_{\mathrm{T}} > 800$ GeV, where H_{T} is the scalar sum of the lepton p_{T}, $E_{\mathrm{T}}^{\mathrm{miss}}$ and the p_{T} of the selected jets. The H_{T} distribution peaks at $\sim 2m_T$ for signal events, which makes the $H_{\mathrm{T}} > 800$ GeV requirement particularly efficient for signal with $m_T \gtrsim 400$ GeV, while rejecting a large fraction of the background. Figure 4(b) shows the distribution of H_{T} after the requirement of $\geq$1 W_{had} candidate and prior to the $H_{\mathrm{T}} > 800$ GeV requirement. In addition, the highest-p_{T} b-jet candidate (b_1) and the next-to-highest-p_{T} b-jet candidate (b_2) are required to have $p_{\mathrm{T}}(b_1) > 160$ GeV and $p_{\mathrm{T}}(b_2) > 110\,(80)$ GeV respectively, in the case of a $W_{\mathrm{had}}^{\mathrm{type\ I}}$ ($W_{\mathrm{had}}^{\mathrm{type\ II}}$) candidate. Finally, the angular separation between the lepton and the reconstructed neutrino is required to satisfy $\Delta R(\ell, \nu) < 0.8\,(1.2)$ in case of a $W_{\mathrm{had}}^{\mathrm{type\ I}}$ ($W_{\mathrm{had}}^{\mathrm{type\ II}}$) candidate. Figure 5(a) shows the distributions of $\Delta R(\ell, \nu)$ after all previous requirements and prior to the $\Delta R(\ell, \nu)$ requirement.

The tight selection adds further requirements that are particularly effective at suppressing $t\bar{t}$ background. First, a large angular separation between the W bosons and the b-jets from the top quark decay is required: $\min(\Delta R(\ell, b_{1,2})) > 1.4$ and $\min(\Delta R(W_{\mathrm{had}}, b_{1,2})) > 1.4$. Figure 5(b) shows the distributions of $\min(\Delta R(\ell, b_{1,2}))$ after loose selection and prior to the $\min(\Delta R(\ell, b_{1,2})) > 1.4$ requirement. Finally, additional requirements are made on $\Delta R(b_1, b_2) > 1.0\,(0.8)$ in the case of a $W_{\mathrm{had}}^{\mathrm{type\ I}}$ ($W_{\mathrm{had}}^{\mathrm{type\ II}}$) candidate and $\Delta m < 250$ GeV only in the case of a $W_{\mathrm{had}}^{\mathrm{type\ I}}$ candidate, where $\Delta m = \min(|m_{\mathrm{reco}}^{\mathrm{lep}} - m_{\mathrm{reco}}^{\mathrm{had}}|)$ is the smallest absolute difference between the reconstructed heavy-quark masses obtained by pairing the W_{lep} and W_{had} candidates with the two b-jet candidates as described in the following. The

JHEP08(2015)105

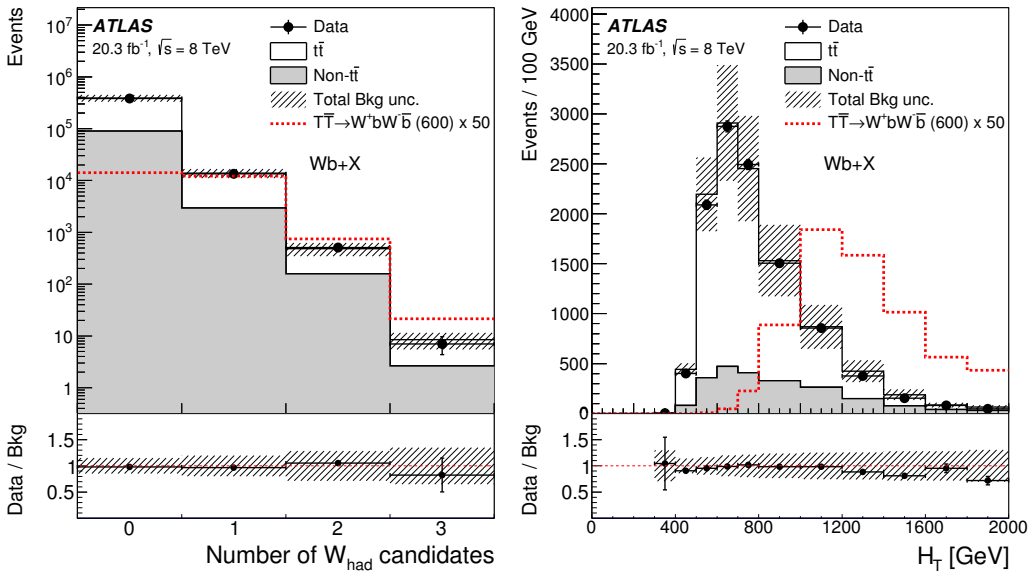

(a) (b)

Figure 4. $T\bar{T} \to Wb$+X search: distribution of (a) the number of hadronically decaying W boson (W_{had}) candidates after preselection requirements, and (b) the scalar sum (H_{T}) of the transverse momenta of the lepton, the selected jets and the missing transverse momentum after preselection and $\geq$1 W_{had} candidate requirements. The data (solid black points) are compared to the SM prediction (stacked histograms). The contributions from backgrounds other than $t\bar{t}$ are combined into a single background source referred to as "Non-$t\bar{t}$". The total uncertainty on the background estimation is shown as a black hashed band. The expected contribution from a vector-like T quark with mass $m_T = 600$ GeV under the assumption $\mathrm{BR}(T \to Wb) = 1$, multiplied by a factor of 50, is also shown (red dashed histogram). The lower panel shows the ratio of data to the SM prediction. The last bin contains the overflow.

reconstruction of the W_{lep} candidate usually yields two solutions, and there are two possible ways to pair the b-jet candidates with the W boson candidates to form the heavy quarks. Among all possible combinations, the one yielding the smallest Δm is chosen. The main discriminating variable used in this search is the reconstructed heavy-quark mass (m_{reco}), built from the W_{had} candidate and one of the two b-jet candidates. The resulting m_{reco} distributions for the loose and tight selections are shown in figure 6 for the sum of $W_{\mathrm{had}}^{\mathrm{type\ I}}$ and $W_{\mathrm{had}}^{\mathrm{type\ II}}$ events. The tight selection has the better expected sensitivity, and only this selection is chosen to derive the final result of the search. The loose selection, displaying a significant $t\bar{t}$ background at low m_{reco} which is in good agreement with the expectation, provides further confidence in the background modelling prior to the application of b-jet isolation requirements in the tight selection.

Table 2 presents a summary of the background estimates for the loose and tight selections, as well as a comparison of the total predicted and observed yields. The quoted uncertainties include both the statistical and systematic contributions. The latter are discussed in section 10. The predicted and observed yields are in agreement within these uncertainties.

JHEP08(2015)105

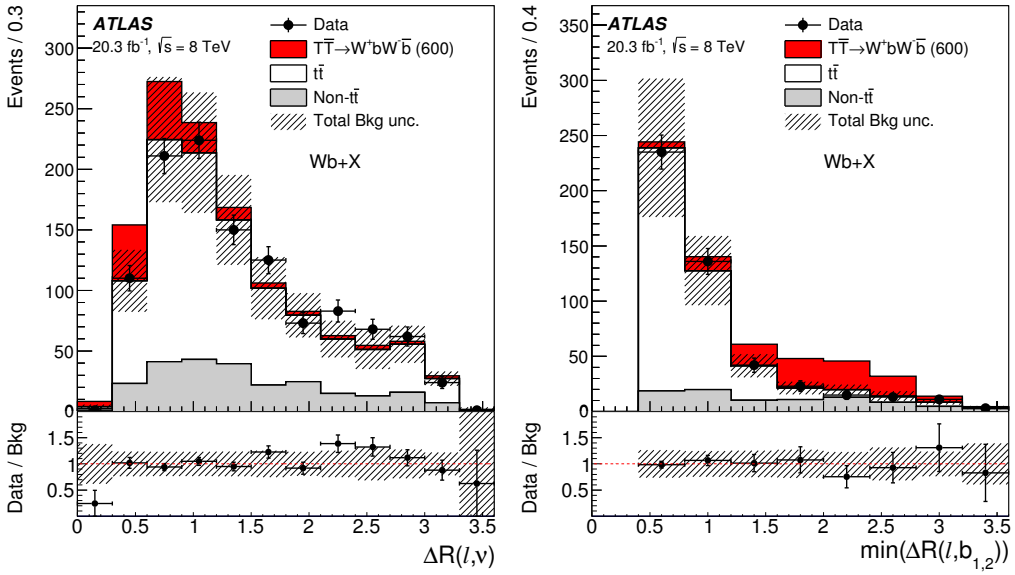

(a) **(b)**

Figure 5. $T\bar{T} \to Wb$+X search: distribution of (a) the angular separation between the lepton and the reconstructed neutrino ($\Delta R(\ell, \nu)$), and (b) the minimum angular separation between the lepton and the two candidate b-jets ($\min(\Delta R(\ell, b_{1,2}))$). The selections made include all previous requirements except for the requirement on each of these variables (see text for details). The data (solid black points) are compared to the SM prediction (stacked histograms). The contributions from backgrounds other than $t\bar{t}$ are combined into a single background source referred to as "Non-$t\bar{t}$". The total uncertainty on the background estimation is shown as a black hashed band. The expected contribution from a vector-like T quark with mass $m_T = 600$ GeV under the assumption $\mathrm{BR}(T \to Wb) = 1$ is also shown (red histogram), stacked on top of the SM background. The lower panel shows the ratio of data to the SM prediction. The last bin contains the overflow.

8 Search for $T\bar{T} \to Ht$+X and $t\bar{t}t\bar{t}$ production

This search is focused on $T\bar{T}$ production where at least one of the T quarks decays into a Higgs boson and a top quark resulting from the following processes: $T\bar{T} \to HtH\bar{t}$, $ZtHt$ and $WbHt$.[8] For the dominant $H \to b\bar{b}$ decay mode, the final-state signature is characterised by high jet and b-tag multiplicities, which provide a powerful experimental handle to suppress the background. Similarly, this search is also sensitive to $T\bar{T} \to ZtZ\bar{t}$ and $WbZt$, with $Z \to b\bar{b}$. High jet and b-tag multiplicities are also characteristic of $t\bar{t}t\bar{t}$ events (both within the SM and in BSM extensions), which makes this search also sensitive to this process. Figure 7(a) compares the jet multiplicity distribution after preselection (described in section 4) between the total background and several signal scenarios. Signal events have, on average, higher jet multiplicity than the background. The higher b-quark content of signal events results in a higher b-tag multiplicity than for the background,

[8] In the following $ZtHt$ is used to denote both $ZtH\bar{t}$ and its charge conjugate, $HtZ\bar{t}$. Similar notation is used for other processes, as appropriate.

JHEP08(2015)105

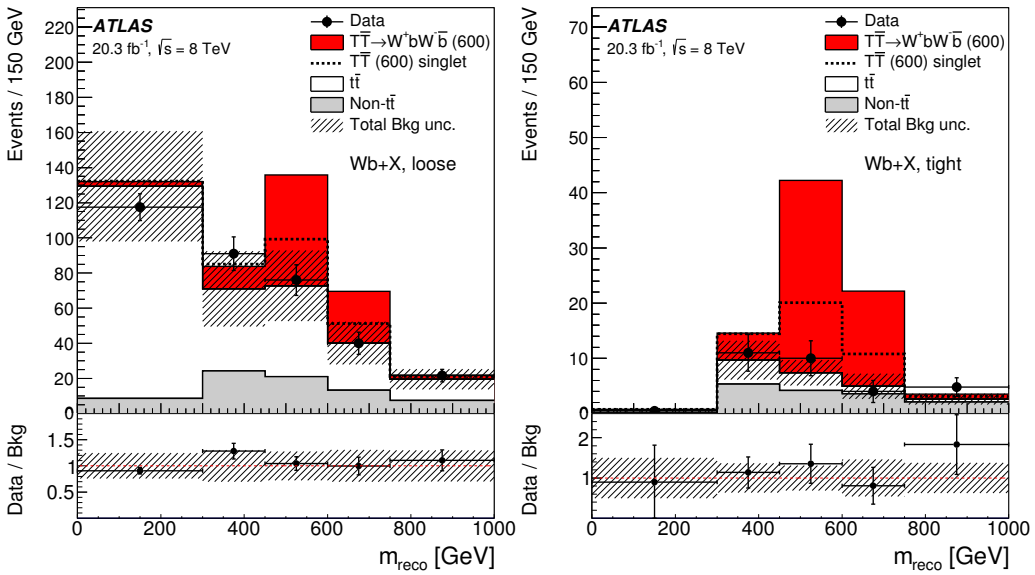

Figure 6. $T\bar{T} \to Wb$+X search: distribution of the reconstructed heavy-quark mass (m_{reco}) after (a) the loose selection and (b) the tight selection, for the sum of $W_{\text{had}}^{\text{type I}}$ and $W_{\text{had}}^{\text{type II}}$ events. The data (solid black points) are compared to the SM prediction (stacked histograms). The contributions from backgrounds other than $t\bar{t}$ are combined into a single background source referred to as "Non-$t\bar{t}$". The total uncertainty on the background estimation is shown as a black hashed band. The expected contributions from a vector-like T quark with mass $m_T = 600$ GeV in two scenarios, BR($T \to Wb$) = 1 (red histogram) and singlet (dashed black histogram), are also shown stacked on top of the SM background. The lower panel shows the ratio of data to the SM prediction. The last bin contains the overflow.

as illustrated in figure 7(b) for events with ≥6 jets. Therefore, after preselection, the final selection requirements are ≥5 jets of which ≥2 jets are b-tagged, leaving a sample completely dominated by $t\bar{t}$+jets background. In order to ensure a non-overlapping analysis sample and to facilitate the combination of results, events accepted by the Wb+X search are rejected. This veto only removes about 2% of the events with ≥6 jets and ≥4 b-tagged jets in data.

In order to optimise the sensitivity of the search, the selected events are categorised into different channels depending on the number of jets (5 and ≥6) and on the number of b-tagged jets (2, 3 and ≥4). The channel with ≥6 jets and ≥4 b-tagged jets has the largest signal-to-background ratio and therefore drives the sensitivity of the search. The channels with two and three b-tagged jets have significantly lower signal-to-background ratio. These are particularly useful to calibrate the $t\bar{t}$+jets background prediction and constrain the related systematic uncertainties. In the case of the channel with ≥6 jets and ≥4 b-tagged jets the background uncertainty is dominated by uncertainties on the b-tagging, jet energy calibration and physics modelling, including the $t\bar{t}$+HF content. A detailed discussion of the systematic uncertainties considered is given in section 10. In addition, events with ≥6

JHEP08(2015)105

	Loose selection	Tight selection
$T\bar{T}$ ($m_T = 600$ GeV)		
BR($T \to Wb$) = 1	115 ± 10	58.9 ± 5.9
Singlet	60.3 ± 5.1	24.5 ± 2.3
$t\bar{t}$	390 ± 110	10.7 ± 4.3
$t\bar{t}V$	6.5 ± 2.5	0.4 ± 0.2
$t\bar{t}H$	1.6 ± 0.4	0.10 ± 0.03
W+jets	38 ± 19	11.4 ± 6.2
Z+jets	1.5 ± 1.2	0.4 ± 0.4
Single top	36 ± 17	2.2 ± 1.5
Diboson	5.6 ± 1.4	1.5 ± 0.6
Multijet	0.3 ± 1.6	0.8 ± 0.7
Total background	480 ± 120	27.6 ± 8.6
Data	478	34

Table 2. $T\bar{T} \to Wb$+X search: number of observed events, integrated over the whole mass spectrum, compared to the SM expectation after the loose and tight selections. The expected signal yields in two different scenarios for a vector-like T quark with $m_T = 600$ GeV, BR($T \to Wb$) = 1 and singlet, are also shown. The quoted uncertainties include both the statistical and systematic contributions.

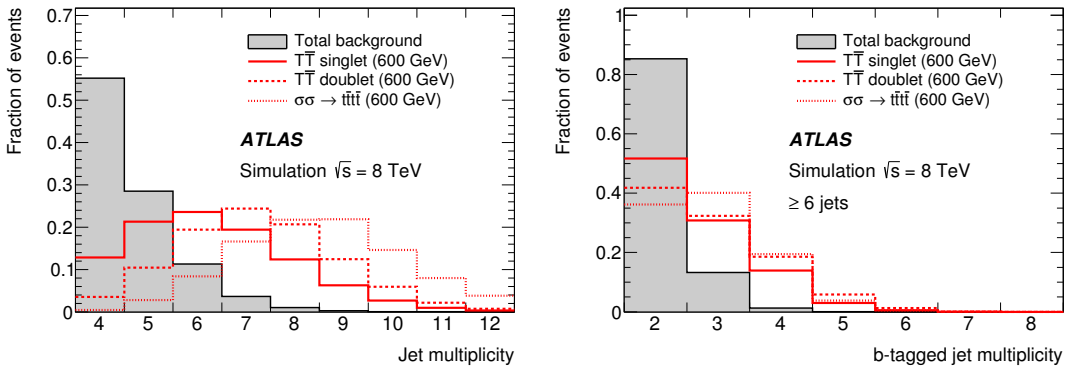

(a) **(b)**

Figure 7. $T\bar{T} \to Ht$+X search (simulated events): comparison of (a) the jet multiplicity distribution after preselection, and (b) the b-tag multiplicity distribution after the requirement of $\geq$6 jets, between the total background (shaded histogram) and several signal scenarios considered in this search: $T\bar{T}$ production in the T quark singlet (red solid histogram) and doublet (red dashed histogram) cases, and sgluon pair production giving a four-top-quark final state (red dotted histogram). A mass of 600 GeV is assumed for the T quark and the sgluon.

JHEP08(2015)105

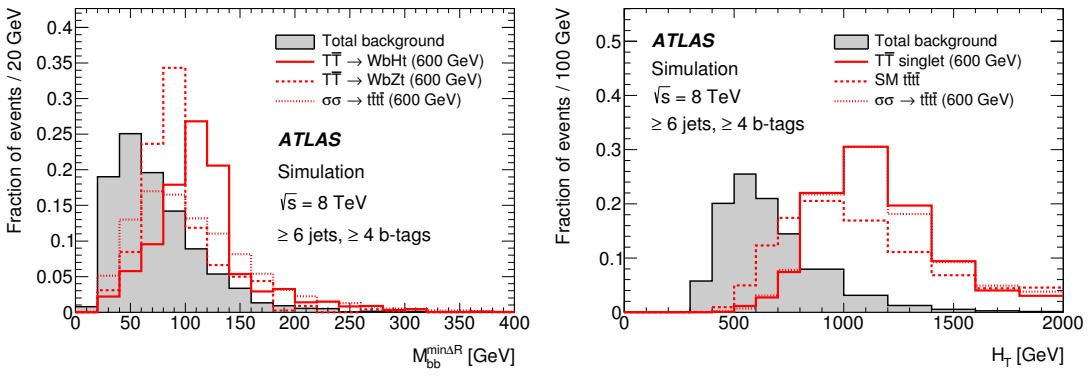

(a) **(b)**

Figure 8. $T\bar{T} \to Ht$+X search (simulated events): comparison of the distributions of (a) the invariant mass of the two b-tagged jets with lowest ΔR separation ($M_{bb}^{\min\Delta R}$), and (b) the scalar sum of the transverse momenta of the lepton, the selected jets and the missing transverse momentum (H_{T}), between the total background (shaded histogram) and several signal scenarios considered in this search: $T\bar{T} \to WbHt$ (red solid histogram), $T\bar{T} \to WbZt$ or SM $t\bar{t}t\bar{t}$ production (red dashed histograms), and sgluon pair production giving a $t\bar{t}t\bar{t}$ final state (red dotted histogram). A mass of 600 GeV is assumed for the T quark and the sgluon. The selection used in both (a) and (b) corresponds to events satisfying the preselection requirements and with ≥6 jets and ≥4 b-tagged jets.

jets and 3 or ≥4 b-tagged jets are split into two channels each depending on the value of the invariant mass of the two b-tagged jets with lowest ΔR separation: $M_{bb}^{\min\Delta R} < 100$ GeV ("low $M_{bb}^{\min\Delta R}$") and $M_{bb}^{\min\Delta R} > 100$ GeV ("high $M_{bb}^{\min\Delta R}$"). For high values of m_T, the Higgs boson from the $T \to Ht$ decay has high p_{T}, and the $b\bar{b}$ pair from the Higgs boson decay has smaller angular separation than other pairs resulting from combinatorial background. As shown in figure 8(a), the $M_{bb}^{\min\Delta R}$ variable provides a good approximation to the reconstructed $H \to b\bar{b}$ invariant mass and allows the separation of these channels into channels depleted or enriched in $T \to Ht$, $H \to b\bar{b}$ decays, the latter having a higher signal-to-background ratio. Therefore, the total number of analysis channels considered in this search is eight: (5 j, 2 b), (5 j, 3 b), (5 j, ≥4 b), (≥6 j, 2 b), (≥6 j, 3 b, low $M_{bb}^{\min\Delta R}$), (≥6 j, 3 b, high $M_{bb}^{\min\Delta R}$), (≥6 j, ≥4 b, low $M_{bb}^{\min\Delta R}$), and (≥6 j, ≥4 b, high $M_{bb}^{\min\Delta R}$), where (n j, m b) indicates n selected jets and m b-tagged jets.

To further improve the separation between signal and background, the distinct kinematic features of the signal are exploited. In particular, the large T quark mass results in energetic leptons and jets in the final state, and H_{T} provides a suitable discriminating variable between signal and background. Figure 8(b) compares the H_{T} distribution between signal and background for events with ≥6 jets and ≥4 b-tagged jets. The H_{T} distribution is quite similar for different signal scenarios corresponding to pair production of exotic particles with the same mass (600 GeV in this case), and significantly different from that of the background. The discrimination between signal and background increases with mass.

JHEP08(2015)105

Figures 9 and 10 show the comparison of data and prediction for the H_{T} distributions in each of the analysis channels considered. The corresponding predicted and observed yields per channel can be found in table 3. Following the statistical procedure outlined in section 11, a fit to the observed H_{T} distributions in data in the eight analysis channels is performed. This provides an improved background prediction with smaller uncertainties, and hence improved sensitivity to a signal. The results are presented in section 12.

9 Search for $B\bar{B} \to Hb$+X production

This search is focused on $B\bar{B}$ production where at least one of the B quarks decays into a Higgs boson and a b quark, a decay mode that was omitted from previous searches [25–27]. In particular, the $B\bar{B} \to HbH\bar{b}$ final state is the least covered one because the most-common Higgs boson decay mode, $H \to b\bar{b}$, leads to a challenging final state with six b-jets and no leptons. In contrast, cleaner experimental signatures involving leptons tend to be suppressed by the small decay branching ratios. However, a sizeable signal rate results from the mixed decay mode where one of the Higgs bosons decays into W^+W^-, while the other Higgs boson decays into $b\bar{b}$: $B\bar{B} \to HbH\bar{b} \to (W^+W^-)b(b\bar{b})\bar{b}$. When one of the W bosons decays leptonically, this leads to the final-state signature considered in this search, involving one lepton and high jet and b-tag multiplicities, analogous to the signature exploited by the $T\bar{T} \to Ht$+X search.

Consequently, this search considers the same discriminating variable, H_{T}, and the same eight analysis channels as the $T\bar{T} \to Ht$+X search. Figure 11(a) illustrates the good separation between signal and background in the H_{T} distribution for events passing the preselection requirements and with ≥ 6 jets and ≥ 4 b-tagged jets. A peculiarity of the $B \to Hb$ decay mode is that the b-jet originating (directly) from the B-quark decay can have very high transverse momentum in the case of a heavy B quark. To exploit this feature, the event selection is tightened relative to that used in the $T\bar{T} \to Ht$+X search by raising the minimum p_{T} requirement on the two highest-p_{T} (leading) b-tagged jets to $p_{\mathrm{T}} > 150$ GeV. Figure 11(b) shows the distribution of the subleading b-jet p_{T} for events passing the preselection requirements and with ≥ 6 jets and ≥ 4 b-tagged jets. The tighter requirement on the subleading b-jet p_{T} rejects about 90% of the $t\bar{t}$ background while retaining a large acceptance for the $B\bar{B} \to Hb$+X signal. This search is also sensitive to other $B\bar{B}$ final states, such as $B\bar{B} \to HbWt$, that typically do not involve multilepton final states in the topologies usually searched for (opposite-sign dileptons with a $Z \to \ell^+\ell^-$ candidate, same-sign dileptons, and trileptons), and is thus complementary to previous searches [25–27].

Figures 12 and 13 show the comparison of data and prediction for the H_{T} distributions in each of the analysis channels considered. The corresponding predicted and observed yields per channel can be found in table 4. The results of the fit to the data to improve the background prediction, as in the $T\bar{T} \to Ht$+X search, are presented in section 12.

JHEP08(2015)105

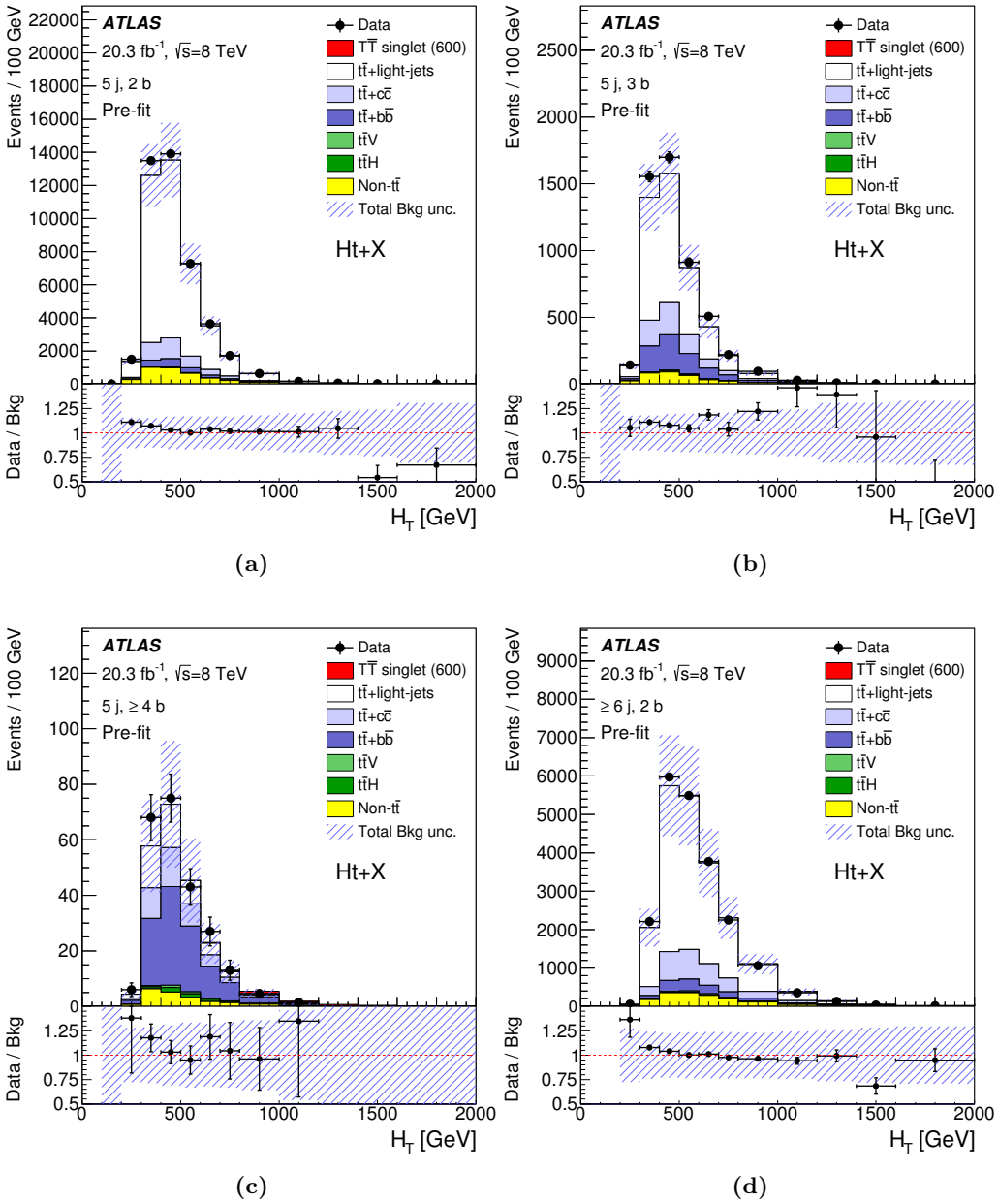

Figure 9. $T\bar{T} \to Ht$+X search: comparison between data and prediction for the distribution of the scalar sum (H_{T}) of the transverse momenta of the lepton, the selected jets and the missing transverse momentum in each of the analysed channels after final selection: (a) (5 j, 2 b), (b) (5 j, 3 b), (c) (5 j, $\geq$4 b), and (d) ($\geq$6 j, 2 b). The background prediction is shown before the fit to data. The contributions from W/Z+jets, single top, diboson and multijet backgrounds are combined into a single background source referred to as "Non-$t\bar{t}$". Also shown is the expected signal contribution from a singlet vector-like T quark with mass $m_T = 600$ GeV. The last bin in all figures contains the overflow. The bottom panel displays the ratio of data to the total background prediction. The hashed area represents the total uncertainty on the background.

JHEP08(2015)105

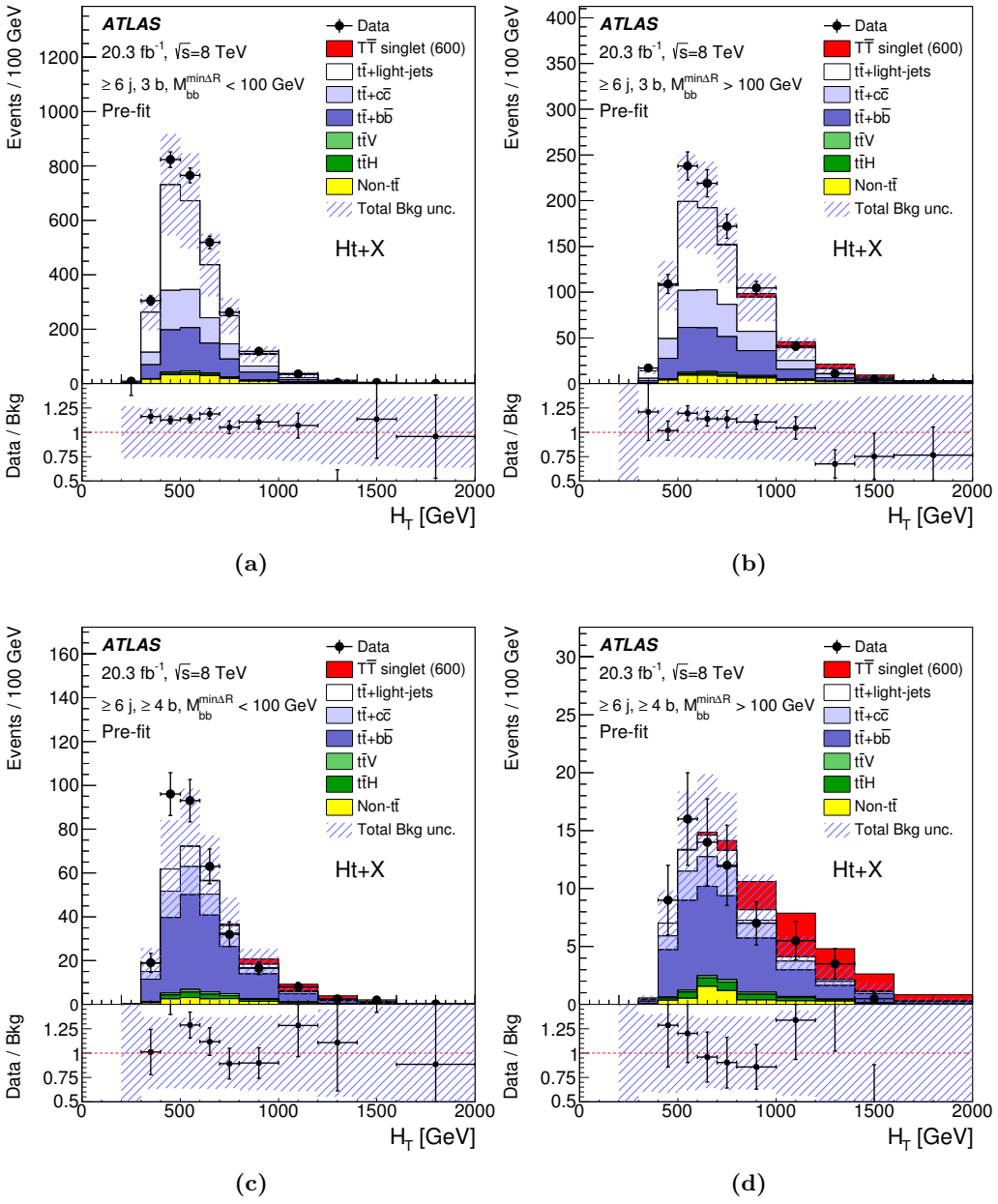

Figure 10. $T\bar{T} \to Ht$+X search: comparison between data and prediction for the distribution of the scalar sum (H_{T}) of the transverse momenta of the lepton, the selected jets and the missing transverse momentum in each of the analysed channels after final selection: (a) (≥6 j, 3 b, low $M_{bb}^{\mathrm{min}\Delta R}$), (b) (≥6 j, 3 b, high $M_{bb}^{\mathrm{min}\Delta R}$), (c) (≥6 j, ≥4 b, low $M_{bb}^{\mathrm{min}\Delta R}$), and (d) (≥6 j, ≥4 b, high $M_{bb}^{\mathrm{min}\Delta R}$). The background prediction is shown before the fit to data. The contributions from W/Z+jets, single top, diboson and multijet backgrounds are combined into a single background source referred to as "Non-$t\bar{t}$". Also shown is the expected signal contribution from a singlet vector-like T quark with mass $m_T = 600$ GeV. The last bin in all figures contains the overflow. The bottom panel displays the ratio of data to the total background prediction. The hashed area represents the total uncertainty on the background.

JHEP08(2015)105

	5 j, 2 b	5 j, 3 b	5 j, ≥4 b	≥6 j, 2 b
$T\bar{T}$ ($m_T = 600$ GeV)				
Singlet	52.5 ± 4.2	19.0 ± 2.3	5.8 ± 1.2	123.3 ± 6.2
(T,B) or (X,T) doublet	25.8 ± 2.0	14.0 ± 1.4	5.0 ± 1.0	154.1 ± 6.4
$\sigma\sigma \to t\bar{t}t\bar{t}$ ($m_\sigma = 800$ GeV)	2.0 ± 0.3	1.4 ± 0.3	0.3 ± 0.1	64.8 ± 4.6
$t\bar{t}t\bar{t}$+X (Tier (1,1), $m_{\mathrm{KK}} = 800$ GeV)	1.0 ± 0.4	0.6 ± 0.3	0.06 ± 0.05	180 ± 29
$t\bar{t}$+light-jets	32400 ± 5300	2930 ± 520	48 ± 12	16200 ± 4000
$t\bar{t} + c\bar{c}$	3800 ± 2100	730 ± 410	42 ± 24	3300 ± 1800
$t\bar{t} + b\bar{b}$	1530 ± 800	800 ± 420	108 ± 58	1300 ± 700
$t\bar{t}V$	140 ± 46	24.9 ± 8.1	2.9 ± 1.0	172 ± 56
$t\bar{t}H$	39.2 ± 1.7	20.8 ± 1.6	5.6 ± 0.7	60.2 ± 4.5
W+jets	1600 ± 1000	111 ± 71	5.0 ± 3.4	770 ± 530
Z+jets	360 ± 120	24.8 ± 8.4	1.2 ± 0.5	185 ± 67
Single top	1630 ± 320	169 ± 36	7.0 ± 1.0	730 ± 200
Diboson	85 ± 27	7.3 ± 2.5	0.4 ± 0.2	45 ± 15
Multijet	133 ± 48	33 ± 12	6.9 ± 2.6	56 ± 20
Total background	41700 ± 6400	4840 ± 900	228 ± 69	22800 ± 5200
Data	43319	5309	244	23001

	≥6 j, 3 b low $M_{bb}^{\min\Delta R}$	≥6 j, 3 b high $M_{bb}^{\min\Delta R}$	≥6 j, ≥4 b low $M_{bb}^{\min\Delta R}$	≥6 j, ≥4 b high $M_{bb}^{\min\Delta R}$
$T\bar{T}$ ($m_T = 600$ GeV)				
Singlet	29.5 ± 2.0	44.0 ± 3.6	17.7 ± 1.9	24.1 ± 3.7
(T,B) or (X,T) doublet	50.2 ± 2.5	68.9 ± 4.1	41.0 ± 3.9	53.8 ± 7.3
$\sigma\sigma \to t\bar{t}t\bar{t}$ ($m_\sigma = 800$ GeV)	22.5 ± 1.6	50.7 ± 3.5	9.3 ± 1.0	16.2 ± 2.6
$t\bar{t}t\bar{t}$+X (Tier (1,1), $m_{\mathrm{KK}} = 800$ GeV)	33.6 ± 2.8	132.5 ± 5.9	27.7 ± 2.3	75 ± 13
$t\bar{t}$+light-jets	1280 ± 350	440 ± 110	38 ± 14	9.3 ± 3.9
$t\bar{t} + c\bar{c}$	550 ± 320	220 ± 120	53 ± 31	14.7 ± 9.0
$t\bar{t} + b\bar{b}$	620 ± 330	250 ± 140	178 ± 95	46 ± 25
$t\bar{t}V$	28.7 ± 9.2	12.5 ± 4.2	6.2 ± 2.0	1.5 ± 0.5
$t\bar{t}H$	24.9 ± 1.9	11.6 ± 1.3	10.6 ± 1.2	4.1 ± 0.6
W+jets	68 ± 46	16 ± 10	6.6 ± 4.8	0.6 ± 0.4
Z+jets	15.7 ± 6.3	3.3 ± 1.3	1.6 ± 0.6	0.3 ± 0.1
Single top	74 ± 22	32 ± 12	7.8 ± 2.2	2.1 ± 1.3
Diboson	4.2 ± 1.6	1.2 ± 0.5	0.4 ± 0.1	0.2 ± 0.1
Multijet	1.9 ± 0.8	4.8 ± 2.1	< 0.01	2.8 ± 1.0
Total background	2670 ± 680	990 ± 260	300 ± 110	81 ± 30
Data	3015	1085	362	84

Table 3. $T\bar{T} \to Ht$+X search: predicted and observed yields in each of the analysis channels considered. The background prediction is shown before the fit to data. Also shown are the signal predictions for different benchmark scenarios considered. The quoted uncertainties are the sum in quadrature of statistical and systematic uncertainties on the yields.

JHEP08(2015)105

	5 j, 2 b	5 j, 3 b	5 j, ≥4 b	≥6 j, 2 b
$B\bar{B}$ ($m_B = 600$ GeV)				
BR($B \to Hb$) = 1	8.6 ± 1.1	9.3 ± 2.2	5.0 ± 1.4	11.9 ± 3.0
Singlet	12.2 ± 1.9	8.8 ± 1.7	3.4 ± 0.8	27.4 ± 4.3
(B, Y) doublet	8.5 ± 1.1	5.8 ± 1.4	2.8 ± 0.8	10.9 ± 2.1
$t\bar{t}$+light-jets	389 ± 93	72 ± 18	2.1 ± 0.7	234 ± 74
$t\bar{t} + c\bar{c}$	56 ± 42	23 ± 15	2.2 ± 1.5	55 ± 40
$t\bar{t} + b\bar{b}$	19 ± 14	25 ± 14	5.5 ± 3.2	22 ± 15
$t\bar{t}V$	4.2 ± 1.4	1.6 ± 0.5	0.3 ± 0.1	5.1 ± 1.7
$t\bar{t}H$	1.0 ± 0.1	1.1 ± 0.2	0.5 ± 0.1	1.5 ± 0.2
W+jets	21 ± 12	3.5 ± 2.1	0.6 ± 0.5	12.5 ± 7.9
Z+jets	8.2 ± 3.3	2.8 ± 2.8	0.5 ± 0.5	4.3 ± 4.1
Single top	41.3 ± 7.2	8.8 ± 1.9	0.6 ± 0.1	28.0 ± 6.8
Diboson	1.9 ± 0.9	0.5 ± 0.3	0.07 ± 0.07	1.2 ± 0.7
Multijet	< 0.01	< 0.01	0.4 ± 0.2	0.2 ± 0.1
Total background	540 ± 120	139 ± 35	12.8 ± 4.9	360 ± 100
Data	576	165	10	375

	≥6 j, 3 b low $M_{bb}^{\min\Delta R}$	≥6 j, 3 b high $M_{bb}^{\min\Delta R}$	≥6 j, ≥4 b low $M_{bb}^{\min\Delta R}$	≥6 j, ≥4 b high $M_{bb}^{\min\Delta R}$
$B\bar{B}$ ($m_B = 600$ GeV)				
BR($B \to Hb$) = 1	3.8 ± 0.6	13.1 ± 1.8	3.2 ± 0.7	9.6 ± 2.0
Singlet	7.1 ± 0.9	15.8 ± 2.5	4.6 ± 0.9	7.5 ± 1.5
(B, Y) doublet	2.7 ± 0.3	7.0 ± 1.3	2.3 ± 0.6	3.9 ± 0.9
$t\bar{t}$+light-jets	21.3 ± 9.0	32.8 ± 9.5	1.4 ± 0.5	1.5 ± 0.6
$t\bar{t} + c\bar{c}$	10.8 ± 7.5	20 ± 15	2.2 ± 1.6	2.9 ± 2.2
$t\bar{t} + b\bar{b}$	13.1 ± 8.5	24 ± 16	7.8 ± 4.8	8.1 ± 5.3
$t\bar{t}V$	1.1 ± 0.4	1.6 ± 0.6	0.6 ± 0.2	0.4 ± 0.2
$t\bar{t}H$	0.7 ± 0.1	1.4 ± 0.2	0.5 ± 0.1	0.9 ± 0.2
W+jets	2.0 ± 1.3	1.1 ± 0.8	0.3 ± 0.3	0.05 ± 0.05
Z+jets	0.11 ± 0.07	0.2 ± 0.1	< 0.01	< 0.01
Single top	3.2 ± 0.6	5.1 ± 2.2	0.8 ± 0.2	0.3 ± 0.2
Diboson	0.2 ± 0.1	0.09 ± 0.03	0.02 ± 0.01	< 0.01
Multijet	< 0.01	0.6 ± 0.2	< 0.01	0.4 ± 0.1
Total background	53 ± 18	87 ± 30	13.7 ± 5.9	14.5 ± 7.3
Data	62	103	23	20

Table 4. $B\bar{B} \to Hb$+X search: predicted and observed yields in each of the analysis channels considered. The background prediction is shown before the fit to data. Also shown are the signal predictions for different benchmark scenarios considered. The quoted uncertainties are the sum in quadrature of statistical and systematic uncertainties on the yields.

JHEP08(2015)105

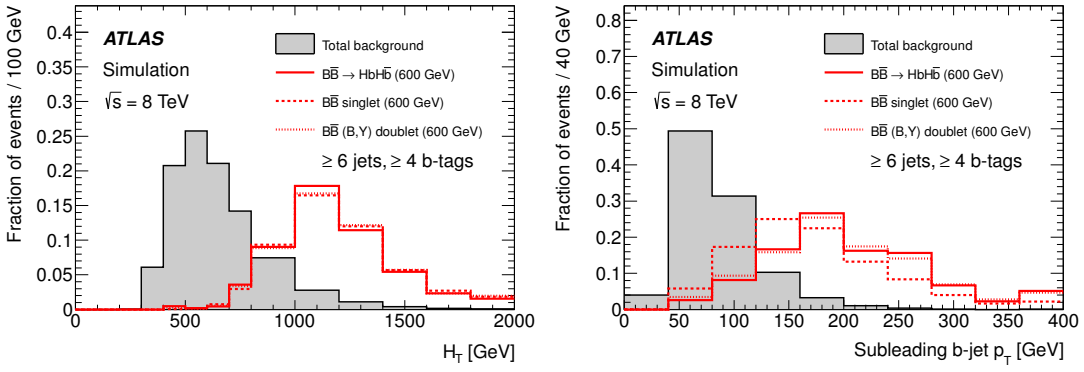

(a) **(b)**

Figure 11. $B\bar{B} \to Hb$+X search (simulated events): comparison of the distributions of (a) the scalar sum of the transverse momenta of the lepton, the selected jets and the missing transverse momentum (H_{T}), and (b) the transverse momentum of the next-to-highest-transverse-momentum b-jet, between the total background (shaded histogram) and several $B\bar{B}$ signal scenarios considered in this search: $\mathrm{BR}(B \to Hb) = 1$ (red solid histogram), B quark singlet (red dashed histogram), and B quark from a (B, Y) doublet (red dotted histogram). In all cases a mass of 600 GeV is assumed for the B quark. The selection used in both (a) and (b) corresponds to events satisfying the preselection requirements and with $\geq$6 jets and $\geq$4 b-tagged jets.

JHEP08(2015)105

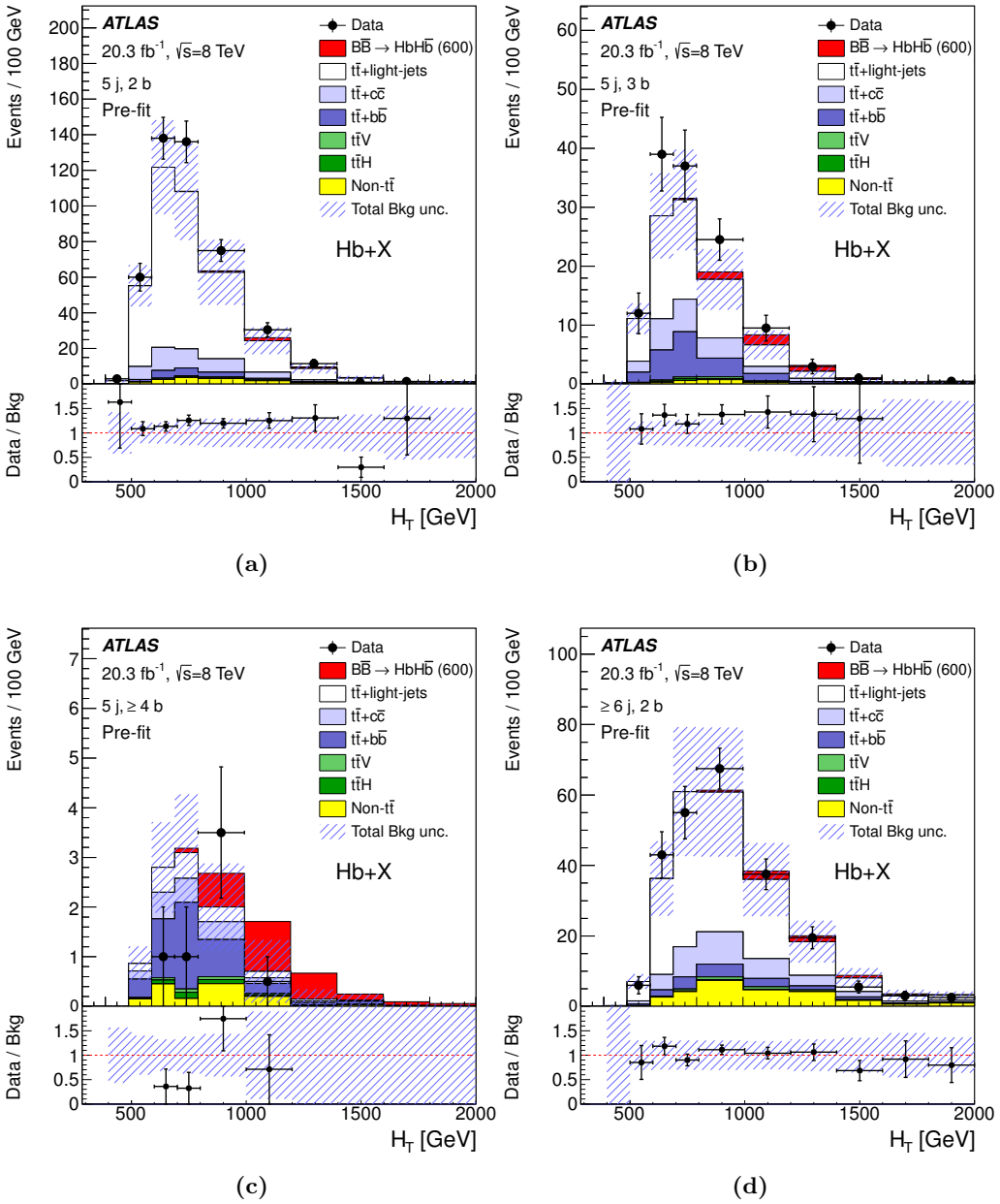

Figure 12. $B\bar{B} \to Hb$+X search: comparison between data and prediction for the distribution of the scalar sum (H_{T}) of the transverse momenta of the lepton, the selected jets and the missing transverse momentum in each of the analysed channels after final selection: a) (5 j, 2 b), (b) (5 j, 3 b), (c) (5 j, ≥4 b), and (d) (≥6 j, 2 b). The background prediction is shown before the fit to data. The contributions from W/Z+jets, single top, diboson and multijet backgrounds are combined into a single background source referred to as "Non-$t\bar{t}$". Also shown is the expected signal contribution from a vector-like B quark with mass $m_B = 600$ GeV under the assumption BR($B \to Hb$) = 1. The last bin in all figures contains the overflow. The bottom panel displays the ratio of data to the total background prediction. The hashed area represents the total uncertainty on the background.

JHEP08(2015)105

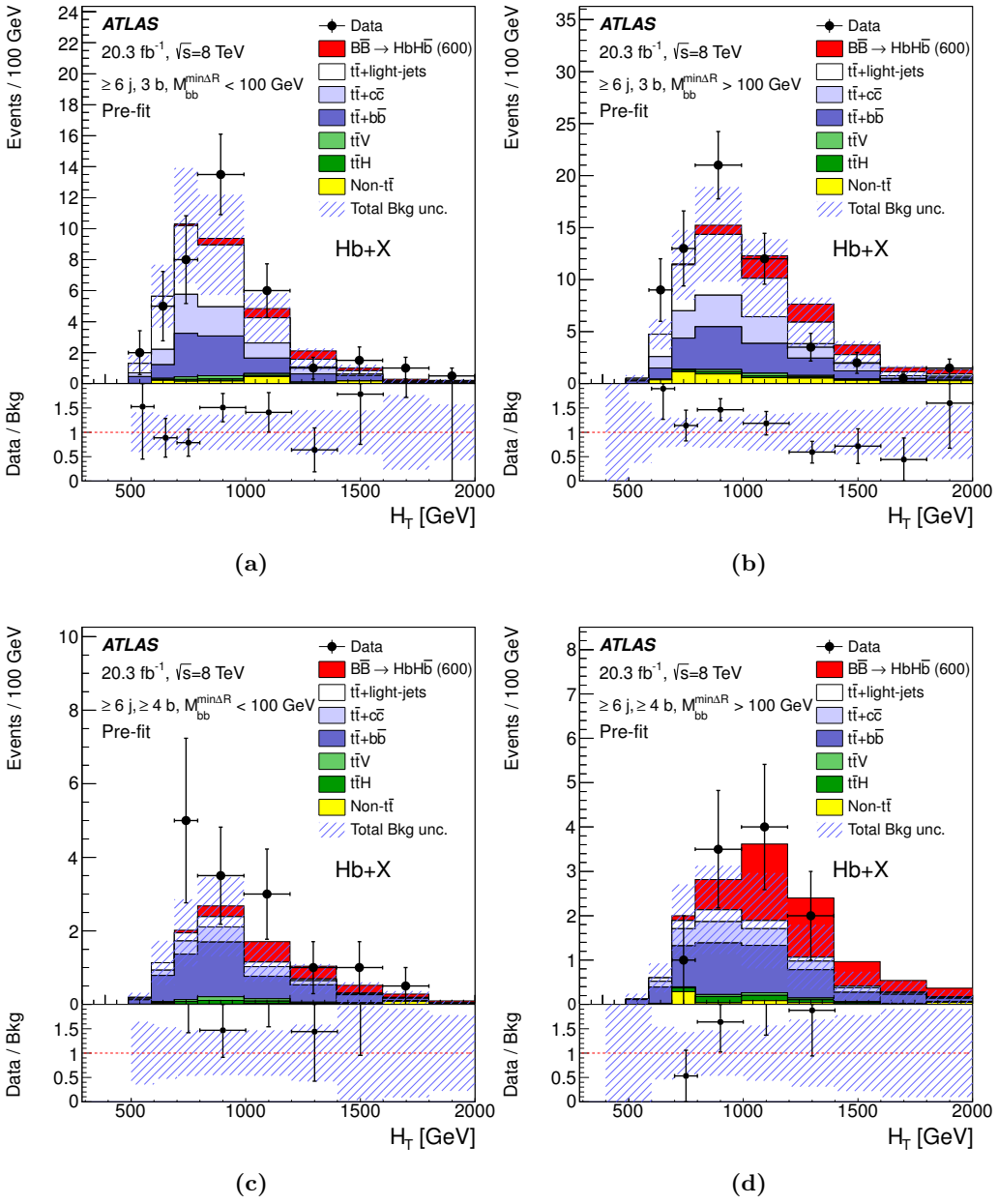

Figure 13. $B\bar{B} \to Hb$+X search: comparison between data and prediction for the distribution of the scalar sum (H_{T}) of the transverse momenta of the lepton, the selected jets and the missing transverse momentum in each of the analysed channels after final selection: (a) (≥6 j, 3 b, low $M_{bb}^{\mathrm{min}\Delta R}$), (b) (≥6 j, 3 b, high $M_{bb}^{\mathrm{min}\Delta R}$), (c) (≥6 j, ≥4 b, low $M_{bb}^{\mathrm{min}\Delta R}$), and (d) (≥6 j, ≥4 b, high $M_{bb}^{\mathrm{min}\Delta R}$). The background prediction is shown before the fit to data. The contributions from W/Z+jets, single top, diboson and multijet backgrounds are combined into a single background source referred to as "Non-$t\bar{t}$". Also shown is the expected signal contribution from a vector-like B quark with mass $m_B = 600$ GeV under the assumption BR($B \to Hb$) = 1. The last bin in all figures contains the overflow. The bottom panel displays the ratio of data to the total background prediction. The hashed area represents the total uncertainty on the background.

JHEP08(2015)105

10 Systematic uncertainties

Several sources of systematic uncertainty are considered that can affect the normalisation of signal and background and/or the shape of their corresponding final discriminant distributions. Individual sources of systematic uncertainty are considered uncorrelated. Correlations of a given systematic uncertainty are maintained across processes and channels. Table 5 presents a list of all systematic uncertainties considered in the analyses and indicates whether they are taken to be normalisation-only, or to affect both shape and normalisation.

Table 6 presents a summary of the systematic uncertainties for the $T\bar{T} \to Wb$+X search and their impact on the normalisation of signal and backgrounds. A similar summary is presented for the $T\bar{T} \to Ht$+X and $B\bar{B} \to Hb$+X searches in tables 7 and 8 respectively, restricted to the highest-sensitivity channel and displaying only the signal and the $t\bar{t}$+jets background categories. Tables 7 and 8 also show the impact of the systematic uncertainties before and after the fit to data.

In the case of the $T\bar{T} \to Wb$+X search, the total systematic uncertainty in the background normalisation is approximately 29%, with the dominant contributions originating from the normalisation of the W+jets background (20%), jet energy scale (+17%/−12%) and the $t\bar{t}$+HF normalisation (11%). The total systematic uncertainty in the signal normalisation is +8%/−10%, with comparable contributions from jet energy scale and b-tagging uncertainties.

The leading sources of systematic uncertainty in the $T\bar{T} \to Ht$+X and $B\bar{B} \to Hb$+X searches vary depending on the analysis channel considered, but they typically originate from $t\bar{t}$+jets modelling (including $t\bar{t}$+HF), jet energy scale and b-tagging. For example, the total systematic uncertainty in the background normalisation in the highest-sensitivity channel ($\geq$6 j, $\geq$4 b, high $M_{bb}^{\min\Delta R}$) of the $T\bar{T} \to Ht$+X search is approximately 37%, with the largest contributions originating from $t\bar{t}$+HF normalisation (23%), jet energy scale (10%) and b-tagging (9%). However, as discussed previously, the fit to data in the eight analysis channels in these searches allows the overall background uncertainty to be reduced significantly, to approximately 5% in the case of the $T\bar{T} \to Ht$+X search. More details about the fit to data can be found in section 12.1. The total systematic uncertainty on the signal normalisation is approximately 15%, almost all due to b-tagging uncertainties.

The following sections describe each of the systematic uncertainties considered in the analyses.

10.1 Luminosity

The uncertainty on the integrated luminosity is 2.8%, affecting the overall normalisation of all processes estimated from the simulation. It is derived following the same methodology as that detailed in ref. [57].

JHEP08(2015)105

Systematic uncertainty	Type	Components
Luminosity	N	1
Reconstructed Objects		
Electron	SN	5
Muon	SN	6
Jet reconstruction	SN	1
Jet vertex fraction	SN	1
Jet energy scale	SN	22
Jet energy resolution	SN	1
Missing transverse momentum	SN	2
b-tagging efficiency	SN	6
c-tagging efficiency	SN	4
Light-jet tagging efficiency	SN	12
High-p_{T} tagging	SN	1
Background Model		
$t\bar{t}$ cross section	N	1
$t\bar{t}$ modelling: p_{T} reweighting	SN	9
$t\bar{t}$ modelling: parton shower	SN	3
$t\bar{t}$+HF: normalisation	N	2
$t\bar{t}$+$c\bar{c}$: HF reweighting	SN	2
$t\bar{t}$+$c\bar{c}$: generator	SN	4
$t\bar{t}$+$b\bar{b}$: NLO Shape	SN	8
W+jets normalisation	N	3
Z+jets normalisation	N	3
Single top cross section	N	1
Single top model	SN	1
Diboson normalisation	N	1
$t\bar{t}V$ cross section	N	1
$t\bar{t}V$ model	SN	1
$t\bar{t}H$ cross section	N	1
$t\bar{t}H$ model	SN	2
Multijet normalisation	N	2

Table 5. List of systematic uncertainties considered. An "N" means that the uncertainty is taken as normalisation-only for all processes and channels affected, whereas "SN" means that the uncertainty is taken on both shape and normalisation. Some of the systematic uncertainties are split into several components for a more accurate treatment.

JHEP08(2015)105

	Signal	$t\bar{t}$	Non-$t\bar{t}$	Total background
Luminosity	±2.8	±2.8	±2.8	±2.8
Lepton efficiencies	±1.6	±1.6	±1.5	±1.6
Jet energy scale	+3.4/−7.2	±16	+19/−9	+17/−12
Jet efficiencies	±1.5	±1.6	±1.6	±1.6
Jet energy resolution	±1.1	±0.6	±2.6	±1.8
b-tagging efficiency	±5.0	±0.7	±2.9	±2.0
c-tagging efficiency	±0.4	±1.2	±2.3	±1.9
Light-jet tagging efficiency	±0.2	±1.3	±1.6	±1.4
High-p_{T} tagging efficiency	±3.2	±1.3	±0.8	±1.1
Missing transverse momentum	–	±2.6	–	±1.0
$t\bar{t}$: reweighting	–	±15	–	±5.9
$t\bar{t}$: parton shower	–	±9.3	–	±3.6
$t\bar{t}$+HF: normalisation	–	+12.0/−5.5	–	+4.5/−2.1
$t\bar{t}$+HF: modelling	–	±30	–	±11
Theoretical cross sections	–	±6.0	±33	±20
Multijet normalisation	–	–	±2.9	±1.8
Non-$t\bar{t}$ modelling	–	–	±2.3	±1.4
Total	+7.7/−10.0	±40	±35	±29

Table 6. $T\bar{T} \to Wb$+X search: summary of the systematic uncertainties considered and their impact (in %) on the normalisation of signal and backgrounds. Only sources of systematic uncertainty resulting in a normalisation change of at least 0.5% are displayed. The signal shown corresponds to a vector-like T quark with mass $m_T = 600$ GeV and $\mathrm{BR}(T \to Wb) = 1$.

10.2 Reconstructed objects

10.2.1 Leptons

Uncertainties associated with leptons arise from the reconstruction, identification and trigger, as well as the lepton momentum scale and resolution. The reconstruction and identification efficiency of electrons and muons, as well as the efficiency of the trigger used to record the events, differ slightly between data and simulation. Scale factors are derived using tag-and-probe techniques on $Z \to \ell^+\ell^-$ ($\ell = e, \mu$) data and simulated samples, and are applied to the simulation to correct for differences. Additional sources of uncertainty originate from the corrections applied to adjust the lepton momentum scale and resolution in the simulation to match those in data, measured using reconstructed distributions of the $Z \to \ell^+\ell^-$ and $J/\psi \to \ell^+\ell^-$ masses, as well as the measured E/p in $W \to e\nu$ events, where E and p are the electron energy and momentum, as measured by the calorimeter and the tracker respectively. The combined effect of all these uncertainties results in an overall normalisation uncertainty on the signal and background of approximately 1.5%.

10.2.2 Jets and missing transverse momentum

Uncertainties associated with jets arise from the efficiency of jet reconstruction and identification based on the JVF variable, as well as the jet energy scale and resolution. The uncertainty associated with the jet reconstruction efficiency is assessed by randomly re-

JHEP08(2015)105

$\geq$6 j, $\geq$4 b, high $M_{bb}^{\min\Delta R}$

	Pre-fit				Post-fit		
	Signal	$t\bar{t}$+light-jets	$t\bar{t}+c\bar{c}$	$t\bar{t}+b\bar{b}$	$t\bar{t}$+light-jets	$t\bar{t}+c\bar{c}$	$t\bar{t}+b\bar{b}$
Luminosity	±2.8	±2.8	±2.8	±2.8	±2.6	±2.6	±2.6
Lepton efficiencies	±1.5	±1.5	±1.5	±1.5	±1.5	±1.4	±1.5
Jet energy scale	±4.4	±15	±11	±12	±8.7	±6.4	±6.7
Jet efficiencies	–	±4.0	±2.2	±1.9	±2.7	±1.5	±1.3
Jet energy resolution	±0.1	±4.4	±3.8	±0.5	±3.1	±2.6	±0.4
b-tagging efficiency	±13	±5.6	±5.4	±9.3	±4.6	±4.6	±6.6
c-tagging efficiency	±1.6	±5.8	±12	±3.1	±5.6	±11	±2.9
Light-jet tagging efficiency	±0.6	±20	±5.7	±2.0	±17	±5.1	±1.8
High-p_{T} tagging efficiency	±4.8	±0.7	±1.7	±1.6	±0.6	±1.3	±1.2
$t\bar{t}$: reweighting	–	±13	±15	–	±10	±10	–
$t\bar{t}$: parton shower	–	±28	±17	±6.2	±13	±11	±4.0
$t\bar{t}$+HF: normalisation	–	–	±50	±50	–	±32	±18
$t\bar{t}$+HF: modelling	–	–	±17	±12	–	±16	±10
Theoretical cross sections	–	±6.3	±6.3	±6.3	±4.6	±4.6	±4.6
Total	±15	±42	±61	±55	±22	±30	±15

Table 7. $T\bar{T} \to Ht$+X search: summary of the systematic uncertainties considered in the ($\geq$6 j, $\geq$4 b, high $M_{bb}^{\min\Delta R}$) channel and their impact (in %) on the normalisation of signal and backgrounds, before and after the fit to data. Only sources of systematic uncertainty resulting in a normalisation change of at least 0.5% are displayed. The signal shown corresponds to a singlet vector-like T quark with mass $m_T = 600$ GeV. The total post-fit uncertainty can be different from the sum in quadrature of individual sources due to the anti-correlations between them resulting from the fit to the data.

moving 0.2% of the jets with p_{T} below 30 GeV, which is the level of disagreement between data and the simulation, and has a negligible impact in the analysis. The per-jet efficiency to satisfy the JVF requirement is measured in $Z(\to \ell^+\ell^-)$+1-jet events in data and simulation, selecting separately events enriched in hard-scatter jets and events enriched in jets from pileup, and good agreement is found. The associated uncertainty is estimated by changing the nominal JVF cut value by ±0.1 and repeating the analysis using the modified cut value, resulting in normalisation uncertainties in the range of 1–5%, depending on the jet multiplicity under consideration and the p_{T} spectra of the jets. The jet energy scale and its uncertainty were derived by combining information from test-beam data, LHC collision data and simulation [54]. The jet energy scale uncertainty is split into 22 uncorrelated sources with their respective jet p_{T} and η dependences and are treated independently in this analysis. It represents one of the leading sources of uncertainty associated with reconstructed objects, affecting the normalisations of signal and backgrounds by approximately 5% and 15% respectively, in the most signal-rich channels considered. The jet energy resolution was measured in data and simulation as a function of jet p_{T} and rapidity using dijet events. They are found to agree within 10%, and the corresponding uncertainty is assessed by smearing the jet p_{T} in the simulation.

JHEP08(2015)105

$\geq$6 j, $\geq$4 b, high $M_{bb}^{\min\Delta R}$

	Pre-fit				Post-fit		
	Signal	$t\bar{t}$+light-jets	$t\bar{t}+c\bar{c}$	$t\bar{t}+b\bar{b}$	$t\bar{t}$+light-jets	$t\bar{t}+c\bar{c}$	$t\bar{t}+b\bar{b}$
Luminosity	±2.8	±2.8	±2.8	±2.8	±2.7	±2.7	±2.7
Lepton efficiencies	±1.6	±1.4	±1.5	±1.7	±1.4	±1.5	±1.6
Jet energy scale	±5.6	±14	±14	±11	±13	±14	±11
Jet efficiencies	±3.1	±3.3	±1.0	±0.9	±3.2	±0.9	±0.8
Jet energy resolution	±0.1	±6.0	±1.1	±1.9	±4.5	±0.9	±1.5
b-tagging efficiency	±16	±7.6	±9.2	±16	±3.9	±5.2	±7.5
c-tagging efficiency	±1.0	±6.1	±15	±3.0	±5.8	±14	±2.8
Light-jet tagging efficiency	–	±19	±6.3	±2.4	±18	±5.8	±2.3
High-p_{T} tagging efficiency	±11	±2.7	±5.3	±5.0	±1.9	±3.8	±3.6
$t\bar{t}$: reweighting	–	±15	±16	–	±14	±15	–
$t\bar{t}$: parton shower	–	±22	±35	±26	±14	±33	±24
$t\bar{t}$+HF: normalisation	–	–	±50	±50	–	±44	±30
$t\bar{t}$+HF: modelling	–	–	±27	±24	–	±28	±21
Theoretical cross sections	–	±6.3	±6.2	±6.3	±5.9	±5.9	±5.9
Total	±21	±38	±73	±65	±24	±46	±27

Table 8. $B\bar{B} \to Hb$+X search: summary of the systematic uncertainties considered in the ($\geq$6 j, $\geq$4 b, high $M_{bb}^{\min\Delta R}$) channel and their impact (in %) on the normalisation of signal and backgrounds, before and after the fit to data. Only sources of systematic uncertainty resulting in a normalisation change of at least 0.5% are displayed. The signal shown corresponds to a vector-like B quark with mass $m_B = 600$ GeV and BR($B \to Hb$) = 1. The total post-fit uncertainty can be different from the sum in quadrature of individual sources due to the anti-correlations between them resulting from the fit to the data.

The $E_{\mathrm{T}}^{\mathrm{miss}}$ reconstruction is affected by uncertainties associated with leptons and jet energy scales and resolutions, which are propagated to $E_{\mathrm{T}}^{\mathrm{miss}}$ and thus are included under the corresponding uncertainty categories in tables 6–8. Additional small uncertainties associated with the modelling of the underlying event, in particular its impact on the p_{T} scale and resolution of unclustered energy, are also taken into account and are displayed in tables 6–8 under the category of "Missing transverse momentum".

10.2.3 Heavy- and light-flavour tagging

Efficiencies to tag jets from b- and c-quarks in the simulation are corrected to match the efficiencies in data by p_{T}-dependent factors in the approximate ranges 0.9–1.0 and 0.9–1.1 respectively, whereas the light-jet efficiency is scaled by p_{T}- and η-dependent scale factors in the range 1.2–1.5 [55, 122]. Uncertainties on these scale factors include a total of six independent sources affecting b-jets and four independent sources affecting c-jets. Each of these uncertainties has different jet p_{T} dependence. Twelve uncertainties are considered for the light-jets tagging, which depend on the jet p_{T} and η regions. These systematic uncertainties are taken as uncorrelated between b-jets, c-jets, and light-jets. An additional uncertainty is included due to the extrapolation of the b-, c-, and light-jet-tagging scale factors for jets with p_{T} beyond the kinematic reach of the data calibration samples used:

JHEP08(2015)105

$p_{\mathrm{T}} > 300$ GeV for b- and c-jets, and $p_{\mathrm{T}} > 750$ GeV for light-jets. This uncertainty is evaluated in the simulation by comparing the tagging efficiencies while varying e.g. the fraction of tracks with shared hits in the silicon detectors or the fraction of fake tracks resulting from random combinations of hits, both of which typically increase at high p_{T} due to growing track multiplicity and density of hits within the jet. These uncertainties are taken to be correlated among the three jet flavours. As an example, the uncertainties on the tagging efficiencies for b-jets and c-jets with 300 GeV $\leq p_{\mathrm{T}} <$ 500 GeV are 14% and 23% respectively.

10.3 Background modelling

10.3.1 $t\bar{t}$+jets

A number of systematic uncertainties affecting the modelling of $t\bar{t}$+jets are considered. These include the uncertainty on the theoretical prediction for the inclusive cross section, uncertainties associated with the reweighting procedure applied to $t\bar{t}$+light-jets and $t\bar{t}+c\bar{c}$ processes, uncertainties affecting the modelling of $t\bar{t}$+HF-jets production, and uncertainties associated with the choice of parton shower and hadronisation model. A summary of these uncertainties can be found below. Additional details can be found in ref. [98].

An uncertainty of $+5\%/-6\%$ is assumed for the inclusive $t\bar{t}$ production cross section [58], including contributions from varying the factorisation and renormalisation scales and uncertainties arising from the PDF, α_{S} and the top quark mass. The PDF and α_{S} uncertainties were calculated using the PDF4LHC prescription.

Uncertainties associated with the reweighting procedure applied to $t\bar{t}$+light-jets and $t\bar{t}+c\bar{c}$ processes include the nine leading sources of uncertainty in the differential cross section measurement at $\sqrt{s} = 7$ TeV [94], dominated by the modelling of initial- and final-state radiation and the choice of event generator for $t\bar{t}$ production.

Uncertainties affecting the modelling of $t\bar{t}+b\bar{b}$ production include those associated with the NLO prediction from Sherpa+OpenLoops, which is used for reweighting of the default Powheg $t\bar{t}+b\bar{b}$ prediction. These include three different scale variations, including changing the functional form of the renormalisation scale, changing the functional form of the factorisation and resummation scales, and varying the renormalisation scale by a factor of two up and down. In addition, a different shower recoil model scheme and two alternative PDF sets (MSTW and NNPDF) are considered. A fraction of the $t\bar{t}+b\bar{b}$ background predicted by Powheg+Pythia originates from multiple parton interactions or final-state radiation from top decay products. Such backgrounds are not part of the NLO prediction, and these two categories are kept separate and subject to additional normalisation uncertainties. The NLO corrections and associated systematic uncertainties are adjusted so that the overall normalisation of the $t\bar{t}+b\bar{b}$ background at the particle level is fixed, i.e. effectively only migrations across categories and distortions to the shape of the kinematic distributions are considered. Detailed comparisons of $t\bar{t}+b\bar{b}$ between Powheg+Pythia and Sherpa+OpenLoops show that the cross sections agree to better than 50%, which is taken as a normalisation uncertainty for $t\bar{t}+b\bar{b}$.

JHEP08(2015)105

Beyond the uncertainties associated with the reweighting procedure, additional uncertainties are assigned to the modelling of the $t\bar{t}+c\bar{c}$ component of the background, which again is not part of the NLO prediction used for $t\bar{t}+b\bar{b}$. These include two uncertainties taken as the full difference between applying and not applying the reweightings of the top quark and $t\bar{t}$ p_{T} spectra. In addition, four uncertainties are considered associated with the choice of LO generator: the full difference between Powheg+Pythia and Madgraph5+Pythia simulations, as well as variations in generator parameters (factorisation and renormalisation scales, matching threshold and c-quark mass), which are derived using Madgraph5+Pythia simulations and applied to the Powheg+Pythia simulation. Analogously to the procedure used in the $t\bar{t}+b\bar{b}$ background estimate, these uncertainties are adjusted so that the overall normalisation of the $t\bar{t}+c\bar{c}$ background at the particle level is fixed. Finally, an overall normalisation uncertainty of 50% is also assigned to the $t\bar{t}+c\bar{c}$ component, taken as uncorrelated with the same normalisation uncertainty applied to $t\bar{t}+b\bar{b}$, since only the $t\bar{t}+b\bar{b}$ process is normalised to a NLO prediction.

An uncertainty due to the choice of parton shower and hadronisation model is derived by comparing events produced by Powheg interfaced to Pythia or Herwig. In the case of $t\bar{t}$+light-jets and $t\bar{t}+c\bar{c}$, a reweighting of the top quark and $t\bar{t}$ p_{T} spectra is also applied to the Powheg+Herwig samples to ensure reliable modelling of the top quark kinematics. The corresponding correction factors were recalculated for Powheg+Herwig in order to match the differential cross section measurements at $\sqrt{s}=7$ TeV. In the case of $t\bar{t}+b\bar{b}$, the various HF categories and the corresponding partonic kinematics in Powheg+Herwig are reweighted to match the NLO prediction of Sherpa+OpenLoops, so that only the effect of changing the hadronisation model is propagated. Given the different effect of this uncertainty on the $t\bar{t}$+light-jets, $t\bar{t}+c\bar{c}$ and $t\bar{t}+b\bar{b}$, it is treated as uncorrelated between the three processes. This treatment prevents an undue reduction of this systematic uncertainty on $t\bar{t}+c\bar{c}$ and $t\bar{t}+b\bar{b}$ by constraining it for $t\bar{t}$+light-jets via the fit to data in the highly populated channels with two b-tagged jets.

10.3.2 W/Z+jets

Uncertainties affecting the modelling of the W/Z+jets background include 5% from their respective normalisations to the theoretical NNLO cross sections [101], as well as an additional 24% normalisation uncertainty added in quadrature for each additional inclusive parton multiplicity bin, based on a comparison among different algorithms for merging LO matrix elements and parton showers [123]. The above uncertainties are taken as uncorrelated between W+jets and Z+jets.

10.3.3 Other simulated background

Uncertainties affecting the modelling of the single-top-quark background include a $+5\%/-4\%$ uncertainty on the total cross section estimated as a weighted average of the theoretical uncertainties on t-, Wt- and s-channel production [105–107], as well as a systematic uncertainty on Wt-channel production concerning the separation between $t\bar{t}$ and Wt at NLO [124]. The latter is estimated by comparing the nominal sample, which uses

JHEP08(2015)105

the so-called "diagram subtraction" scheme, with an alternative sample using the "diagram removal" scheme.

Uncertainties on the diboson background normalisation include 5% from the NLO theoretical cross sections [108] added in quadrature to an uncertainty of 24% due to the extrapolation to the high jet multiplicity channels, following the procedure discussed in section 10.3.2.

Uncertainties on the $t\bar{t}V$ and $t\bar{t}H$ normalisations are 30% and $+9\%/-12\%$ respectively, from the uncertainties on their respective NLO theoretical cross sections [112, 120, 125]. Additional small uncertainties arising from scale variations, which change the amount of initial-state radiation and thus the event kinematics, are also included.

10.3.4 Multijet

Uncertainties on the data-driven multijet background estimate receive contributions from the limited sample size in data, particularly at high jet and b-tag multiplicities, as well as from the uncertainty on the rate of fake leptons, estimated in different control regions (e.g. selected with either an upper $E_{\mathrm{T}}^{\mathrm{miss}}$ or m_{T}^{W} requirement). A combined normalisation uncertainty of 50% due to all these effects is assigned, which is taken as correlated across jet and b-tag multiplicity bins, but uncorrelated between electron and muon channels. No explicit shape uncertainty is assigned since the large statistical uncertainties associated with the multijet background prediction, which are uncorrelated bin-to-bin in the final discriminating variable, effectively cover all possible shape uncertainties.

11 Statistical analysis

For a given search, the distributions of the final discriminating variables in each of the analysis channels considered are combined to test for the presence of a signal. The statistical analysis is based on a binned likelihood function $\mathcal{L}(\mu, \theta)$ constructed as a product of Poisson probability terms over all bins considered in the analysis. This function depends on the signal-strength parameter μ, a multiplicative factor to the theoretical signal production cross section, and θ, a set of nuisance parameters that encode the effect of systematic uncertainties on the signal and background expectations and are implemented in the likelihood function as Gaussian or log-normal priors. Therefore, the total number of expected events in a given bin depends on μ and θ. The nuisance parameters θ allow variations of the expectations for signal and background according to the corresponding systematic uncertainties, and their fitted values correspond to the deviations from the nominal expectations that globally provide the best fit to the data. This procedure allows a reduction of the impact of systematic uncertainties on the search sensitivity by taking advantage of the highly populated background-dominated channels included in the likelihood fit. It requires a good understanding of the systematic effects affecting the shapes of the discriminant distributions. Detailed validation studies of the fitting procedure have been performed using the simulation. To verify the improved background prediction, fits are performed under the background-only hypothesis. Differences between the data and the background prediction

JHEP08(2015)105

are checked relative to the smaller post-fit uncertainties in kinematic variables other than the ones used in the fit.

The test statistic q_μ is defined as the profile likelihood ratio: $q_\mu = -2\ln(\mathcal{L}(\mu, \hat{\hat{\theta}}_\mu)/\mathcal{L}(\hat{\mu}, \hat{\theta}))$, where $\hat{\mu}$ and $\hat{\theta}$ are the values of the parameters that maximise the likelihood function (with the constraint $0 \leq \hat{\mu} \leq \mu$), and $\hat{\hat{\theta}}_\mu$ are the values of the nuisance parameters that maximise the likelihood function for a given value of μ. Statistical uncertainties in each bin of the discriminant distributions are also taken into account via dedicated parameters in the fit. The test statistic q_μ is implemented in the RooFit package [126, 127] and is used to measure the compatibility of the observed data with the background-only hypothesis (i.e. the discovery test) setting $\mu = 0$ in the profile likelihood ratio: $q_0 = -2\ln(\mathcal{L}(0, \hat{\hat{\theta}}_0)/\mathcal{L}(\hat{\mu}, \hat{\theta}))$. The p-value (referred to as p_0) representing the compatibility of the data with the background-only hypothesis is estimated by integrating the distribution of q_0 from background-only pseudo-experiments, approximated using the asymptotic formulae given in ref. [128], above the observed value of q_0. Some model dependence exists in the estimation of the p_0-value, as a given signal scenario needs to be assumed in the calculation of the denominator of q_μ, even if the overall signal normalisation is left floating and fitted to data. The observed p_0-value is checked for each explored signal scenario. In the absence of any significant excess above the background expectation, upper limits on the signal production cross section for each of the signal scenarios considered are derived by using q_μ in the $\mathrm{CL_s}$ method [129, 130]. For a given signal scenario, values of the production cross section (parameterised by μ) yielding $\mathrm{CL_s}<0.05$, where $\mathrm{CL_s}$ is computed using the asymptotic approximation [128], are excluded at $\geq$95% CL.

12 Results

This section presents the results obtained from the searches discussed in sections 7–9, following the statistical analysis discussed in section 11.

12.1 Likelihood fits to data

The consideration of high-statistics background-dominated channels in the analysis allows an improved background prediction with significantly reduced systematic uncertainties to be obtained during the statistical analysis, as discussed in section 11. This is the strategy adopted in the $T\bar{T} \to Ht$+X and $B\bar{B} \to Hb$+X searches. In contrast, the small number of data events in the $T\bar{T} \to Wb$+X search results in virtually the same background prediction and uncertainties both pre-fit and post-fit. Figures 14 and 15 show the comparison of data and the post-fit background prediction for the H_{T} distributions in each of the analysis channels considered in the $T\bar{T} \to Ht$+X search. The corresponding comparisons for the $B\bar{B} \to Hb$+X search can be found in figures 16 and 17. The fit to the data is performed under the background-only hypothesis. Tables with the corresponding predicted and observed yields per channel can be found in appendix A.

Compared to the pre-fit distributions shown in sections 8 and 9, the total background uncertainty is significantly reduced after the fit, not only in the background-dominated channels, but also in the signal-rich channels. The reduced uncertainty results from the

JHEP08(2015)105

significant constraints provided by the data on some systematic uncertainties, as well as the anti-correlations among sources of systematic uncertainty resulting from the fit to the data. For example, the uncertainty in the $t\bar{t} + b\bar{b}$ background in the highest-sensitivity channel ($\geq$6 j, $\geq$4 b, high $M_{bb}^{\min\Delta R}$) is reduced from about 60% prior to the fit to about 15% and 30% in the $T\bar{T} \to Ht$+X and the $B\bar{B} \to Hb$+X searches, respectively. The larger post-fit uncertainty in the case of the $B\bar{B} \to Hb$+X search is partly caused by the smaller number of data events due to the selection requirements being tighter than in the $T\bar{T} \to Ht$+X search.

12.2 Limits on $T\bar{T}$ production

The compatibility of the data with the background prediction is assessed by computing the p_0-value for each signal scenario considered, defined by the assumed values for the heavy quark mass (see section 5.1) and the three decay branching ratios, which are varied in steps of 0.05 requiring that they add up to unity. In the case of the $T\bar{T} \to Wb$+X search alone, the smallest p_0-value found, 0.023, is obtained for $m_T = 600$ GeV, BR($T \to Wb$) = 0.30 and BR($T \to Ht$) = 0.65 [BR($T \to Zt$) = 1 − BR($T \to Wb$) − BR($T \to Ht$) = 0.05], and corresponds to a local significance of 2.0 standard deviations above the background-only prediction. In the case of the $T\bar{T} \to Ht$+X search, the smallest p_0-value found, 0.44, is obtained for $m_T = 600$ GeV, BR($T \to Wb$) = 0.0, BR($T \to Ht$) = 0.0, and BR($T \to Zt$) = 1.0, and corresponds to a local significance of 0.2 standard deviations above the background-only prediction. Thus, no significant excess above the background expectation is found in either of the two searches.

Since the two searches have complementary sensitivity to different decay modes of a vector-like T quark, they are combined in a single likelihood function taking into account the correlation of systematic uncertainties. Upper limits at 95% CL on the $T\bar{T}$ production cross section are set in several benchmark scenarios as a function of the T quark mass m_T and are compared to the theoretical prediction from Top++, as shown in figure 18. The resulting lower limits on m_T correspond to the central value of the theoretical cross section. The scenarios considered involve different assumptions on the decay branching ratios: BR($T \to Wb$) = 1, singlet and doublet. Only the $T\bar{T} \to Wb$+X search is sensitive to a T quark with BR($T \to Wb$) = 1, yielding an observed (expected) 95% CL lower limit of $m_T > 770\,(795)$ GeV. This represents the most stringent limit to date, and is also applicable to a Y vector-like quark with electric charge of $-4/3$ and decaying into a W^- boson and a b quark. Both searches are sensitive to a vector-like singlet T quark. The $T\bar{T} \to Wb$+X and $T\bar{T} \to Ht$+X searches yield observed (expected) 95% CL limits of $m_T > 660\,(670)$ GeV and $m_T > 765\,(720)$ GeV respectively. The combination of both analyses results in a slight improvement over the $T\bar{T} \to Ht$+X search alone, yielding $m_T > 800\,(755)$ GeV. Finally, only the $T\bar{T} \to Ht$+X search is sensitive to a vector-like doublet T quark, yielding an observed (expected) 95% CL lower limit of $m_T > 855\,(820)$ GeV.

The same searches are used to derive exclusion limits on vector-like T quark production for different values of m_T and as a function of BR($T \to Wb$) and BR($T \to Ht$). To probe this branching ratio plane, the signal samples are reweighted by the ratio of the desired branching ratio to the original branching ratio in Protos, and the complete analysis is

JHEP08(2015)105

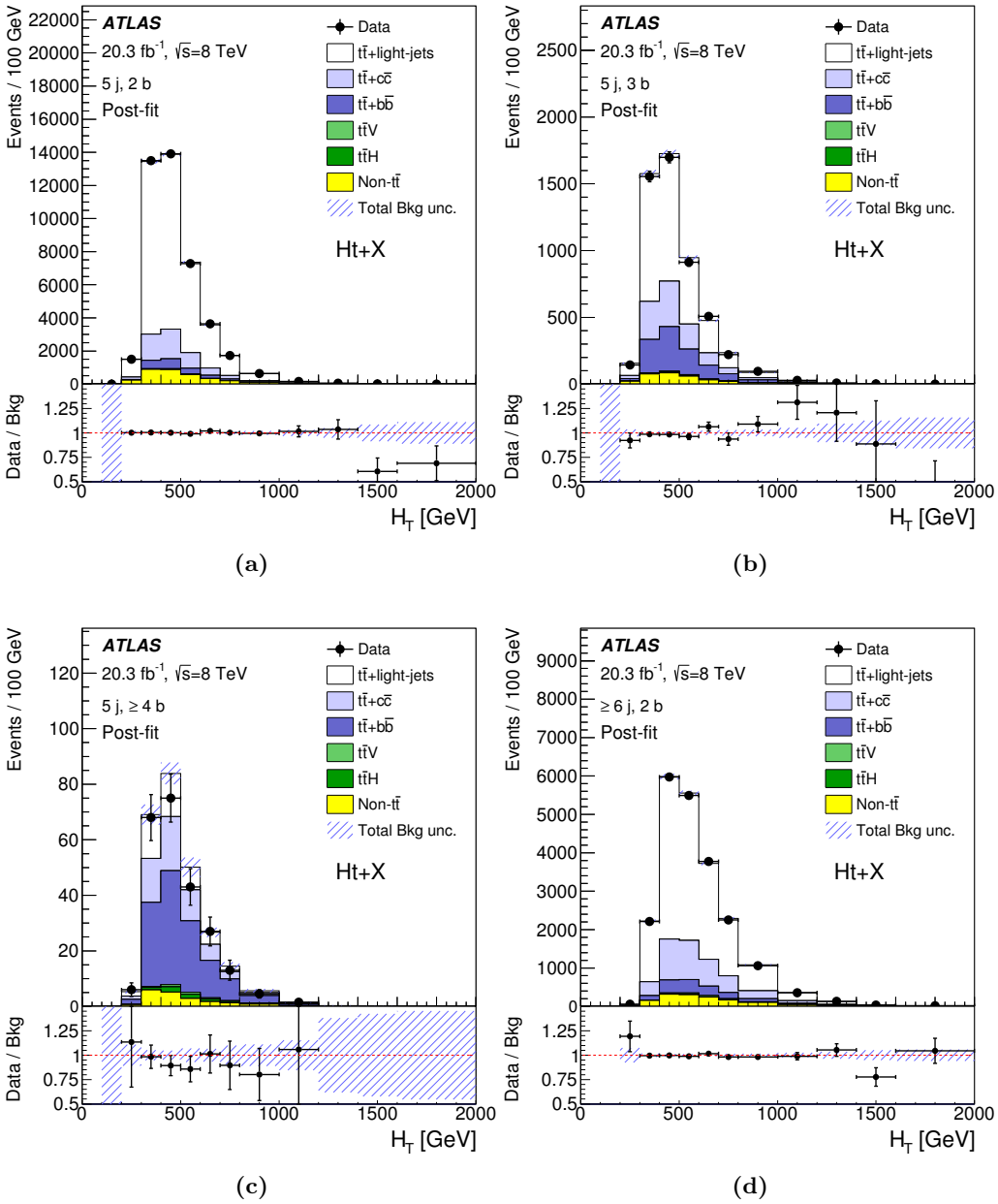

Figure 14. $T\bar{T} \to Ht$+X search: comparison between data and prediction for the distribution of the scalar sum (H_{T}) of the transverse momenta of the lepton, the selected jets and the missing transverse momentum in each of the analysed channels after final selection: (a) (5 j, 2 b), (b) (5 j, 3 b), (c) (5 j, ≥4 b), and (d) (≥6 j, 2 b). The background prediction is shown after the fit to data under the background-only hypothesis. The small contributions from W/Z+jets, single top, diboson and multijet backgrounds are combined into a single background source referred to as "Non-$t\bar{t}$". The last bin in all figures contains the overflow. The bottom panel displays the ratio of data to the total background prediction. The hashed area represents the total uncertainty on the background.

JHEP08(2015)105

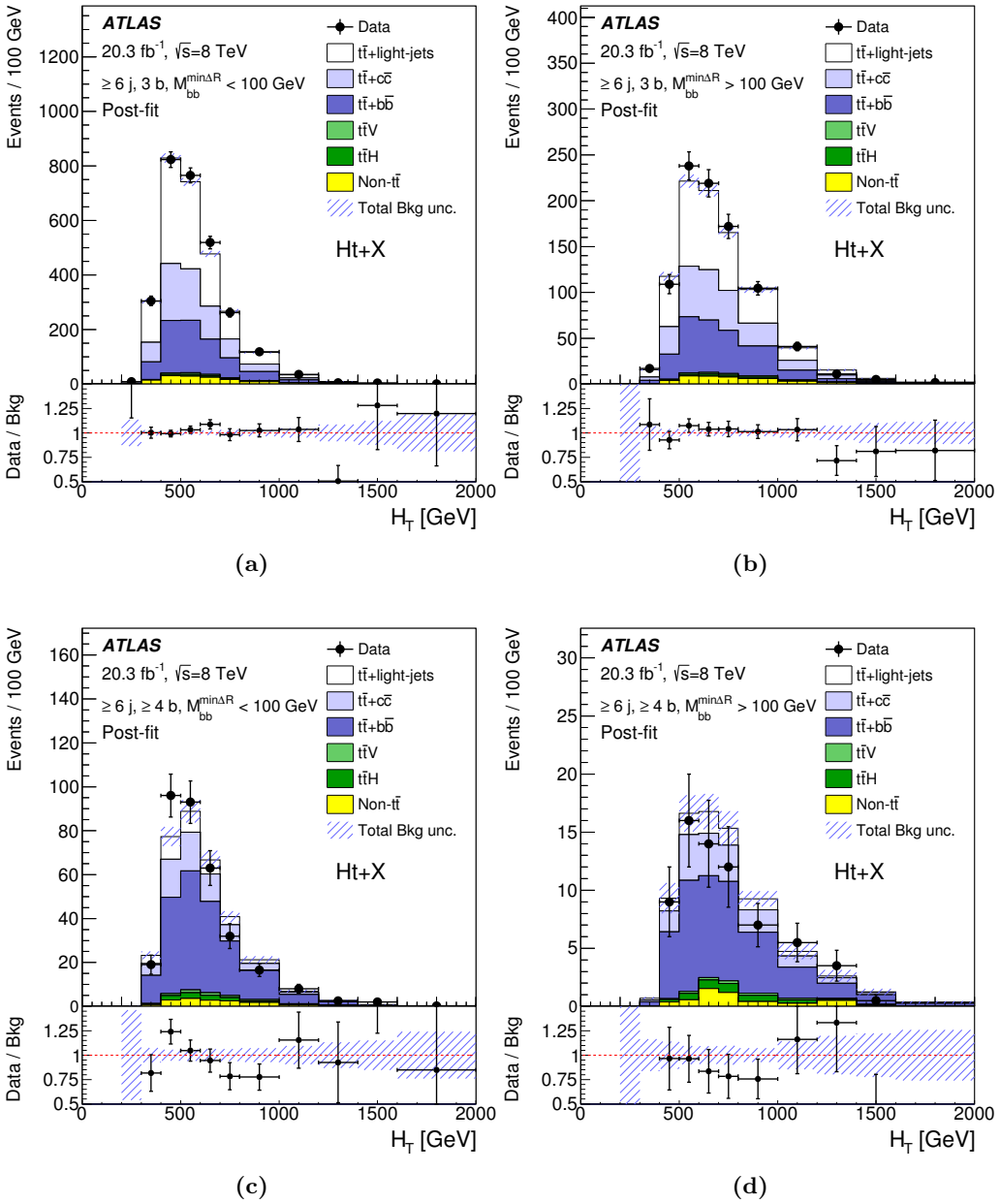

Figure 15. $T\bar{T} \to Ht$+X search: comparison between data and prediction for the distribution of the scalar sum (H_{T}) of the transverse momenta of the lepton, the selected jets and the missing transverse momentum in each of the analysed channels after final selection: (a) (≥6 j, 3 b, low $M_{bb}^{\mathrm{min}\Delta R}$), (b) (≥6 j, 3 b, high $M_{bb}^{\mathrm{min}\Delta R}$), (c) (≥6 j, ≥4 b, low $M_{bb}^{\mathrm{min}\Delta R}$), and (d) (≥6 j, ≥4 b, high $M_{bb}^{\mathrm{min}\Delta R}$). The background prediction is shown after the fit to data under the background-only hypothesis. The small contributions from W/Z+jets, single top, diboson and multijet backgrounds are combined into a single background source referred to as "Non-$t\bar{t}$". The last bin in all figures contains the overflow. The bottom panel displays the ratio of data to the total background prediction. The hashed area represents the total uncertainty on the background.

JHEP08(2015)105

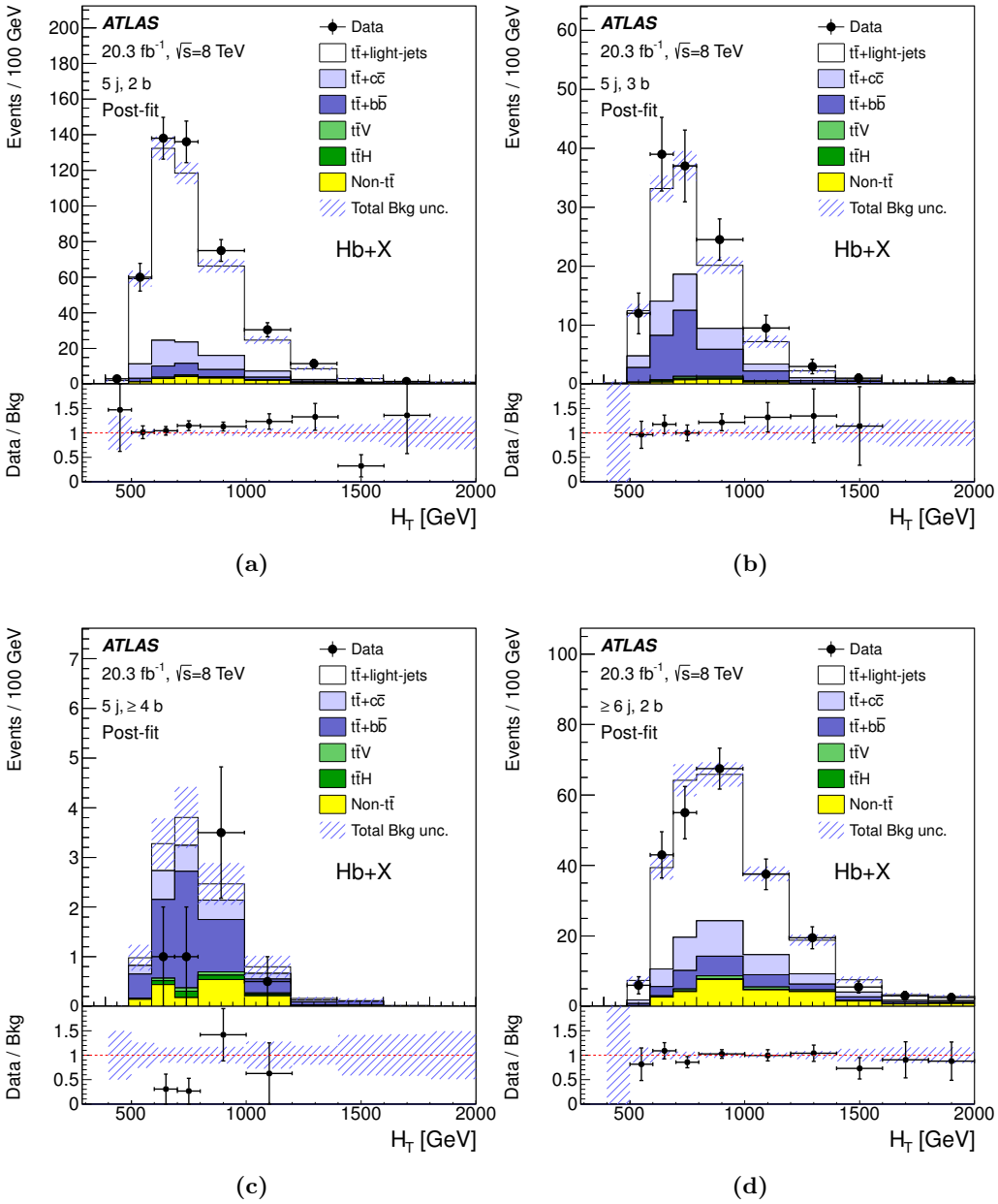

Figure 16. $B\bar{B} \to Hb$+X search: comparison between data and prediction for the distribution of the scalar sum (H_{T}) of the transverse momenta of the lepton, the selected jets and the missing transverse momentum in each of the analysed channels after final selection: (a) (5 j, 2 b), (b) (5 j, 3 b), (c) (5 j, ≥4 b), and (d) (≥6 j, 2 b). The background prediction is shown after the fit to data under the background-only hypothesis. The small contributions from W/Z+jets, single top, diboson and multijet backgrounds are combined into a single background source referred to as "Non-$t\bar{t}$". The last bin in all figures contains the overflow. The bottom panel displays the ratio of data to the total background prediction. The hashed area represents the total uncertainty on the background.

JHEP08(2015)105

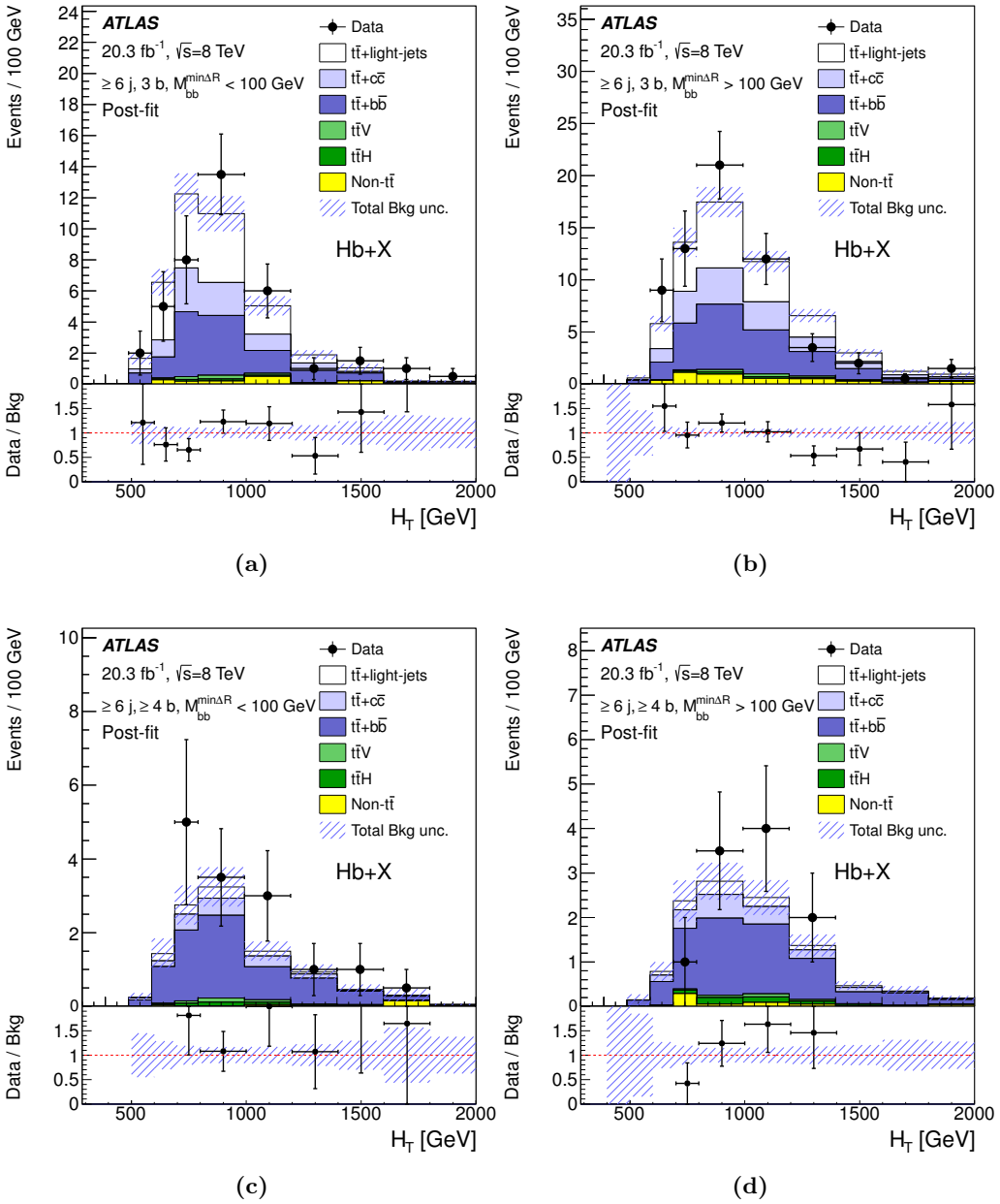

Figure 17. $B\bar{B} \to Hb$+X search: comparison between data and prediction for the distribution of the scalar sum (H_{T}) of the transverse momenta of the lepton, the selected jets and the missing transverse momentum in each of the analysed channels after final selection: (a) (≥6 j, 3 b, low $M_{bb}^{\mathrm{min}\Delta R}$), (b) (≥6 j, 3 b, high $M_{bb}^{\mathrm{min}\Delta R}$), (c) (≥6 j, ≥4 b, low $M_{bb}^{\mathrm{min}\Delta R}$), and (d) (≥6 j, ≥4 b, high $M_{bb}^{\mathrm{min}\Delta R}$). The background prediction is shown after the fit to data under the background-only hypothesis. The small contributions from W/Z+jets, single top, diboson and multijet backgrounds are combined into a single background source referred to as "Non-$t\bar{t}$". The last bin in all figures contains the overflow. The bottom panel displays the ratio of data to the total background prediction. The hashed area represents the total uncertainty on the background.

JHEP08(2015)105

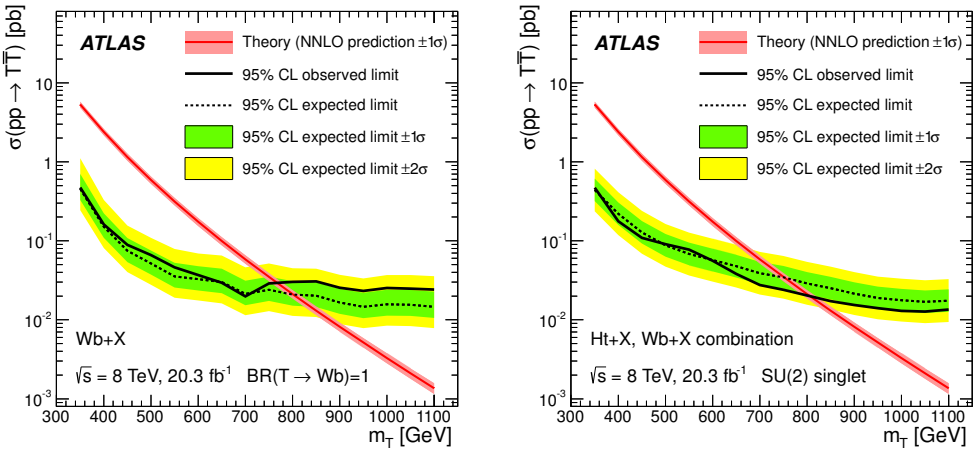

(a)

(b)

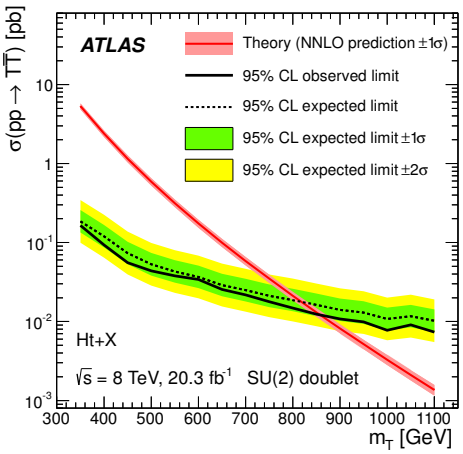

(c)

Figure 18. Observed (solid line) and expected (dashed line) 95% CL upper limits on the $T\bar{T}$ cross section as a function of the T quark mass (a) under the assumption $\mathrm{BR}(T \to Wb) = 1$, (b) for a T quark singlet, and (c) for a T quark doublet. The surrounding shaded bands correspond to ± 1 and ± 2 standard deviations around the expected limit. The thin red line and band show the theoretical prediction and its ± 1 standard deviation uncertainty.

repeated. The resulting 95% CL exclusion limits are shown in figure 19 for the combination of the $T\bar{T} \to Wb$+X and $T\bar{T} \to Ht$+X searches, for different values of m_T. Figure 20 presents the corresponding observed and expected T quark mass limits in the plane of $\mathrm{BR}(T \to Ht)$ versus $\mathrm{BR}(T \to Wb)$, obtained by linear interpolation of the estimated $\mathrm{CL_s}$ versus m_T.

The combined results set observed lower limits on the T quark mass ranging between 715 GeV and 950 GeV for all possible values of the branching ratios into the three decay modes. This implies that any branching ratio scenario is excluded at 95% CL for a T

JHEP08(2015)105

quark with mass below 715 GeV. The corresponding range of expected lower limits is between 675 GeV and 885 GeV. The exclusion limits for the individual searches can be found in appendix B. These figures illustrate the complementarity of these searches and how their combination improves over simply taking the most sensitive search for each assumed branching ratio scenario, leading to large regions in the branching ratio plane being excluded.

In addition to the combined $T\bar{T} \to Wb$+X and $T\bar{T} \to Ht$+X result discussed in this paper, the ATLAS Collaboration has performed searches for $T\bar{T}$ production in several multilepton final states: same-sign dileptons and trileptons [27] and opposite-sign dileptons and trileptons with a Z boson candidate [25] (referred to as the Zb/t+X search). These searches have overlapping selections and have not been combined. Figure 21 summarises the most restrictive observed and expected T quark mass limits in the plane of BR($T \to Ht$) versus BR($T \to Wb$), set by any of these searches. The observed lower limits on the T quark mass range between 730 GeV and 950 GeV for all possible values of the branching ratios into the three decay modes, representing an improvement over previous results [28]. The corresponding range of expected lower limits is between 715 GeV and 885 GeV.

12.3 Limits on $B\bar{B}$ production

In the case of the $B\bar{B} \to Hb$+X search, the smallest p_0-value found, 0.023, is obtained for $m_B = 450$ GeV, BR($B \to Wt$) = 0.0 and BR($B \to Hb$) = 0.3 [BR($B \to Zb$) = 1 − BR($B \to Wt$) − BR($B \to Hb$) = 0.7), and corresponds to a local significance of 2.0 standard deviations above the background-only prediction.

Upper limits at 95% CL on the $B\bar{B}$ production cross section are set for two benchmark scenarios as a function of the B quark mass, as shown in figure 22. Assuming BR($B \to Hb$) = 1, the intervals $350 < m_B < 580$ GeV and $635 < m_B < 700$ GeV are excluded at 95% CL. The expected exclusion is $m_B > 625$ GeV at 95% CL. For branching ratios corresponding to a B singlet, the observed (expected) 95% CL limit is $m_B > 735\,(635)$ GeV. Exclusion limits are set for values of m_B and as a function of BR($B \to Wt$) and BR($B \to Hb$), shown in figure 23. The search is particularly sensitive at large BR($B \to Hb$), and also at large BR($B \to Wt$). Figure 24 presents the corresponding observed and expected B quark mass limits in the plane of BR($B \to Hb$) versus BR($B \to Wt$).

Beyond the $B\bar{B} \to Hb$+X search presented in this paper, which focuses on the $B \to Hb$ decay, the ATLAS Collaboration has performed several other searches for $B\bar{B}$ production that are complementary to each other. A search in the lepton-plus-jets final state [26], referred to as $B\bar{B} \to Wt$+X, and the search in same-sign dilepton and multilepton events [27], probe primarily the $B \to Wt$ decay mode. The Zb/t+X search [25] is most sensitive to $B \to Zb$ production. Figure 25 summarises the most restrictive observed and expected B quark mass limits in the plane of BR($B \to Hb$) versus BR($B \to Wt$), set by any of these searches. The observed lower limits on the B quark mass range between 575 GeV and 813 GeV for all possible values of the branching ratios into the three decay modes. The corresponding range of expected lower limits is between 615 GeV and 800 GeV.

JHEP08(2015)105

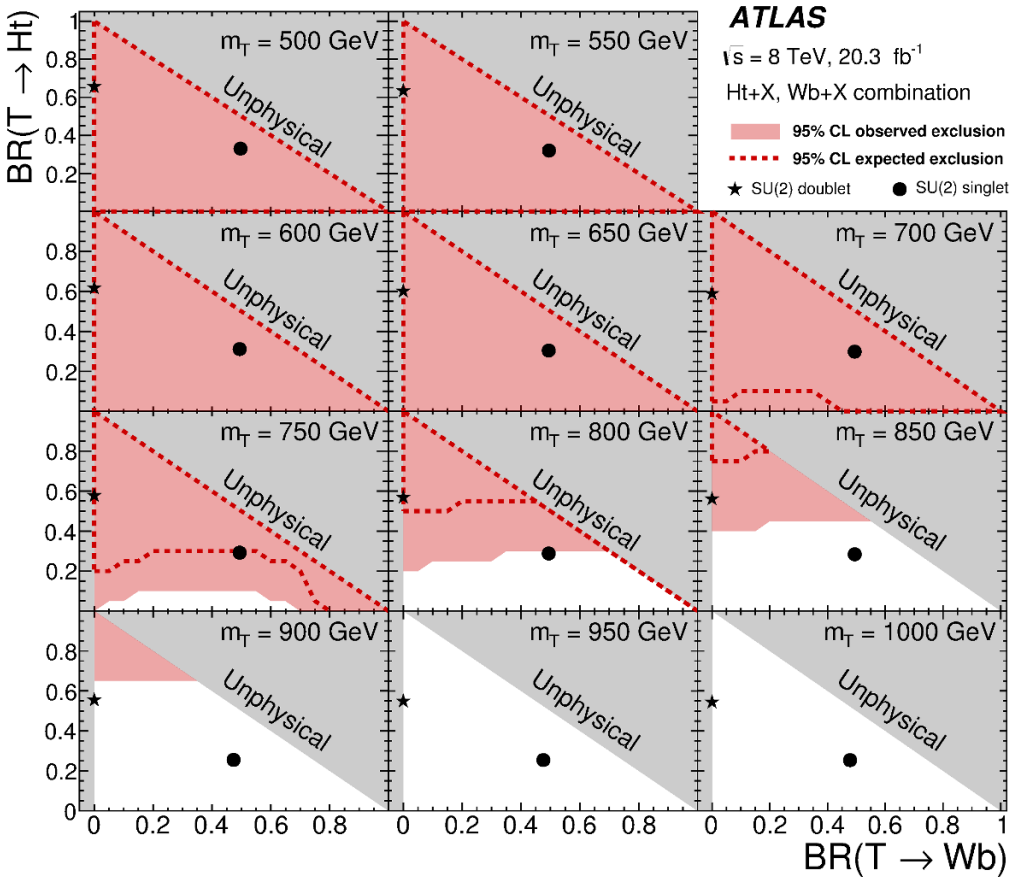

Figure 19. Observed (red filled area) and expected (red dashed line) 95% CL exclusion in the plane of BR($T \to Wb$) versus BR($T \to Ht$) from the combination of the $T\bar{T} \to Wb$+X and $T\bar{T} \to Ht$+X searches, for different values of the vector-like T quark mass. The grey (dark shaded) area corresponds to the unphysical region where the sum of branching ratios exceeds unity. The default branching ratio values from the PROTOS event generator for the weak-isospin singlet and doublet cases are shown as plain circle and star symbols respectively.

12.4 Limits on $t\bar{t}t\bar{t}$ production

The Ht+X analysis is also used to set limits on four-top-quark production considering different signal benchmark scenarios: SM-like $t\bar{t}t\bar{t}$, $t\bar{t}t\bar{t}$ via an EFT model with a four-top-quark contact interaction, sgluon pair production with decay into $t\bar{t}$, and $t\bar{t}t\bar{t}$+X via the 2UED/RPP model. Except for the case of SM-like $t\bar{t}t\bar{t}$ production, for which the ATLAS multilepton search [27] achieves the best expected sensitivity, in all other benchmark scenarios this analysis achieves the most restrictive expected bounds.

In the case of $t\bar{t}t\bar{t}$ production with the SM kinematics, the observed (expected) 95% CL upper limit on the production cross section is 23 fb (32 fb), or 34 (47) times the SM prediction. In this scenario the expected sensitivity of this analysis is comparable to that of previous searches [27, 42]. In the case of $t\bar{t}t\bar{t}$ production via an EFT model, the observed (expected) 95% CL upper limit on the production cross section is 12 fb (16 fb). The improved sensitivity in the case of the EFT model results from the harder H_{T} spectrum

JHEP08(2015)105

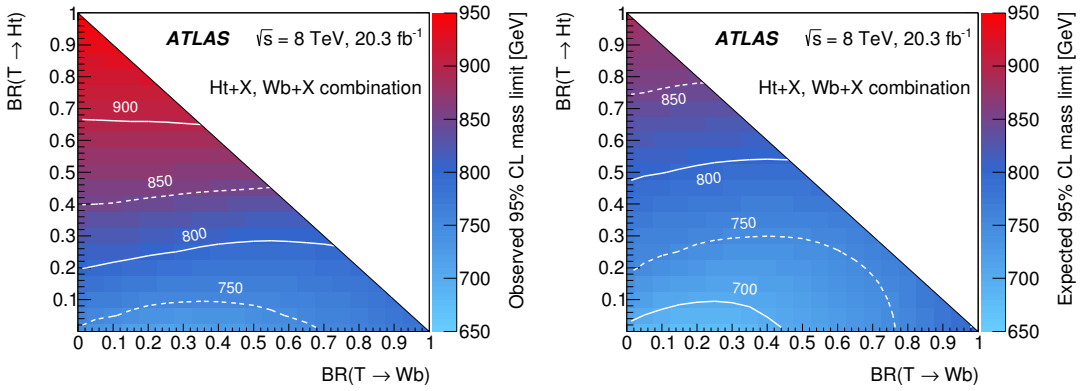

(a) (b)

Figure 20. (a) Observed and (b) expected limit (95% CL) on the mass of the T quark in the plane of BR($T \to Ht$) versus BR($T \to Wb$) for the combination of the $T\bar{T} \to Wb$+X and $T\bar{T} \to Ht$+X searches. Contour lines are provided to guide the eye.

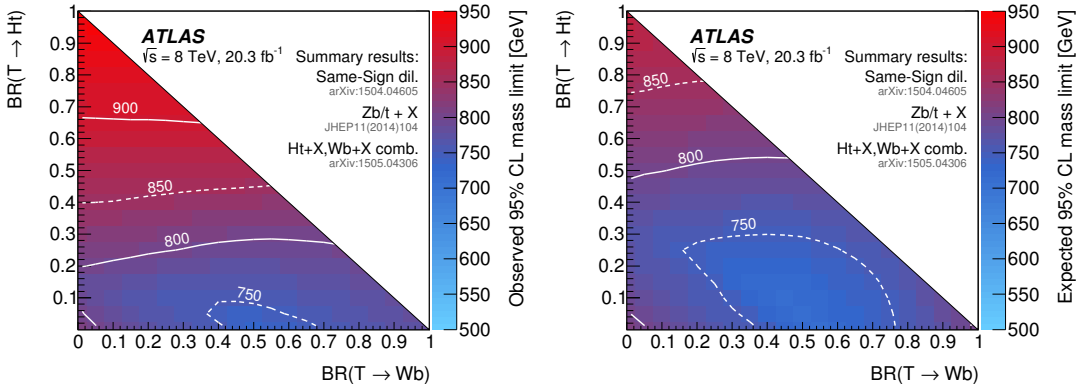

(a) (b)

Figure 21. Summary of the most restrictive (a) observed and (b) expected limit (95% CL) on the mass of the T quark in the plane of BR($T \to Ht$) versus BR($T \to Wb$) from all ATLAS searches for $T\bar{T}$ production (see text for details). Contour lines are provided to guide the eye.

compared to that of SM $t\bar{t}t\bar{t}$ production. The upper limit on the production cross section can be translated into an observed (expected) limit on the free parameter of the model, $|C_{4t}|/\Lambda^2 < 6.6$ TeV^{-2} (7.7 TeV^{-2}).

The resulting observed and expected upper limits on the sgluon pair production cross section times branching ratio are shown in figure 26 as a function of the sgluon mass and are compared to the theoretical prediction. The observed (expected) 95% CL limit on the sgluon mass is 1.06 TeV (1.02 TeV).

Finally, in the context of the 2UED/RPP model, the observed and expected upper limits on the production cross section times branching ratio are shown in figure 27 as a function of m_{KK} for the symmetric case ($\xi = R_4/R_5 = 1$), assuming production by tier

JHEP08(2015)105

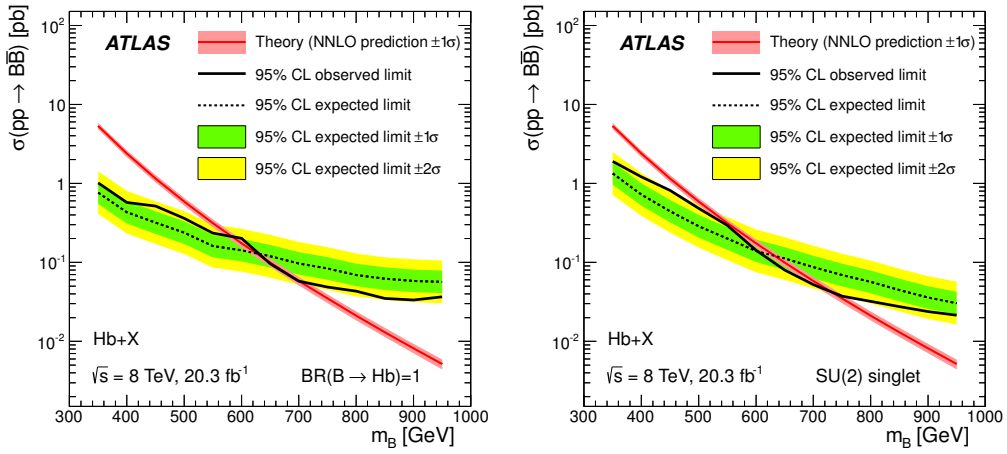

(a) **(b)**

Figure 22. Observed (solid line) and expected (dashed line) 95% CL upper limits on the $B\bar{B}$ cross section as a function of the B quark mass (a) under the assumption BR($B \to Hb$) = 1 and (b) for a B quark singlet. The surrounding shaded bands correspond to ±1 and ±2 standard deviations around the expected limit. The thin red line and band show the theoretical prediction and its ±1 standard deviation uncertainty.

(1,1) alone. The comparison to the LO theoretical cross section translates into an observed (expected) 95% CL limit on m_{KK} of 1.12 TeV (1.10 TeV). Four-top-quark events can also arise from tiers (2,0) and (0,2). In those tiers the theoretical production cross sections can be calculated, leading to more robust results (i.e. there is no need to assume a particular branching ratio). The dependence of the tier kinematics on the tier mass also allows the extrapolation of constraints on tier (1,1) to tiers (2,0) and (0,2). Excluding a given production cross section for tier (1,1) at a given m_{KK} is equivalent to excluding this production cross section for tier (2,0) alone at $m_{\mathrm{KK}}/\sqrt{2}$ and for tier (0,2) at $m_{\mathrm{KK}}/\sqrt{2}\xi$. The contribution of tier (0,2) vanishes as ξ increases (highly asymmetric case). Figure 28 presents the observed and expected upper limits on the production cross section times branching ratio as function of m_{KK} for two scenarios: tiers (2,0)+(0,2) alone in the symmetric case, and tier (2,0) alone in the highly asymmetric case. In both cases a branching ratio of $A^{(1,1)} \to t\bar{t}$ of 0% is assumed. The corresponding observed (expected) 95% CL limits on m_{KK} are 0.61 TeV (0.60 TeV) and 0.57 TeV (0.55 TeV) respectively.

JHEP08(2015)105

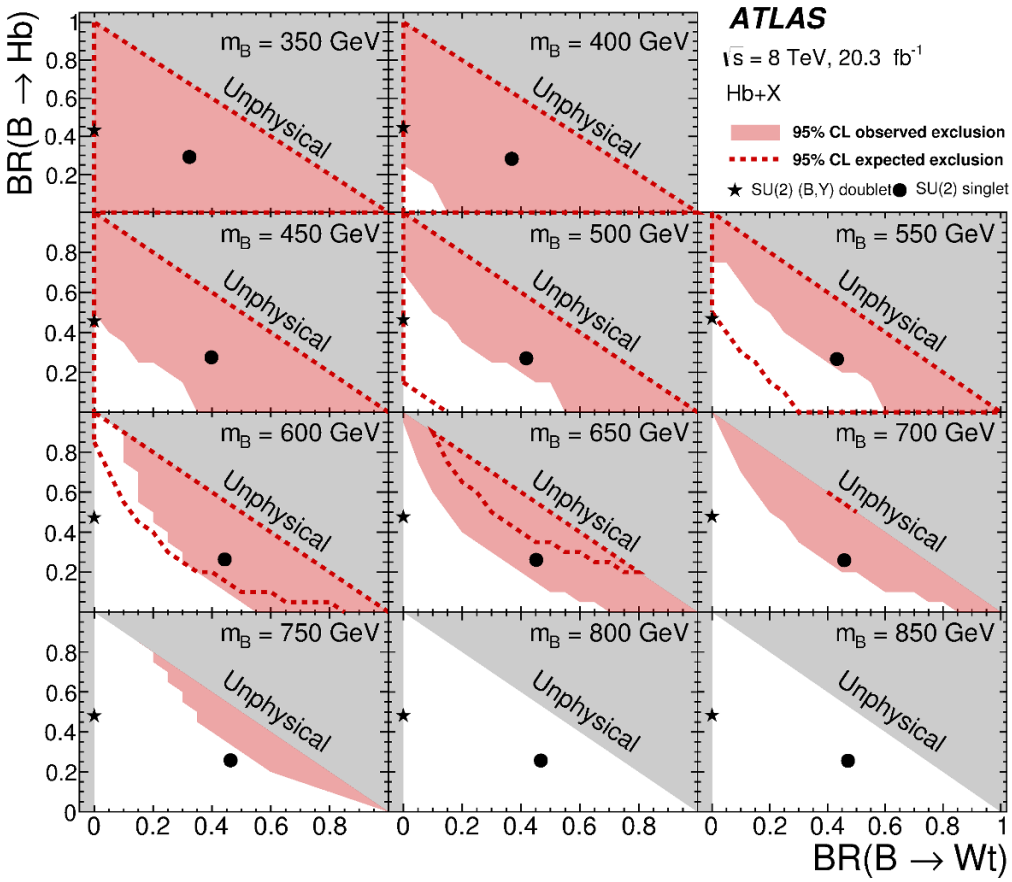

Figure 23. Observed (red filled area) and expected (red dashed line) 95% CL exclusion in the plane of BR($B \to Wt$) versus BR($B \to Hb$) from the $B\bar{B} \to Hb$+X search, for different values of the vector-like B quark mass. The grey (dark shaded) area corresponds to the unphysical region where the sum of branching ratios exceeds unity. The default branching ratio values from the PROTOS event generator for the weak-isospin singlet and (B,Y) doublet cases are shown as plain circle and star symbols respectively.

JHEP08(2015)105

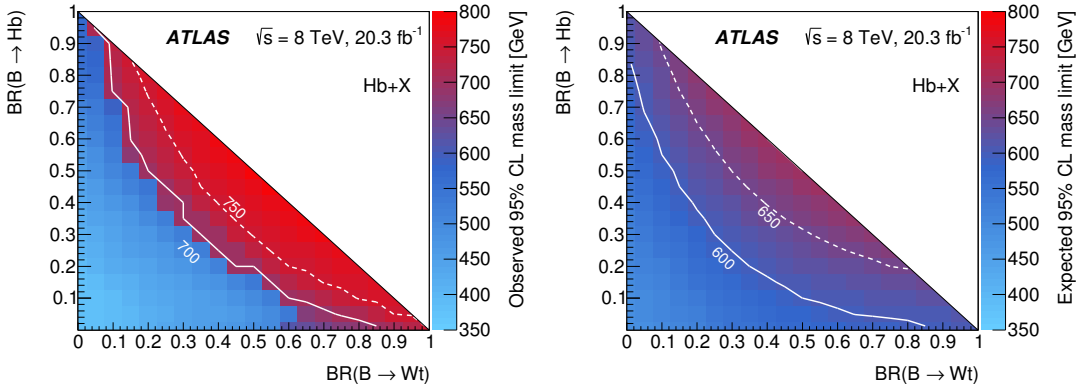

(a) (b)

Figure 24. (a) Observed and (b) expected limit (95% CL) on the mass of the B quark in the plane of BR($B \to Hb$) versus BR($B \to Wt$) for the $B\bar{B} \to Hb$+X search. Contour lines are provided to guide the eye.

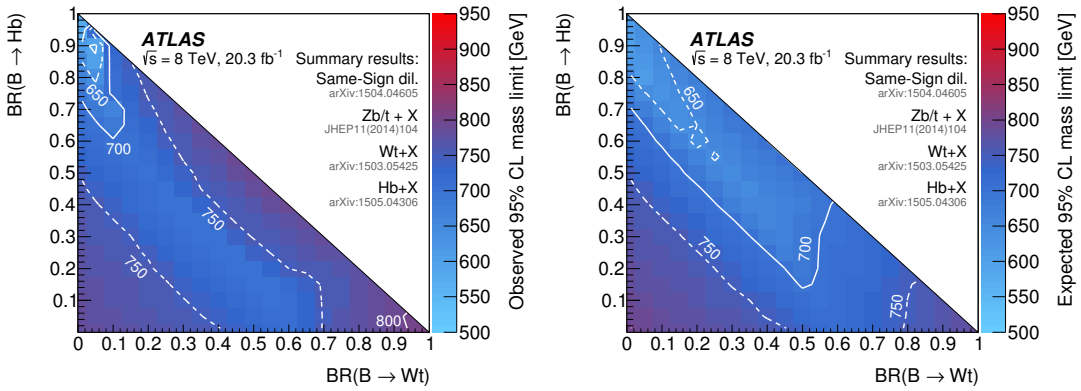

(a) (b)

Figure 25. Summary of the most restrictive (a) observed and (b) expected limit (95% CL) on the mass of the B quark in the plane of BR($B \to Hb$) versus BR($B \to Wt$) from all ATLAS searches for $B\bar{B}$ production (see text for details). Contour lines are provided to guide the eye.

JHEP08(2015)105

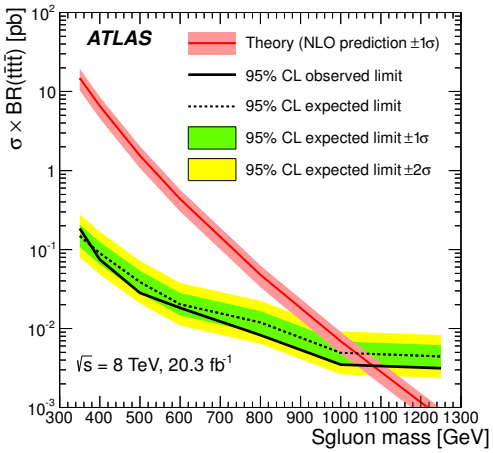

Figure 26. Observed (solid line) and expected (dashed line) 95% CL upper limits on the sgluon pair production cross section times branching ratio as a function of the sgluon mass. The surrounding shaded bands correspond to ±1 and ±2 standard deviations around the expected limit. The thin red line and band show the theoretical prediction and its ±1 standard deviation uncertainty.

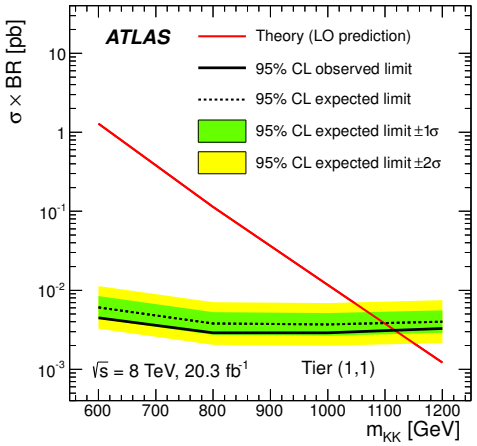

Figure 27. Observed (solid line) and expected (dashed line) 95% CL upper limits on the production cross section times branching ratio of four-top-quark events as a function of the Kaluza-Klein mass (m_{KK}) from tier (1,1) in the symmetric case. The surrounding shaded bands correspond to ±1 and ±2 standard deviations around the expected limit. The thin red line shows the theoretical prediction for the production cross section of four-top-quark events by tier (1,1) assuming $\mathrm{BR}(A^{(1,1)} \to t\bar{t}) = 1$, where $A^{(1,1)}$ is the lightest particle of this tier.

JHEP08(2015)105

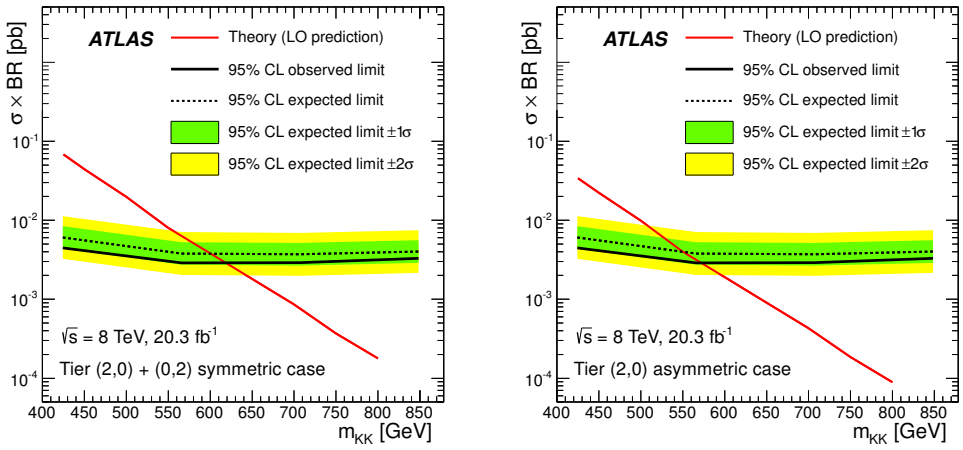

(a) **(b)**

Figure 28. Observed (solid line) and expected (dashed line) 95% CL upper limits on the production cross section times branching ratio of four-top-quark events as a function of the Kaluza-Klein mass (m_{KK}) from (a) tiers (2,0)+(0,2) alone in the symmetric case and (b) tier (2,0) alone in the highly asymmetric case. The surrounding shaded bands correspond to ± 1 and ± 2 standard deviations around the expected limit. The thin red line shows the theoretical prediction for the production cross section of four-top-quark events.

JHEP08(2015)105

13 Conclusion

A search for pair production of vector-like quarks, both up-type (T) and down-type (B), as well as four-top-quark production has been performed using pp collision data at $\sqrt{s} = 8$ TeV corresponding to an integrated luminosity of $20.3\,\text{fb}^{-1}$ recorded with the ATLAS detector at the CERN Large Hadron Collider. The final states considered have an isolated electron or muon with high transverse momentum, large missing transverse momentum and at least four jets. Three different analyses are optimised to reach the best sensitivity to the decay channels $T\bar{T} \to Wb$+X, $T\bar{T} \to Ht$+X and $B\bar{B} \to Hb$+X.

No significant deviation from the Standard Model expectation is observed and lower limits on the masses of the vector-like T (B) quark are derived as a function of the branching ratios BR($T \to Wb$), BR($T \to Zt$), and BR($T \to Ht$) (respectively BR($B \to Wt$), BR($B \to Zb$), and BR($B \to Hb$)). The combination of the $T\bar{T} \to Wb$+X, $T\bar{T} \to Ht$+X analyses yields observed lower limits on the T quark mass ranging between 715 GeV and 950 GeV for all possible values of the branching ratios into three decay modes, and are the most stringent constraints to date. The $B\bar{B} \to Hb$+X analysis is the first search to target specifically this decay mode and leads to an observed lower limit on the B quark mass of 580 GeV for BR($B \to Hb$) = 1. Finally, a summary of all ATLAS vector-like quark pair production searches is given. For $B\bar{B}$ production, the observed lower limits on the B quark mass range between 575 GeV and 813 GeV for all possible values of the branching ratios into the three decay modes.

The $T\bar{T} \to Ht$+X analysis is also used to set limits on four-top-quark production, both in the Standard Model and in several new physics scenarios, including a four-fermion contact interaction, sgluon pair production and a universal extra dimensions model. In the case of Standard Model production, a cross section larger than 23 fb is excluded at the 95% CL. The most restrictive limits to date are obtained for four-top-quark production in the various new physics scenarios considered.

Acknowledgments

We thank CERN for the very successful operation of the LHC, as well as the support staff from our institutions without whom ATLAS could not be operated efficiently.

We acknowledge the support of ANPCyT, Argentina; YerPhI, Armenia; ARC, Australia; BMWFW and FWF, Austria; ANAS, Azerbaijan; SSTC, Belarus; CNPq and FAPESP, Brazil; NSERC, NRC and CFI, Canada; CERN; CONICYT, Chile; CAS, MOST and NSFC, China; COLCIENCIAS, Colombia; MSMT CR, MPO CR and VSC CR, Czech Republic; DNRF, DNSRC and Lundbeck Foundation, Denmark; EPLANET, ERC and NSRF, European Union; IN2P3-CNRS, CEA-DSM/IRFU, France; GNSF, Georgia; BMBF, DFG, HGF, MPG and AvH Foundation, Germany; GSRT and NSRF, Greece; RGC, Hong Kong SAR, China; ISF, MINERVA, GIF, I-CORE and Benoziyo Center, Israel; INFN, Italy; MEXT and JSPS, Japan; CNRST, Morocco; FOM and NWO, Netherlands; BRF and RCN, Norway; MNiSW and NCN, Poland; GRICES and FCT, Portugal; MNE/IFA, Romania; MES of Russia and NRC KI, Russian Federation; JINR; MSTD,

JHEP08(2015)105

Serbia; MSSR, Slovakia; ARRS and MIZŠ, Slovenia; DST/NRF, South Africa; MINECO, Spain; SRC and Wallenberg Foundation, Sweden; SER, SNSF and Cantons of Bern and Geneva, Switzerland; NSC, Taiwan; TAEK, Turkey; STFC, the Royal Society and Leverhulme Trust, United Kingdom; DOE and NSF, United States of America.

The crucial computing support from all WLCG partners is acknowledged gratefully, in particular from CERN and the ATLAS Tier-1 facilities at TRIUMF (Canada), NDGF (Denmark, Norway, Sweden), CC-IN2P3 (France), KIT/GridKA (Germany), INFN-CNAF (Italy), NL-T1 (Netherlands), PIC (Spain), ASGC (Taiwan), RAL (U.K.) and BNL (U.S.A.) and in the Tier-2 facilities worldwide.

JHEP08(2015)105

A Post-fit event yields

Table 9 presents the observed and predicted background yields in each of the analysis channels for the $T\bar{T} \to Ht$+X search, after the fit to the data under the background-only hypothesis. The corresponding observed and predicted yields for the $B\bar{B} \to Hb$+X search are summarised in table 10.

	5 j, 2 b	5 j, 3 b	5 j, ≥4 b	≥6 j, 2 b
$t\bar{t}$+light-jets	32200 ± 1500	2940 ± 220	49.1 ± 8.8	16000 ± 1000
$t\bar{t} + c\bar{c}$	5600 ± 1700	1000 ± 310	61 ± 17	4300 ± 1300
$t\bar{t} + b\bar{b}$	1820 ± 360	990 ± 180	124 ± 19	1440 ± 280
$t\bar{t}V$	139 ± 44	25.0 ± 7.9	3.1 ± 1.0	164 ± 52
$t\bar{t}H$	39.8 ± 1.4	22.0 ± 1.2	6.1 ± 0.5	58.7 ± 2.9
W+jets	1200 ± 580	86 ± 41	4.3 ± 2.0	560 ± 280
Z+jets	390 ± 120	27.6 ± 8.7	1.6 ± 0.5	190 ± 60
Single top	1600 ± 260	172 ± 31	7.1 ± 0.8	710 ± 150
Diboson	88 ± 27	7.7 ± 2.6	0.4 ± 0.2	43 ± 13
Multijet	125 ± 40	31 ± 10	6.4 ± 2.2	52 ± 16
Total background	43240 ± 320	5360 ± 79	263 ± 10	23100 ± 240
Data	43319	5309	244	23001

	≥6 j, 3 b low $M_{bb}^{\min\Delta R}$	≥6 j, 3 b high $M_{bb}^{\min\Delta R}$	≥6 j, ≥4 b low $M_{bb}^{\min\Delta R}$	≥6 j, ≥4 b high $M_{bb}^{\min\Delta R}$
$t\bar{t}$+light-jets	1260 ± 130	421 ± 43	38.3 ± 8.1	9.5 ± 2.1
$t\bar{t} + c\bar{c}$	760 ± 210	278 ± 79	72 ± 20	20.4 ± 6.2
$t\bar{t} + b\bar{b}$	730 ± 120	285 ± 51	211 ± 29	52.0 ± 7.9
$t\bar{t}V$	28.1 ± 8.9	12.3 ± 3.9	6.3 ± 2.0	1.5 ± 0.5
$t\bar{t}H$	25.0 ± 1.3	11.7 ± 0.9	11.1 ± 0.9	4.2 ± 0.4
W+jets	50 ± 25	12.0 ± 6.1	5.4 ± 2.9	0.4 ± 0.2
Z+jets	16.8 ± 5.5	3.3 ± 1.2	1.6 ± 0.5	0.3 ± 0.1
Single top	76 ± 17	33 ± 10	11.3 ± 3.2	2.8 ± 1.5
Diboson	4.3 ± 1.5	1.4 ± 0.5	0.4 ± 0.1	0.2 ± 0.1
Multijet	1.7 ± 0.7	4.3 ± 1.8	< 0.01	2.6 ± 0.8
Total background	2948 ± 54	1062 ± 25	357 ± 16	93.9 ± 5.0
Data	3015	1085	362	84

Table 9. $T\bar{T} \to Ht$+X search: predicted and observed yields in each of the analysis channels considered. The background prediction is shown after the fit to data under the background-only hypothesis. The quoted uncertainties are the sum in quadrature of statistical and systematic uncertainties on the yields, computed taking into account correlations among nuisance parameters and among processes.

JHEP08(2015)105

	5 j, 2 b	5 j, 3 b	5 j, ≥4 b	≥6 j, 2 b
$t\bar{t}$+light-jets	406 ± 35	77.8 ± 8.8	2.3 ± 0.5	239 ± 26
$t\bar{t} + c\bar{c}$	60 ± 31	25 ± 11	2.4 ± 1.1	58 ± 26
$t\bar{t} + b\bar{b}$	28 ± 10	35.4 ± 9.3	7.4 ± 1.9	33 ± 11
$t\bar{t}V$	4.2 ± 1.3	1.7 ± 0.5	0.3 ± 0.1	5.1 ± 1.6
$t\bar{t}H$	1.0 ± 0.1	1.2 ± 0.1	0.5 ± 0.1	1.5 ± 0.2
W+jets	23 ± 12	3.9 ± 2.0	0.8 ± 0.5	13.9 ± 7.5
Z+jets	7.2 ± 2.7	2.0 ± 2.2	0.6 ± 0.5	4.0 ± 3.1
Single top	41.5 ± 4.9	9.1 ± 1.2	0.6 ± 0.1	26.8 ± 4.2
Diboson	1.9 ± 0.8	0.5 ± 0.3	0.05 ± 0.05	1.2 ± 0.6
Multijet	< 0.01	< 0.01	0.3 ± 0.2	0.18 ± 0.01
Total background	573 ± 20	156.3 ± 8.5	15.2 ± 1.9	383 ± 16
Data	576	165	10	375

	≥6 j, 3 b low $M_{bb}^{\min\Delta R}$	≥6 j, 3 b high $M_{bb}^{\min\Delta R}$	≥6 j, ≥4 b low $M_{bb}^{\min\Delta R}$	≥6 j, ≥4 b high $M_{bb}^{\min\Delta R}$
$t\bar{t}$+light-jets	23.4 ± 4.5	34.6 ± 4.9	1.5 ± 0.3	1.6 ± 0.4
$t\bar{t} + c\bar{c}$	12.0 ± 5.2	22 ± 10	2.5 ± 1.2	3.1 ± 1.4
$t\bar{t} + b\bar{b}$	19.6 ± 6.2	36 ± 11	11.8 ± 3.0	11.8 ± 3.1
$t\bar{t}V$	1.2 ± 0.4	1.7 ± 0.5	0.6 ± 0.2	0.4 ± 0.1
$t\bar{t}H$	0.7 ± 0.1	1.4 ± 0.2	0.5 ± 0.1	0.9 ± 0.1
W+jets	2.3 ± 1.3	1.3 ± 0.8	0.5 ± 0.5	0.07 ± 0.06
Z+jets	0.1 ± 0.1	0.2 ± 0.1	< 0.01	< 0.01
Single top	3.1 ± 0.4	4.7 ± 1.4	0.8 ± 0.1	0.4 ± 0.2
Diboson	0.2 ± 0.1	0.10 ± 0.03	0.02 ± 0.01	0.01 ± 0.01
Multijet	< 0.01	0.6 ± 0.2	< 0.01	0.4 ± 0.1
Total background	62.6 ± 5.3	101.9 ± 7.3	18.3 ± 2.6	18.6 ± 2.6
Data	62	103	23	20

Table 10. $B\bar{B} \to Hb$+X search: predicted and observed yields in each of the analysis channels considered. The background prediction is shown after the fit to data under the background-only hypothesis. The quoted uncertainties are the sum in quadrature of statistical and systematic uncertainties on the yields, computed taking into account correlations among nuisance parameters and among processes.

JHEP08(2015)105

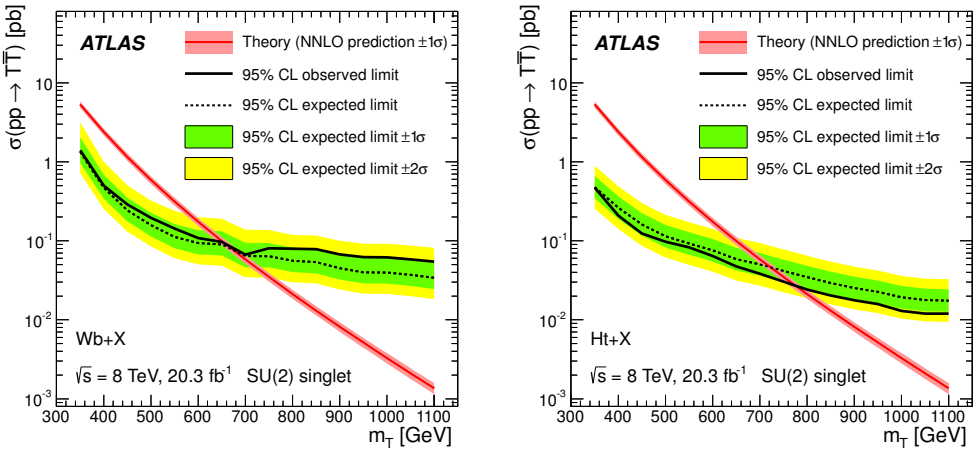

(a) **(b)**

Figure 29. Observed (solid line) and expected (dashed line) 95% CL upper limits on the $T\bar{T}$ cross section for a vector-like singlet T quark as a function of the T quark mass from (a) the $T\bar{T} \to Wb$+X search and (b) $T\bar{T} \to Ht$+X search. The surrounding shaded bands correspond to ± 1 and ± 2 standard deviations around the expected limit. The thin red line and band show the theoretical prediction and its ± 1 standard deviation uncertainty.

B Limits on $T\bar{T}$ production from individual searches

Figure 29 shows 95% CL upper limits on the $T\bar{T}$ production cross section as a function of the T quark mass obtained by the individual $T\bar{T} \to Wb$+X and $T\bar{T} \to Ht$+X searches for the singlet scenario. The $T\bar{T} \to Wb$+X and $T\bar{T} \to Ht$+X searches yield observed (expected) 95% CL limits of $m_T > 660\,(665)$ GeV and $m_T > 765\,(720)$ GeV respectively. Figure 30 shows the 95% CL exclusion limits on vector-like T quark production, for different values of m_T and as a function of the two branching ratios BR($T \to Wb$) and BR($T \to Ht$), obtained by the $T\bar{T} \to Wb$+X search. Figure 31(a,b) present the corresponding expected and observed T quark mass limits respectively, in the plane of BR($T \to Ht$) versus BR($T \to Wb$). The exclusion limits obtained by the $T\bar{T} \to Ht$+X search can be found in figures 32 and 33. The $T\bar{T} \to Wb$+X search sets observed (expected) lower limits on the T quark mass ranging between 350 GeV and 760 GeV (350 GeV and 800 GeV) for all possible values of the branching ratios into the three decay modes. The $T\bar{T} \to Ht$+X search sets observed (expected) lower limits on the T quark mass ranging between 510 GeV and 950 GeV (505 GeV and 885 GeV) for all possible values of the branching ratios into the three decay modes.

JHEP08(2015)105

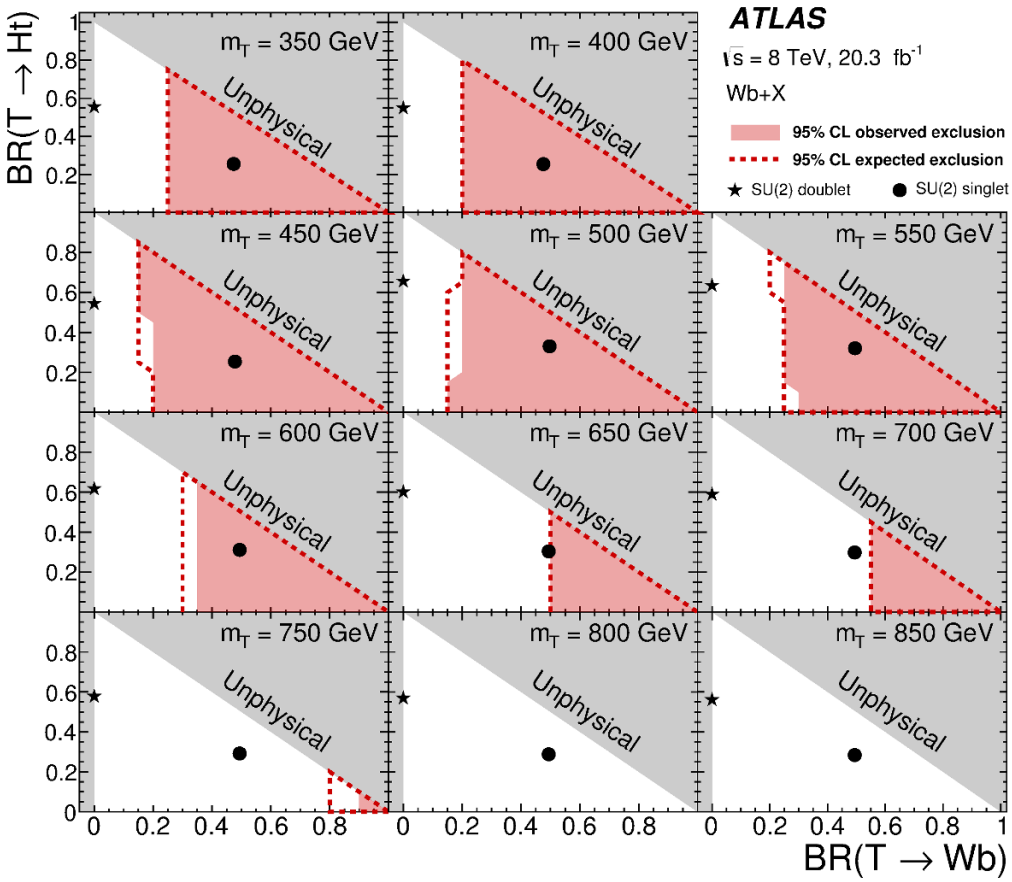

Figure 30. Observed (red filled area) and expected (red dashed line) 95% CL exclusion in the plane of BR($T \to Wb$) versus BR($T \to Ht$) for the $T\bar{T} \to Wb$+X search, for different values of the vector-like T quark mass. The grey (dark shaded) area corresponds to the unphysical region where the sum of branching ratios exceeds unity. The default branching ratio values from the PROTOS event generator for the weak-isospin singlet and doublet cases are shown as plain circle and star symbols respectively.

JHEP08(2015)105

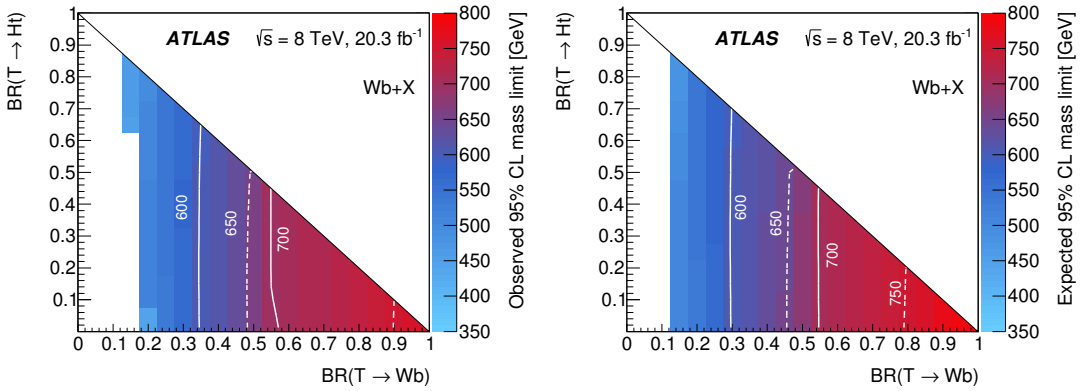

(a) **(b)**

Figure 31. (a) Observed and (b) expected limit (95% CL) on the mass of the T quark in the plane of BR($T \to Ht$) versus BR($T \to Wb$) for the $T\bar{T} \to Wb$+X search. Contour lines are provided to guide the eye. The region shown in white is not excluded for any values of the T quark mass probed.

JHEP08(2015)105

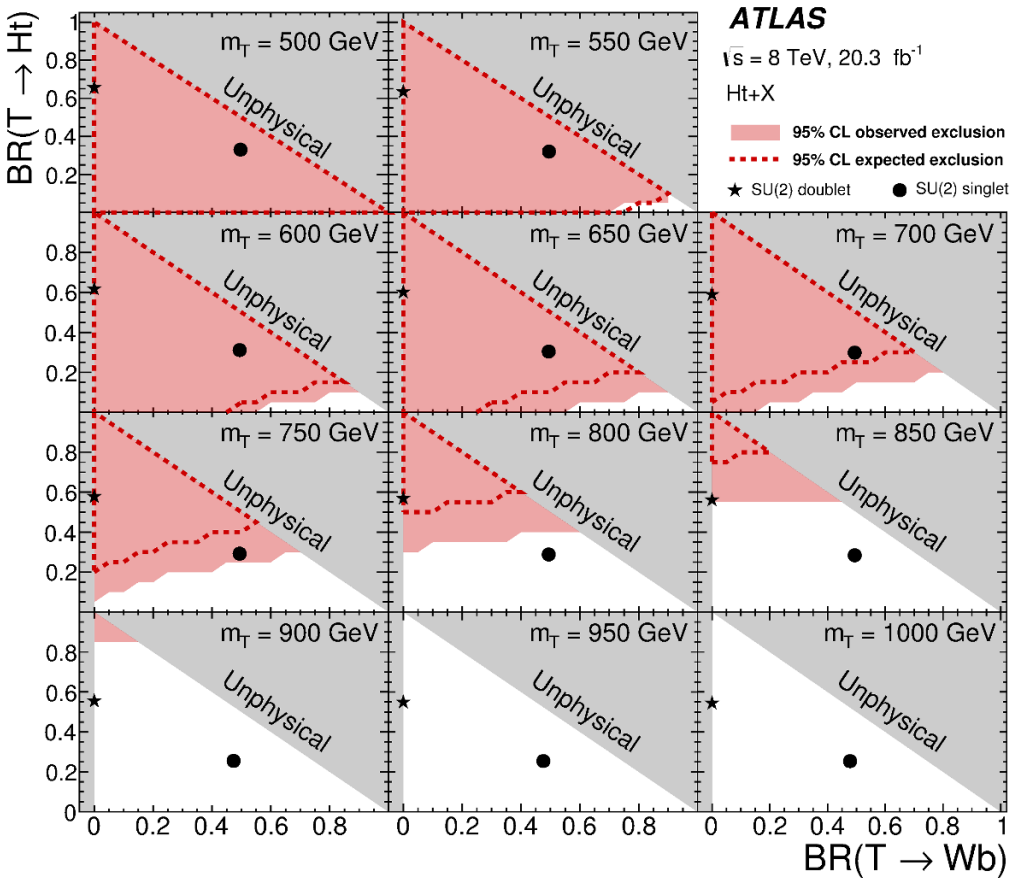

Figure 32. Observed (red filled area) and expected (red dashed line) 95% CL exclusion in the plane of BR($T \to Wb$) versus BR($T \to Ht$) for the $T\bar{T} \to Ht$+X search, for different values of the vector-like T quark mass. The grey (dark shaded) area corresponds to the unphysical region where the sum of branching ratios exceeds unity. The default branching ratio values from the PROTOS event generator for the weak-isospin singlet and doublet cases are shown as plain circle and star symbols respectively.

JHEP08(2015)105

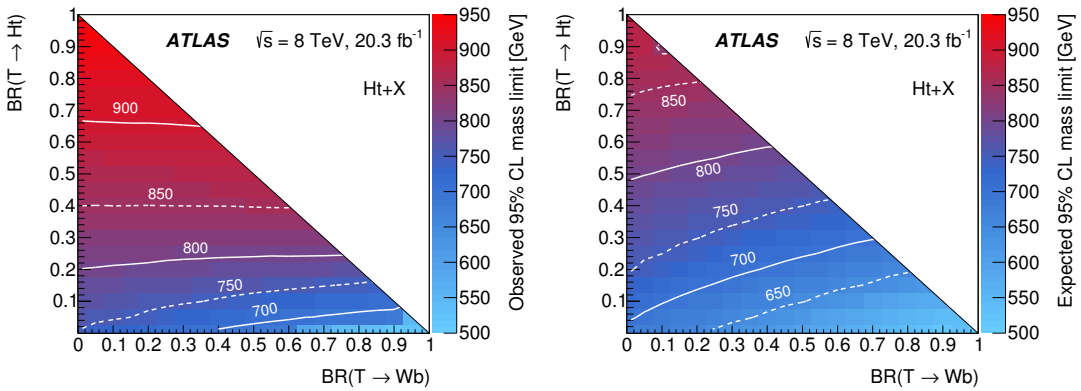

(a) **(b)**

Figure 33. (a) Observed and (b) expected limit (95% CL) on the mass of the T quark in the plane of BR($T \to Ht$) versus BR($T \to Wb$) for the $T\bar{T} \to Ht$+X search. Contour lines are provided to guide the eye.

JHEP08(2015)105

Open Access. This article is distributed under the terms of the Creative Commons Attribution License (CC-BY 4.0), which permits any use, distribution and reproduction in any medium, provided the original author(s) and source are credited.

References

[1] ATLAS collaboration, *Observation of a new particle in the search for the Standard Model Higgs boson with the ATLAS detector at the LHC*, *Phys. Lett.* **B 716** (2012) 1 [arXiv:1207.7214] [INSPIRE].

[2] CMS collaboration, *Observation of a new boson at a mass of 125 GeV with the CMS experiment at the LHC*, *Phys. Lett.* **B 716** (2012) 30 [arXiv:1207.7235] [INSPIRE].

[3] L. Susskind, *Dynamics of Spontaneous Symmetry Breaking in the Weinberg-Salam Theory*, *Phys. Rev.* **D 20** (1979) 2619 [INSPIRE].

[4] N. Arkani-Hamed, A.G. Cohen, E. Katz and A.E. Nelson, *The Littlest Higgs*, *JHEP* **07** (2002) 034 [hep-ph/0206021] [INSPIRE].

[5] M. Schmaltz and D. Tucker-Smith, *Little Higgs review*, *Ann. Rev. Nucl. Part. Sci.* **55** (2005) 229 [hep-ph/0502182] [INSPIRE].

[6] D.B. Kaplan, H. Georgi and S. Dimopoulos, *Composite Higgs Scalars*, *Phys. Lett.* **B 136** (1984) 187 [INSPIRE].

[7] K. Agashe, R. Contino and A. Pomarol, *The minimal composite Higgs model*, *Nucl. Phys.* **B 719** (2005) 165 [hep-ph/0412089] [INSPIRE].

[8] C.T. Hill and E.H. Simmons, *Strong dynamics and electroweak symmetry breaking*, *Phys. Rept.* **381** (2003) 235 [*Erratum ibid.* **390** (2004) 553] [hep-ph/0203079] [INSPIRE].

[9] F. del Aguila and M.J. Bowick, *The Possibility of New Fermions With $\Delta I = 0$ Mass*, *Nucl. Phys.* **B 224** (1983) 107 [INSPIRE].

[10] J.A. Aguilar-Saavedra, *Identifying top partners at LHC*, *JHEP* **11** (2009) 030 [arXiv:0907.3155] [INSPIRE].

[11] J.A. Aguilar-Saavedra, *Mixing with vector-like quarks: constraints and expectations*, *EPJ Web Conf.* **60** (2013) 16012 [arXiv:1306.4432] [INSPIRE].

[12] J.A. Aguilar-Saavedra, R. Benbrik, S. Heinemeyer and M. Pérez-Victoria, *Handbook of vectorlike quarks: Mixing and single production*, *Phys. Rev.* **D 88** (2013) 094010 [arXiv:1306.0572] [INSPIRE].

[13] A. Atre, M. Carena, T. Han and J. Santiago, *Heavy Quarks Above the Top at the Tevatron*, *Phys. Rev.* **D 79** (2009) 054018 [arXiv:0806.3966] [INSPIRE].

[14] A. Atre et al., *Model-Independent Searches for New Quarks at the LHC*, *JHEP* **08** (2011) 080 [arXiv:1102.1987] [INSPIRE].

[15] ATLAS collaboration, *Search for pair production of a heavy up-type quark decaying to a W boson and a b quark in the lepton+jets channel with the ATLAS detector*, *Phys. Rev. Lett.* **108** (2012) 261802 [arXiv:1202.3076] [INSPIRE].

[16] ATLAS collaboration, *Search for pair-produced heavy quarks decaying to Wq in the two-lepton channel at $\sqrt{s} = 7$ TeV with the ATLAS detector*, *Phys. Rev.* **D 86** (2012) 012007 [arXiv:1202.3389] [INSPIRE].

JHEP08(2015)105

[17] CMS collaboration, *Search for pair produced fourth-generation up-type quarks in pp collisions at $\sqrt{s} = 7$ TeV with a lepton in the final state*, *Phys. Lett.* **B 718** (2012) 307 [arXiv:1209.0471] [INSPIRE].

[18] CMS collaboration, *Search for heavy, top-like quark pair production in the dilepton final state in pp collisions at $\sqrt{s} = 7$ TeV*, *Phys. Lett.* **B 716** (2012) 103 [arXiv:1203.5410] [INSPIRE].

[19] ATLAS collaboration, *Search for pair production of a new quark that decays to a Z boson and a bottom quark with the ATLAS detector*, *Phys. Rev. Lett.* **109** (2012) 071801 [arXiv:1204.1265] [INSPIRE].

[20] CMS collaboration, *Search for heavy quarks decaying into a top quark and a W or Z boson using lepton + jets events in pp collisions at $\sqrt{s} = 7$ TeV*, *JHEP* **01** (2013) 154 [arXiv:1210.7471] [INSPIRE].

[21] CMS collaboration, *Search for a Vector-like Quark with Charge 2/3 in t + Z Events from pp Collisions at $\sqrt{s} = 7$ TeV*, *Phys. Rev. Lett.* **107** (2011) 271802 [arXiv:1109.4985] [INSPIRE].

[22] ATLAS collaboration, *Search for down-type fourth generation quarks with the ATLAS detector in events with one lepton and hadronically decaying W bosons*, *Phys. Rev. Lett.* **109** (2012) 032001 [arXiv:1202.6540] [INSPIRE].

[23] CMS collaboration, *Search for heavy bottom-like quarks in 4.9 inverse femtobarns of pp collisions at $\sqrt{s} = 7$ TeV*, *JHEP* **05** (2012) 123 [arXiv:1204.1088] [INSPIRE].

[24] ATLAS collaboration, *Search for pair production of heavy top-like quarks decaying to a high-p_{T} W boson and a b quark in the lepton plus jets final state at $\sqrt{s} = 7$ TeV with the ATLAS detector*, *Phys. Lett.* **B 718** (2013) 1284 [arXiv:1210.5468] [INSPIRE].

[25] ATLAS collaboration, *Search for pair and single production of new heavy quarks that decay to a Z boson and a third-generation quark in pp collisions at $\sqrt{s} = 8$ TeV with the ATLAS detector*, *JHEP* **11** (2014) 104 [arXiv:1409.5500] [INSPIRE].

[26] ATLAS collaboration, *Search for vectorlike B quarks in events with one isolated lepton, missing transverse momentum and jets at $\sqrt{s} = 8$ TeV with the ATLAS detector*, *Phys. Rev.* **D 91** (2015) 112011 [arXiv:1503.05425] [INSPIRE].

[27] ATLAS collaboration, *Analysis of events with b-jets and a pair of leptons of the same charge in pp collisions at $\sqrt{s} = 8$ TeV with the ATLAS detector*, arXiv:1504.04605 [INSPIRE].

[28] CMS collaboration, *Inclusive search for a vector-like T quark with charge $\frac{2}{3}$ in pp collisions at $\sqrt{s} = 8$ TeV*, *Phys. Lett.* **B 729** (2014) 149 [arXiv:1311.7667] [INSPIRE].

[29] A. Pomarol and J. Serra, *Top Quark Compositeness: Feasibility and Implications*, *Phys. Rev.* **D 78** (2008) 074026 [arXiv:0806.3247] [INSPIRE].

[30] B. Lillie, J. Shu and T.M.P. Tait, *Top Compositeness at the Tevatron and LHC*, *JHEP* **04** (2008) 087 [arXiv:0712.3057] [INSPIRE].

[31] K. Kumar, T.M.P. Tait and R. Vega-Morales, *Manifestations of Top Compositeness at Colliders*, *JHEP* **05** (2009) 022 [arXiv:0901.3808] [INSPIRE].

[32] M. Guchait, F. Mahmoudi and K. Sridhar, *Associated production of a Kaluza-Klein excitation of a gluon with a $t\bar{t}$ pair at the LHC*, *Phys. Lett.* **B 666** (2008) 347 [arXiv:0710.2234] [INSPIRE].

[33] T. Plehn and T.M.P. Tait, *Seeking Sgluons*, *J. Phys.* **G 36** (2009) 075001 [arXiv:0810.3919] [INSPIRE].

JHEP08(2015)105

[34] S.Y. Choi, M. Drees, J. Kalinowski, J.M. Kim, E. Popenda and P.M. Zerwas, *Color-Octet Scalars of $N = 2$ Supersymmetry at the LHC*, *Phys. Lett.* **B 672** (2009) 246 [arXiv:0812.3586] [INSPIRE].

[35] C. Kilic, T. Okui and R. Sundrum, *Vectorlike Confinement at the LHC*, *JHEP* **02** (2010) 018 [arXiv:0906.0577] [INSPIRE].

[36] C. Kilic, T. Okui and R. Sundrum, *Colored Resonances at the Tevatron: Phenomenology and Discovery Potential in Multijets*, *JHEP* **07** (2008) 038 [arXiv:0802.2568] [INSPIRE].

[37] G. Burdman, B.A. Dobrescu and E. Pontón, *Resonances from two universal extra dimensions*, *Phys. Rev.* **D 74** (2006) 075008 [hep-ph/0601186] [INSPIRE].

[38] S. Calvet, B. Fuks, P. Gris and L. Valéry, *Searching for sgluons in multitop events at a center-of-mass energy of 8 TeV*, *JHEP* **04** (2013) 043 [arXiv:1212.3360] [INSPIRE].

[39] G. Cacciapaglia, A. Deandrea and J. Llodra-Perez, *A Dark Matter candidate from Lorentz Invariance in 6D*, *JHEP* **03** (2010) 083 [arXiv:0907.4993] [INSPIRE].

[40] G. Cacciapaglia, R. Chierici, A. Deandrea, L. Panizzi, S. Perries and S. Tosi, *Four tops on the real projective plane at LHC*, *JHEP* **10** (2011) 042 [arXiv:1107.4616] [INSPIRE].

[41] A. Arbey, G. Cacciapaglia, A. Deandrea and B. Kubik, *Dark Matter in a twisted bottle*, *JHEP* **01** (2013) 147 [arXiv:1210.0384] [INSPIRE].

[42] CMS collaboration, *Search for standard model production of four top quarks in the lepton + jets channel in pp collisions at $\sqrt{s} = 8$ TeV*, *JHEP* **11** (2014) 154 [arXiv:1409.7339] [INSPIRE].

[43] ATLAS collaboration, *The ATLAS Experiment at the CERN Large Hadron Collider*, 2008 *JINST* **3** S08003 [INSPIRE].

[44] ATLAS collaboration, *Performance of the ATLAS Trigger System in 2010*, *Eur. Phys. J.* **C 72** (2012) 1849 [arXiv:1110.1530] [INSPIRE].

[45] ATLAS collaboration, *Electron reconstruction and identification efficiency measurements with the ATLAS detector using the 2011 LHC proton-proton collision data*, *Eur. Phys. J.* **C 74** (2014) 2941 [arXiv:1404.2240] [INSPIRE].

[46] ATLAS collaboration, *Muon reconstruction efficiency and momentum resolution of the ATLAS experiment in proton-proton collisions at $\sqrt{s} = 7$ TeV in 2010*, *Eur. Phys. J.* **C 74** (2014) 3034 [arXiv:1404.4562] [INSPIRE].

[47] ATLAS collaboration, *Measurement of the muon reconstruction performance of the ATLAS detector using 2011 and 2012 LHC proton-proton collision data*, *Eur. Phys. J.* **C 74** (2014) 3130 [arXiv:1407.3935] [INSPIRE].

[48] M. Cacciari, G.P. Salam and G. Soyez, *The anti-k_t jet clustering algorithm*, *JHEP* **04** (2008) 063 [arXiv:0802.1189] [INSPIRE].

[49] M. Cacciari and G.P. Salam, *Dispelling the N^3 myth for the k_t jet-finder*, *Phys. Lett.* **B 641** (2006) 57 [hep-ph/0512210] [INSPIRE].

[50] M. Cacciari, G.P. Salam and G. Soyez, *FastJet User Manual*, *Eur. Phys. J.* **C 72** (2012) 1896 [arXiv:1111.6097] [INSPIRE].

[51] C. Cojocaru et al., *Hadronic calibration of the ATLAS liquid argon end-cap calorimeter in the pseudorapidity region $1.6 < |\eta| < 1.8$ in beam tests*, *Nucl. Instrum. Meth.* **A 531** (2004) 481 [physics/0407009] [INSPIRE].

JHEP08(2015)105

[52] W. Lampl et al., *Calorimeter Clustering Algorithms: Description and Performance*, ATL-LARG-PUB-2008-002 (2008).

[53] ATLAS collaboration, *Jet energy measurement with the ATLAS detector in proton-proton collisions at* $\sqrt{s} = 7$ *TeV*, *Eur. Phys. J.* **C 73** (2013) 2304 [arXiv:1112.6426] [INSPIRE].

[54] ATLAS collaboration, *Jet energy measurement and its systematic uncertainty in proton-proton collisions at* $\sqrt{s} = 7$ *TeV with the ATLAS detector*, *Eur. Phys. J.* **C 75** (2015) 17 [arXiv:1406.0076] [INSPIRE].

[55] ATLAS collaboration, *Calibration of the performance of b-tagging for c and light-flavour jets in the 2012 ATLAS data*, ATLAS-CONF-2014-046 (2014).

[56] ATLAS collaboration, *Performance of Missing Transverse Momentum Reconstruction in Proton-Proton Collisions at 7 TeV with ATLAS*, *Eur. Phys. J.* **C 72** (2012) 1844 [arXiv:1108.5602] [INSPIRE].

[57] ATLAS collaboration, *Improved luminosity determination in pp collisions at* $\sqrt{s} = 7$ *TeV using the ATLAS detector at the LHC*, *Eur. Phys. J.* **C 73** (2013) 2518 [arXiv:1302.4393] [INSPIRE].

[58] M. Czakon and A. Mitov, *Top++: A Program for the Calculation of the Top-Pair Cross-Section at Hadron Colliders*, *Comput. Phys. Commun.* **185** (2014) 2930 [arXiv:1112.5675] [INSPIRE].

[59] M. Cacciari, M. Czakon, M. Mangano, A. Mitov and P. Nason, *Top-pair production at hadron colliders with next-to-next-to-leading logarithmic soft-gluon resummation*, *Phys. Lett.* **B 710** (2012) 612 [arXiv:1111.5869] [INSPIRE].

[60] P. Bärnreuther, M. Czakon and A. Mitov, *Percent Level Precision Physics at the Tevatron: First Genuine NNLO QCD Corrections to* $q\bar{q} \to t\bar{t} + X$, *Phys. Rev. Lett.* **109** (2012) 132001 [arXiv:1204.5201] [INSPIRE].

[61] M. Czakon and A. Mitov, *NNLO corrections to top-pair production at hadron colliders: the all-fermionic scattering channels*, *JHEP* **12** (2012) 054 [arXiv:1207.0236] [INSPIRE].

[62] M. Czakon and A. Mitov, *NNLO corrections to top pair production at hadron colliders: the quark-gluon reaction*, *JHEP* **01** (2013) 080 [arXiv:1210.6832] [INSPIRE].

[63] M. Czakon, P. Fiedler and A. Mitov, *Total Top-Quark Pair-Production Cross section at Hadron Colliders Through* $O(\alpha_S^4)$, *Phys. Rev. Lett.* **110** (2013) 252004 [arXiv:1303.6254] [INSPIRE].

[64] A.D. Martin, W.J. Stirling, R.S. Thorne and G. Watt, *Parton distributions for the LHC*, *Eur. Phys. J.* **C 63** (2009) 189 [arXiv:0901.0002] [INSPIRE].

[65] A.D. Martin, W.J. Stirling, R.S. Thorne and G. Watt, *Uncertainties on* α_s *in global PDF analyses and implications for predicted hadronic cross sections*, *Eur. Phys. J.* **C 64** (2009) 653 [arXiv:0905.3531] [INSPIRE].

[66] M. Botje et al., *The PDF4LHC Working Group Interim Recommendations*, arXiv:1101.0538 [INSPIRE].

[67] H.-L. Lai et al., *New parton distributions for collider physics*, *Phys. Rev.* **D 82** (2010) 074024 [arXiv:1007.2241] [INSPIRE].

[68] J. Gao et al., *CT10 next-to-next-to-leading order global analysis of QCD*, *Phys. Rev.* **D 89** (2014) 033009 [arXiv:1302.6246] [INSPIRE].

[69] R.D. Ball et al., *Parton distributions with LHC data*, *Nucl. Phys.* **B 867** (2013) 244 [arXiv:1207.1303] [INSPIRE].

[70] J.A. Aguilar-Saavedra, *PROTOS, a PROgram for TOp Simulations*, http://jaguilar.web.cern.ch/jaguilar/protos/.

[71] T. Sjöstrand, S. Mrenna and P.Z. Skands, *PYTHIA 6.4 Physics and Manual*, *JHEP* **05** (2006) 026 [hep-ph/0603175] [INSPIRE].

[72] ATLAS collaboration, *ATLAS tunes of PYTHIA 6 and PYTHIA 8 for MC11*, ATL-PHYS-PUB-2011-009 (2011).

[73] V.D. Barger, A.L. Stange and R.J.N. Phillips, *Four heavy quark hadroproduction*, *Phys. Rev.* **D 44** (1991) 1987 [INSPIRE].

[74] V. Barger, W.-Y. Keung and B. Yencho, *Triple-Top Signal of New Physics at the LHC*, *Phys. Lett.* **B 687** (2010) 70 [arXiv:1001.0221] [INSPIRE].

[75] C. Degrande, J.-M. Gerard, C. Grojean, F. Maltoni and G. Servant, *Non-resonant New Physics in Top Pair Production at Hadron Colliders*, *JHEP* **03** (2011) 125 [arXiv:1010.6304] [INSPIRE].

[76] H. Georgi, L. Kaplan, D. Morin and A. Schenk, *Effects of top compositeness*, *Phys. Rev.* **D 51** (1995) 3888 [hep-ph/9410307] [INSPIRE].

[77] J. Alwall, M. Herquet, F. Maltoni, O. Mattelaer and T. Stelzer, *MadGraph 5: Going Beyond*, *JHEP* **06** (2011) 128 [arXiv:1106.0522] [INSPIRE].

[78] T. Sjöstrand, S. Mrenna and P.Z. Skands, *A Brief Introduction to PYTHIA 8.1*, *Comput. Phys. Commun.* **178** (2008) 852 [arXiv:0710.3820] [INSPIRE].

[79] ATLAS collaboration, *Summary of ATLAS PYTHIA 8 tunes*, ATL-PHYS-PUB-2012-003 (2012).

[80] P. Meade and M. Reece, *BRIDGE: Branching ratio inquiry/decay generated events*, hep-ph/0703031 [INSPIRE].

[81] P.M. Nadolsky et al., *Implications of CTEQ global analysis for collider observables*, *Phys. Rev.* **D 78** (2008) 013004 [arXiv:0802.0007] [INSPIRE].

[82] D. Gonçalves-Netto, D. López-Val, K. Mawatari, T. Plehn and I. Wigmore, *Sgluon Pair Production to Next-to-Leading Order*, *Phys. Rev.* **D 85** (2012) 114024 [arXiv:1203.6358] [INSPIRE].

[83] ATLAS collaboration, *The ATLAS Simulation Infrastructure*, *Eur. Phys. J.* **C 70** (2010) 823 [arXiv:1005.4568] [INSPIRE].

[84] GEANT4 collaboration, S. Agostinelli et al., *GEANT4: A simulation toolkit*, *Nucl. Instrum. Meth.* **A 506** (2003) 250 [INSPIRE].

[85] P. Golonka and Z. Was, *PHOTOS Monte Carlo: A precision tool for QED corrections in Z and W decays*, *Eur. Phys. J.* **C 45** (2006) 97 [hep-ph/0506026] [INSPIRE].

[86] S. Jadach, J.H. Kuhn and Z. Was, *TAUOLA: a library of Monte Carlo programs to simulate decays of polarized τ leptons*, *Comput. Phys. Commun.* **64** (1991) 275 [CERN-TH-5856-90].

[87] S. Frixione, P. Nason and G. Ridolfi, *A positive-weight next-to-leading-order Monte Carlo for heavy flavour hadroproduction*, *JHEP* **09** (2007) 126 [arXiv:0707.3088] [INSPIRE].

[88] P. Nason, *A new method for combining NLO QCD with shower Monte Carlo algorithms*, *JHEP* **11** (2004) 040 [hep-ph/0409146] [INSPIRE].

JHEP08(2015)105

[89] S. Frixione, P. Nason and C. Oleari, *Matching NLO QCD computations with Parton Shower simulations: the POWHEG method*, *JHEP* **11** (2007) 070 [arXiv:0709.2092] [INSPIRE].

[90] S. Alioli, P. Nason, C. Oleari and E. Re, *A general framework for implementing NLO calculations in shower Monte Carlo programs: the POWHEG BOX*, *JHEP* **06** (2010) 043 [arXiv:1002.2581] [INSPIRE].

[91] P.Z. Skands, *Tuning Monte Carlo Generators: The Perugia Tunes*, *Phys. Rev.* **D 82** (2010) 074018 [arXiv:1005.3457] [INSPIRE].

[92] G. Corcella et al., *HERWIG 6: An event generator for hadron emission reactions with interfering gluons (including supersymmetric processes)*, *JHEP* **01** (2001) 010 [hep-ph/0011363] [INSPIRE].

[93] J.M. Butterworth, J.R. Forshaw and M.H. Seymour, *Multiparton interactions in photoproduction at HERA*, *Z. Phys.* **C 72** (1996) 637 [hep-ph/9601371] [INSPIRE].

[94] ATLAS collaboration, *Measurements of normalized differential cross sections for $t\bar{t}$ production in pp collisions at $\sqrt{s} = 7$ TeV using the ATLAS detector*, *Phys. Rev.* **D 90** (2014) 072004 [arXiv:1407.0371] [INSPIRE].

[95] F. Cascioli, P. Maierhöfer, N. Moretti, S. Pozzorini and F. Siegert, *NLO matching for $t\bar{t}b\bar{b}$ production with massive b-quarks*, *Phys. Lett.* **B 734** (2014) 210 [arXiv:1309.5912] [INSPIRE].

[96] T. Gleisberg et al., *Event generation with SHERPA 1.1*, *JHEP* **02** (2009) 007 [arXiv:0811.4622] [INSPIRE].

[97] F. Cascioli, P. Maierhofer and S. Pozzorini, *Scattering Amplitudes with Open Loops*, *Phys. Rev. Lett.* **108** (2012) 111601 [arXiv:1111.5206] [INSPIRE].

[98] ATLAS collaboration, *Search for the Standard Model Higgs boson produced in association with top quarks and decaying into $b\bar{b}$ in pp collisions at $\sqrt{s} = 8$ TeV with the ATLAS detector*, *Eur. Phys. J.* **C 75** (2015) 349 [arXiv:1503.05066] [INSPIRE].

[99] M.L. Mangano, M. Moretti, F. Piccinini, R. Pittau and A.D. Polosa, *ALPGEN, a generator for hard multiparton processes in hadronic collisions*, *JHEP* **07** (2003) 001 [hep-ph/0206293] [INSPIRE].

[100] M.L. Mangano, M. Moretti and R. Pittau, *Multijet matrix elements and shower evolution in hadronic collisions: $Wb\bar{b}$ + n jets as a case study*, *Nucl. Phys.* **B 632** (2002) 343 [hep-ph/0108069] [INSPIRE].

[101] K. Melnikov and F. Petriello, *Electroweak gauge boson production at hadron colliders through $O(\alpha_s^2)$*, *Phys. Rev.* **D 74** (2006) 114017 [hep-ph/0609070] [INSPIRE].

[102] S. Alioli, P. Nason, C. Oleari and E. Re, *NLO single-top production matched with shower in POWHEG: s- and t-channel contributions*, *JHEP* **09** (2009) 111 [*Erratum ibid.* **1002** (2010) 011] [arXiv:0907.4076] [INSPIRE].

[103] E. Re, *Single-top Wt-channel production matched with parton showers using the POWHEG method*, *Eur. Phys. J.* **C 71** (2011) 1547 [arXiv:1009.2450] [INSPIRE].

[104] S. Frixione, E. Laenen, P. Motylinski and B.R. Webber, *Single-top production in MC@NLO*, *JHEP* **03** (2006) 092 [hep-ph/0512250] [INSPIRE].

[105] N. Kidonakis, *Next-to-next-to-leading-order collinear and soft gluon corrections for t-channel single top quark production*, *Phys. Rev.* **D 83** (2011) 091503 [arXiv:1103.2792] [INSPIRE].

JHEP08(2015)105

[106] N. Kidonakis, *Two-loop soft anomalous dimensions for single top quark associated production with a W^- or H^-*, *Phys. Rev.* **D 82** (2010) 054018 [arXiv:1005.4451] [INSPIRE].

[107] N. Kidonakis, *NNLL resummation for s-channel single top quark production*, *Phys. Rev.* **D 81** (2010) 054028 [arXiv:1001.5034] [INSPIRE].

[108] J.M. Campbell and R.K. Ellis, *An update on vector boson pair production at hadron colliders*, *Phys. Rev.* **D 60** (1999) 113006 [hep-ph/9905386] [INSPIRE].

[109] M.V. Garzelli, A. Kardos, C.G. Papadopoulos and Z. Trócsányi, *Standard Model Higgs boson production in association with a top anti-top pair at NLO with parton showering*, *Europhys. Lett.* **96** (2011) 11001 [arXiv:1108.0387] [INSPIRE].

[110] G. Bevilacqua et al., *HELAC-NLO*, *Comput. Phys. Commun.* **184** (2013) 986 [arXiv:1110.1499] [INSPIRE].

[111] ATLAS collaboration, *New ATLAS event generator tunes to 2010 data*, ATL-PHYS-PUB-2011-008 (2011).

[112] M.V. Garzelli, A. Kardos, C.G. Papadopoulos and Z. Trócsányi, *$t\bar{t}W^{\pm}$ and $t\bar{t}Z$ Hadroproduction at NLO accuracy in QCD with Parton Shower and Hadronization effects*, *JHEP* **11** (2012) 056 [arXiv:1208.2665] [INSPIRE].

[113] S. Dawson, C. Jackson, L.H. Orr, L. Reina and D. Wackeroth, *Associated Higgs production with top quarks at the large hadron collider: NLO QCD corrections*, *Phys. Rev.* **D 68** (2003) 034022 [hep-ph/0305087] [INSPIRE].

[114] W. Beenakker, S. Dittmaier, M. Krämer, B. Plumper, M. Spira and P.M. Zerwas, *NLO QCD corrections to $t\bar{t}H$ production in hadron collisions*, *Nucl. Phys.* **B 653** (2003) 151 [hep-ph/0211352] [INSPIRE].

[115] W. Beenakker, S. Dittmaier, M. Krämer, B. Plumper, M. Spira and P.M. Zerwas, *Higgs radiation off top quarks at the Tevatron and the LHC*, *Phys. Rev. Lett.* **87** (2001) 201805 [hep-ph/0107081] [INSPIRE].

[116] A. Djouadi, J. Kalinowski and M. Spira, *HDECAY: A program for Higgs boson decays in the standard model and its supersymmetric extension*, *Comput. Phys. Commun.* **108** (1998) 56 [hep-ph/9704448] [INSPIRE].

[117] A. Bredenstein, A. Denner, S. Dittmaier and M.M. Weber, *Precise predictions for the Higgs-boson decay $H \to WW/ZZ \to 4$ leptons*, *Phys. Rev.* **D 74** (2006) 013004 [hep-ph/0604011] [INSPIRE].

[118] S. Actis, G. Passarino, C. Sturm and S. Uccirati, *NNLO Computational Techniques: The Cases $H \to \gamma\gamma$ and $H \to gg$*, *Nucl. Phys.* **B 811** (2009) 182 [arXiv:0809.3667] [INSPIRE].

[119] A. Denner, S. Heinemeyer, I. Puljak, D. Rebuzzi and M. Spira, *Standard Model Higgs-Boson Branching Ratios with Uncertainties*, *Eur. Phys. J.* **C 71** (2011) 1753 [arXiv:1107.5909] [INSPIRE].

[120] LHC Higgs Cross section Working Group, S. Dittmaier et al., *Handbook of LHC Higgs Cross sections: 1. Inclusive Observables*, arXiv:1101.0593 [INSPIRE].

[121] ATLAS collaboration, *Measurement of the top quark-pair production cross section with ATLAS in pp collisions at $\sqrt{s} = 7$ TeV*, *Eur. Phys. J.* **C 71** (2011) 1577 [arXiv:1012.1792] [INSPIRE].

JHEP08(2015)105

[122] ATLAS collaboration, *Calibration of b-tagging using dileptonic top pair events in a combinatorial likelihood approach with the ATLAS experiment*, ATLAS-CONF-2014-004 (2014).

[123] J. Alwall et al., *Comparative study of various algorithms for the merging of parton showers and matrix elements in hadronic collisions*, *Eur. Phys. J.* **C 53** (2008) 473 [arXiv:0706.2569] [INSPIRE].

[124] S. Frixione, E. Laenen, P. Motylinski, B.R. Webber and C.D. White, *Single-top hadroproduction in association with a W boson*, *JHEP* **07** (2008) 029 [arXiv:0805.3067] [INSPIRE].

[125] J.M. Campbell and R.K. Ellis, $t\bar{t}W^{+-}$ *production and decay at NLO*, *JHEP* **07** (2012) 052 [arXiv:1204.5678] [INSPIRE].

[126] W. Verkerke and D.P. Kirkby, *The RooFit toolkit for data modeling*, *eConf* **C 0303241** (2003) MOLT007 [physics/0306116] [INSPIRE].

[127] W. Verkerke and D. Kirkby, *RooFit Users Manual*, http://roofit.sourceforge.net/.

[128] G. Cowan, K. Cranmer, E. Gross and O. Vitells, *Asymptotic formulae for likelihood-based tests of new physics*, *Eur. Phys. J.* **C 71** (2011) 1554 [*Erratum ibid.* **C 73** (2013) 2501] [arXiv:1007.1727] [INSPIRE].

[129] T. Junk, *Confidence level computation for combining searches with small statistics*, *Nucl. Instrum. Meth.* **A 434** (1999) 435 [hep-ex/9902006] [INSPIRE].

[130] A.L. Read, *Presentation of search results: The CL(s) technique*, *J. Phys.* **G 28** (2002) 2693 [INSPIRE].

JHEP08(2015)105

The ATLAS collaboration

G. Aad[85], B. Abbott[113], J. Abdallah[151], O. Abdinov[11], R. Aben[107], M. Abolins[90], O.S. AbouZeid[158], H. Abramowicz[153], H. Abreu[152], R. Abreu[30], Y. Abulaiti[146a,146b], B.S. Acharya[164a,164b,a], L. Adamczyk[38a], D.L. Adams[25], J. Adelman[108], S. Adomeit[100], T. Adye[131], A.A. Affolder[74], T. Agatonovic-Jovin[13], J.A. Aguilar-Saavedra[126a,126f], S.P. Ahlen[22], F. Ahmadov[65,b], G. Aielli[133a,133b], H. Akerstedt[146a,146b], T.P.A. Åkesson[81], G. Akimoto[155], A.V. Akimov[96], G.L. Alberghi[20a,20b], J. Albert[169], S. Albrand[55], M.J. Alconada Verzini[71], M. Aleksa[30], I.N. Aleksandrov[65], C. Alexa[26a], G. Alexander[153], T. Alexopoulos[10], M. Alhroob[113], G. Alimonti[91a], L. Alio[85], J. Alison[31], S.P. Alkire[35], B.M.M. Allbrooke[18], P.P. Allport[74], A. Aloisio[104a,104b], A. Alonso[36], F. Alonso[71], C. Alpigiani[76], A. Altheimer[35], B. Alvarez Gonzalez[30], D. Álvarez Piqueras[167], M.G. Alviggi[104a,104b], B.T. Amadio[15], K. Amako[66], Y. Amaral Coutinho[24a], C. Amelung[23], D. Amidei[89], S.P. Amor Dos Santos[126a,126c], A. Amorim[126a,126b], S. Amoroso[48], N. Amram[153], G. Amundsen[23], C. Anastopoulos[139], L.S. Ancu[49], N. Andari[30], T. Andeen[35], C.F. Anders[58b], G. Anders[30], J.K. Anders[74], K.J. Anderson[31], A. Andreazza[91a,91b], V. Andrei[58a], S. Angelidakis[9], I. Angelozzi[107], P. Anger[44], A. Angerami[35], F. Anghinolfi[30], A.V. Anisenkov[109,c], N. Anjos[12], A. Annovi[124a,124b], M. Antonelli[47], A. Antonov[98], J. Antos[144b], F. Anulli[132a], M. Aoki[66], L. Aperio Bella[18], G. Arabidze[90], Y. Arai[66], J.P. Araque[126a], A.T.H. Arce[45], F.A. Arduh[71], J-F. Arguin[95], S. Argyropoulos[42], M. Arik[19a], A.J. Armbruster[30], O. Arnaez[30], V. Arnal[82], H. Arnold[48], M. Arratia[28], O. Arslan[21], A. Artamonov[97], G. Artoni[23], S. Asai[155], N. Asbah[42], A. Ashkenazi[153], B. Åsman[146a,146b], L. Asquith[149], K. Assamagan[25], R. Astalos[144a], M. Atkinson[165], N.B. Atlay[141], B. Auerbach[6], K. Augsten[128], M. Aurousseau[145b], G. Avolio[30], B. Axen[15], M.K. Ayoub[117], G. Azuelos[95,d], M.A. Baak[30], A.E. Baas[58a], C. Bacci[134a,134b], H. Bachacou[136], K. Bachas[154], M. Backes[30], M. Backhaus[30], P. Bagiacchi[132a,132b], P. Bagnaia[132a,132b], Y. Bai[33a], T. Bain[35], J.T. Baines[131], O.K. Baker[176], P. Balek[129], T. Balestri[148], F. Balli[84], E. Banas[39], Sw. Banerjee[173], A.A.E. Bannoura[175], H.S. Bansil[18], L. Barak[30], E.L. Barberio[88], D. Barberis[50a,50b], M. Barbero[85], T. Barillari[101], M. Barisonzi[164a,164b], T. Barklow[143], N. Barlow[28], S.L. Barnes[84], B.M. Barnett[131], R.M. Barnett[15], Z. Barnovska[5], A. Baroncelli[134a], G. Barone[49], A.J. Barr[120], F. Barreiro[82], J. Barreiro Guimarães da Costa[57], R. Bartoldus[143], A.E. Barton[72], P. Bartos[144a], A. Basalaev[123], A. Bassalat[117], A. Basye[165], R.L. Bates[53], S.J. Batista[158], J.R. Batley[28], M. Battaglia[137], M. Bauce[132a,132b], F. Bauer[136], H.S. Bawa[143,e], J.B. Beacham[111], M.D. Beattie[72], T. Beau[80], P.H. Beauchemin[161], R. Beccherle[124a,124b], P. Bechtle[21], H.P. Beck[17,f], K. Becker[120], M. Becker[83], S. Becker[100], M. Beckingham[170], C. Becot[117], A.J. Beddall[19c], A. Beddall[19c], V.A. Bednyakov[65], C.P. Bee[148], L.J. Beemster[107], T.A. Beermann[175], M. Begel[25], J.K. Behr[120], C. Belanger-Champagne[87], W.H. Bell[49], G. Bella[153], L. Bellagamba[20a], A. Bellerive[29], M. Bellomo[86], K. Belotskiy[98], O. Beltramello[30], O. Benary[153], D. Benchekroun[135a], M. Bender[100], K. Bendtz[146a,146b], N. Benekos[10], Y. Benhammou[153], E. Benhar Noccioli[49], J.A. Benitez Garcia[159b], D.P. Benjamin[45], J.R. Bensinger[23], S. Bentvelsen[107], L. Beresford[120], M. Beretta[47], D. Berge[107], E. Bergeaas Kuutmann[166], N. Berger[5], F. Berghaus[169], J. Beringer[15], C. Bernard[22], N.R. Bernard[86], C. Bernius[110], F.U. Bernlochner[21], T. Berry[77], P. Berta[129], C. Bertella[83], G. Bertoli[146a,146b], F. Bertolucci[124a,124b], C. Bertsche[113], D. Bertsche[113], M.I. Besana[91a], G.J. Besjes[106], O. Bessidskaia Bylund[146a,146b], M. Bessner[42], N. Besson[136], C. Betancourt[48], S. Bethke[101], A.J. Bevan[76], W. Bhimji[46], R.M. Bianchi[125], L. Bianchini[23], M. Bianco[30], O. Biebel[100], S.P. Bieniek[78], M. Biglietti[134a], J. Bilbao De Mendizabal[49], H. Bilokon[47], M. Bindi[54], S. Binet[117], A. Bingul[19c], C. Bini[132a,132b], C.W. Black[150], J.E. Black[143], K.M. Black[22], D. Blackburn[138], R.E. Blair[6], J.-B. Blanchard[136], J.E. Blanco[77], T. Blazek[144a], I. Bloch[42], C. Blocker[23], W. Blum[83,*], U. Blumenschein[54], G.J. Bobbink[107],

JHEP08(2015)105

V.S. Bobrovnikov[109,c], S.S. Bocchetta[81], A. Bocci[45], C. Bock[100], M. Boehler[48], J.A. Bogaerts[30], A.G. Bogdanchikov[109], C. Bohm[146a], V. Boisvert[77], T. Bold[38a], V. Boldea[26a], A.S. Boldyrev[99], M. Bomben[80], M. Bona[76], M. Boonekamp[136], A. Borisov[130], G. Borissov[72], S. Borroni[42], J. Bortfeldt[100], V. Bortolotto[60a,60b,60c], K. Bos[107], D. Boscherini[20a], M. Bosman[12], J. Boudreau[125], J. Bouffard[2], E.V. Bouhova-Thacker[72], D. Boumediene[34], C. Bourdarios[117], N. Bousson[114], A. Boveia[30], J. Boyd[30], I.R. Boyko[65], I. Bozic[13], J. Bracinik[18], A. Brandt[8], G. Brandt[54], O. Brandt[58a], U. Bratzler[156], B. Brau[86], J.E. Brau[116], H.M. Braun[175,*], S.F. Brazzale[164a,164c], K. Brendlinger[122], A.J. Brennan[88], L. Brenner[107], R. Brenner[166], S. Bressler[172], K. Bristow[145c], T.M. Bristow[46], D. Britton[53], D. Britzger[42], F.M. Brochu[28], I. Brock[21], R. Brock[90], J. Bronner[101], G. Brooijmans[35], T. Brooks[77], W.K. Brooks[32b], J. Brosamer[15], E. Brost[116], J. Brown[55], P.A. Bruckman de Renstrom[39], D. Bruncko[144b], R. Bruneliere[48], A. Bruni[20a], G. Bruni[20a], M. Bruschi[20a], L. Bryngemark[81], T. Buanes[14], Q. Buat[142], P. Buchholz[141], A.G. Buckley[53], S.I. Buda[26a], I.A. Budagov[65], F. Buehrer[48], L. Bugge[119], M.K. Bugge[119], O. Bulekov[98], D. Bullock[8], H. Burckhart[30], S. Burdin[74], B. Burghgrave[108], S. Burke[131], I. Burmeister[43], E. Busato[34], D. Büscher[48], V. Büscher[83], P. Bussey[53], J.M. Butler[22], A.I. Butt[3], C.M. Buttar[53], J.M. Butterworth[78], P. Butti[107], W. Buttinger[25], A. Buzatu[53], A.R. Buzykaev[109,c], S. Cabrera Urbán[167], D. Caforio[128], V.M. Cairo[37a,37b], O. Cakir[4a], P. Calafiura[15], A. Calandri[136], G. Calderini[80], P. Calfayan[100], L.P. Caloba[24a], D. Calvet[34], S. Calvet[34], R. Camacho Toro[31], S. Camarda[42], P. Camarri[133a,133b], D. Cameron[119], L.M. Caminada[15], R. Caminal Armadans[12], S. Campana[30], M. Campanelli[78], A. Campoverde[148], V. Canale[104a,104b], A. Canepa[159a], M. Cano Bret[76], J. Cantero[82], R. Cantrill[126a], T. Cao[40], M.D.M. Capeans Garrido[30], I. Caprini[26a], M. Caprini[26a], M. Capua[37a,37b], R. Caputo[83], R. Cardarelli[133a], T. Carli[30], G. Carlino[104a], L. Carminati[91a,91b], S. Caron[106], E. Carquin[32a], G.D. Carrillo-Montoya[8], J.R. Carter[28], J. Carvalho[126a,126c], D. Casadei[78], M.P. Casado[12], M. Casolino[12], E. Castaneda-Miranda[145b], A. Castelli[107], V. Castillo Gimenez[167], N.F. Castro[126a,g], P. Catastini[57], A. Catinaccio[30], J.R. Catmore[119], A. Cattai[30], J. Caudron[83], V. Cavaliere[165], D. Cavalli[91a], M. Cavalli-Sforza[12], V. Cavasinni[124a,124b], F. Ceradini[134a,134b], B.C. Cerio[45], K. Cerny[129], A.S. Cerqueira[24b], A. Cerri[149], L. Cerrito[76], F. Cerutti[15], M. Cerv[30], A. Cervelli[17], S.A. Cetin[19b], A. Chafaq[135a], D. Chakraborty[108], I. Chalupkova[129], P. Chang[165], B. Chapleau[87], J.D. Chapman[28], D.G. Charlton[18], C.C. Chau[158], C.A. Chavez Barajas[149], S. Cheatham[152], A. Chegwidden[90], S. Chekanov[6], S.V. Chekulaev[159a], G.A. Chelkov[65,h], M.A. Chelstowska[89], C. Chen[64], H. Chen[25], K. Chen[148], L. Chen[33d,i], S. Chen[33c], X. Chen[33f], Y. Chen[67], H.C. Cheng[89], Y. Cheng[31], A. Cheplakov[65], E. Cheremushkina[130], R. Cherkaoui El Moursli[135e], V. Chernyatin[25,*], E. Cheu[7], L. Chevalier[136], V. Chiarella[47], J.T. Childers[6], G. Chiodini[73a], A.S. Chisholm[18], R.T. Chislett[78], A. Chitan[26a], M.V. Chizhov[65], K. Choi[61], S. Chouridou[9], B.K.B. Chow[100], V. Christodoulou[78], D. Chromek-Burckhart[30], M.L. Chu[151], J. Chudoba[127], A.J. Chuinard[87], J.J. Chwastowski[39], L. Chytka[115], G. Ciapetti[132a,132b], A.K. Ciftci[4a], D. Cinca[53], V. Cindro[75], I.A. Cioara[21], A. Ciocio[15], Z.H. Citron[172], M. Ciubancan[26a], A. Clark[49], B.L. Clark[57], P.J. Clark[46], R.N. Clarke[15], W. Cleland[125], C. Clement[146a,146b], Y. Coadou[85], M. Cobal[164a,164c], A. Coccaro[138], J. Cochran[64], L. Coffey[23], J.G. Cogan[143], B. Cole[35], S. Cole[108], A.P. Colijn[107], J. Collot[55], T. Colombo[58c], G. Compostella[101], P. Conde Muiño[126a,126b], E. Coniavitis[48], S.H. Connell[145b], I.A. Connelly[77], S.M. Consonni[91a,91b], V. Consorti[48], S. Constantinescu[26a], C. Conta[121a,121b], G. Conti[30], F. Conventi[104a,j], M. Cooke[15], B.D. Cooper[78], A.M. Cooper-Sarkar[120], T. Cornelissen[175], M. Corradi[20a], F. Corriveau[87,k], A. Corso-Radu[163], A. Cortes-Gonzalez[12], G. Cortiana[101], G. Costa[91a], M.J. Costa[167], D. Costanzo[139], D. Côté[8], G. Cottin[28], G. Cowan[77], B.E. Cox[84], K. Cranmer[110], G. Cree[29], S. Crépé-Renaudin[55], F. Crescioli[80], W.A. Cribbs[146a,146b], M. Crispin Ortuzar[120], M. Cristinziani[21], V. Croft[106],

JHEP08(2015)105

G. Crosetti[37a,37b], T. Cuhadar Donszelmann[139], J. Cummings[176], M. Curatolo[47], C. Cuthbert[150], H. Czirr[141], P. Czodrowski[3], S. D'Auria[53], M. D'Onofrio[74], M.J. Da Cunha Sargedas De Sousa[126a,126b], C. Da Via[84], W. Dabrowski[38a], A. Dafinca[120], T. Dai[89], O. Dale[14], F. Dallaire[95], C. Dallapiccola[86], M. Dam[36], J.R. Dandoy[31], N.P. Dang[48], A.C. Daniells[18], M. Danninger[168], M. Dano Hoffmann[136], V. Dao[48], G. Darbo[50a], S. Darmora[8], J. Dassoulas[3], A. Dattagupta[61], W. Davey[21], C. David[169], T. Davidek[129], E. Davies[120,l], M. Davies[153], P. Davison[78], Y. Davygora[58a], E. Dawe[88], I. Dawson[139], R.K. Daya-Ishmukhametova[86], K. De[8], R. de Asmundis[104a], S. De Castro[20a,20b], S. De Cecco[80], N. De Groot[106], P. de Jong[107], H. De la Torre[82], F. De Lorenzi[64], L. De Nooij[107], D. De Pedis[132a], A. De Salvo[132a], U. De Sanctis[149], A. De Santo[149], J.B. De Vivie De Regie[117], W.J. Dearnaley[72], R. Debbe[25], C. Debenedetti[137], D.V. Dedovich[65], I. Deigaard[107], J. Del Peso[82], T. Del Prete[124a,124b], D. Delgove[117], F. Deliot[136], C.M. Delitzsch[49], M. Deliyergiyev[75], A. Dell'Acqua[30], L. Dell'Asta[22], M. Dell'Orso[124a,124b], M. Della Pietra[104a,j], D. della Volpe[49], M. Delmastro[5], P.A. Delsart[55], C. Deluca[107], D.A. DeMarco[158], S. Demers[176], M. Demichev[65], A. Demilly[80], S.P. Denisov[130], D. Derendarz[39], J.E. Derkaoui[135d], F. Derue[80], P. Dervan[74], K. Desch[21], C. Deterre[42], P.O. Deviveiros[30], A. Dewhurst[131], S. Dhaliwal[23], A. Di Ciaccio[133a,133b], L. Di Ciaccio[5], A. Di Domenico[132a,132b], C. Di Donato[104a,104b], A. Di Girolamo[30], B. Di Girolamo[30], A. Di Mattia[152], B. Di Micco[134a,134b], R. Di Nardo[47], A. Di Simone[48], R. Di Sipio[158], D. Di Valentino[29], C. Diaconu[85], M. Diamond[158], F.A. Dias[46], M.A. Diaz[32a], E.B. Diehl[89], J. Dietrich[16], S. Diglio[85], A. Dimitrievska[13], J. Dingfelder[21], P. Dita[26a], S. Dita[26a], F. Dittus[30], F. Djama[85], T. Djobava[51b], J.I. Djuvsland[58a], M.A.B. do Vale[24c], D. Dobos[30], M. Dobre[26a], C. Doglioni[49], T. Dohmae[155], J. Dolejsi[129], Z. Dolezal[129], B.A. Dolgoshein[98,*], M. Donadelli[24d], S. Donati[124a,124b], P. Dondero[121a,121b], J. Donini[34], J. Dopke[131], A. Doria[104a], M.T. Dova[71], A.T. Doyle[53], E. Drechsler[54], M. Dris[10], E. Dubreuil[34], E. Duchovni[172], G. Duckeck[100], O.A. Ducu[26a,85], D. Duda[175], A. Dudarev[30], L. Duflot[117], L. Duguid[77], M. Dührssen[30], M. Dunford[58a], H. Duran Yildiz[4a], M. Düren[52], A. Durglishvili[51b], D. Duschinger[44], M. Dyndal[38a], C. Eckardt[42], K.M. Ecker[101], R.C. Edgar[89], W. Edson[2], N.C. Edwards[46], W. Ehrenfeld[21], T. Eifert[30], G. Eigen[14], K. Einsweiler[15], T. Ekelof[166], M. El Kacimi[135c], M. Ellert[166], S. Elles[5], F. Ellinghaus[83], A.A. Elliot[169], N. Ellis[30], J. Elmsheuser[100], M. Elsing[30], D. Emeliyanov[131], Y. Enari[155], O.C. Endner[83], M. Endo[118], J. Erdmann[43], A. Ereditato[17], G. Ernis[175], J. Ernst[2], M. Ernst[25], S. Errede[165], E. Ertel[83], M. Escalier[117], H. Esch[43], C. Escobar[125], B. Esposito[47], A.I. Etienvre[136], E. Etzion[153], H. Evans[61], A. Ezhilov[123], L. Fabbri[20a,20b], G. Facini[31], R.M. Fakhrutdinov[130], S. Falciano[132a], R.J. Falla[78], J. Faltova[129], Y. Fang[33a], M. Fanti[91a,91b], A. Farbin[8], A. Farilla[134a], T. Farooque[12], S. Farrell[15], S.M. Farrington[170], P. Farthouat[30], F. Fassi[135e], P. Fassnacht[30], D. Fassouliotis[9], M. Faucci Giannelli[77], A. Favareto[50a,50b], L. Fayard[117], P. Federic[144a], O.L. Fedin[123,m], W. Fedorko[168], S. Feigl[30], L. Feligioni[85], C. Feng[33d], E.J. Feng[6], H. Feng[89], A.B. Fenyuk[130], P. Fernandez Martinez[167], S. Fernandez Perez[30], J. Ferrando[53], A. Ferrari[166], P. Ferrari[107], R. Ferrari[121a], D.E. Ferreira de Lima[53], A. Ferrer[167], D. Ferrere[49], C. Ferretti[89], A. Ferretto Parodi[50a,50b], M. Fiascaris[31], F. Fiedler[83], A. Filipčič[75], M. Filipuzzi[42], F. Filthaut[106], M. Fincke-Keeler[169], K.D. Finelli[150], M.C.N. Fiolhais[126a,126c], L. Fiorini[167], A. Firan[40], A. Fischer[2], C. Fischer[12], J. Fischer[175], W.C. Fisher[90], E.A. Fitzgerald[23], M. Flechl[48], I. Fleck[141], P. Fleischmann[89], S. Fleischmann[175], G.T. Fletcher[139], G. Fletcher[76], T. Flick[175], A. Floderus[81], L.R. Flores Castillo[60a], M.J. Flowerdew[101], A. Formica[136], A. Forti[84], D. Fournier[117], H. Fox[72], S. Fracchia[12], P. Francavilla[80], M. Franchini[20a,20b], D. Francis[30], L. Franconi[119], M. Franklin[57], M. Fraternali[121a,121b], D. Freeborn[78], S.T. French[28], F. Friedrich[44], D. Froidevaux[30], J.A. Frost[120], C. Fukunaga[156], E. Fullana Torregrosa[83], B.G. Fulsom[143], J. Fuster[167], C. Gabaldon[55], O. Gabizon[175], A. Gabrielli[20a,20b], A. Gabrielli[132a,132b], S. Gadatsch[107],

JHEP08(2015)105

S. Gadomski[49], G. Gagliardi[50a,50b], P. Gagnon[61], C. Galea[106], B. Galhardo[126a,126c], E.J. Gallas[120], B.J. Gallop[131], P. Gallus[128], G. Galster[36], K.K. Gan[111], J. Gao[33b,85], Y. Gao[46], Y.S. Gao[143,e], F.M. Garay Walls[46], F. Garberson[176], C. García[167], J.E. García Navarro[167], M. Garcia-Sciveres[15], R.W. Gardner[31], N. Garelli[143], V. Garonne[119], C. Gatti[47], A. Gaudiello[50a,50b], G. Gaudio[121a], B. Gaur[141], L. Gauthier[95], P. Gauzzi[132a,132b], I.L. Gavrilenko[96], C. Gay[168], G. Gaycken[21], E.N. Gazis[10], P. Ge[33d], Z. Gecse[168], C.N.P. Gee[131], D.A.A. Geerts[107], Ch. Geich-Gimbel[21], M.P. Geisler[58a], C. Gemme[50a], M.H. Genest[55], S. Gentile[132a,132b], M. George[54], S. George[77], D. Gerbaudo[163], A. Gershon[153], H. Ghazlane[135b], B. Giacobbe[20a], S. Giagu[132a,132b], V. Giangiobbe[12], P. Giannetti[124a,124b], B. Gibbard[25], S.M. Gibson[77], M. Gilchriese[15], T.P.S. Gillam[28], D. Gillberg[30], G. Gilles[34], D.M. Gingrich[3,d], N. Giokaris[9], M.P. Giordani[164a,164c], F.M. Giorgi[20a], F.M. Giorgi[16], P.F. Giraud[136], P. Giromini[47], D. Giugni[91a], C. Giuliani[48], M. Giulini[58b], B.K. Gjelsten[119], S. Gkaitatzis[154], I. Gkialas[154], E.L. Gkougkousis[117], L.K. Gladilin[99], C. Glasman[82], J. Glatzer[30], P.C.F. Glaysher[46], A. Glazov[42], M. Goblirsch-Kolb[101], J.R. Goddard[76], J. Godlewski[39], S. Goldfarb[89], T. Golling[49], D. Golubkov[130], A. Gomes[126a,126b,126d], R. Gonçalo[126a], J. Goncalves Pinto Firmino Da Costa[136], L. Gonella[21], S. González de la Hoz[167], G. Gonzalez Parra[12], S. Gonzalez-Sevilla[49], L. Goossens[30], P.A. Gorbounov[97], H.A. Gordon[25], I. Gorelov[105], B. Gorini[30], E. Gorini[73a,73b], A. Gorišek[75], E. Gornicki[39], A.T. Goshaw[45], C. Gössling[43], M.I. Gostkin[65], D. Goujdami[135c], A.G. Goussiou[138], N. Govender[145b], H.M.X. Grabas[137], L. Graber[54], I. Grabowska-Bold[38a], P. Grafström[20a,20b], K-J. Grahn[42], J. Gramling[49], E. Gramstad[119], S. Grancagnolo[16], V. Grassi[148], V. Gratchev[123], H.M. Gray[30], E. Graziani[134a], Z.D. Greenwood[79,n], K. Gregersen[78], I.M. Gregor[42], P. Grenier[143], J. Griffiths[8], A.A. Grillo[137], K. Grimm[72], S. Grinstein[12,o], Ph. Gris[34], J.-F. Grivaz[117], J.P. Grohs[44], A. Grohsjean[42], E. Gross[172], J. Grosse-Knetter[54], G.C. Grossi[79], Z.J. Grout[149], L. Guan[33b], J. Guenther[128], F. Guescini[49], D. Guest[176], O. Gueta[153], E. Guido[50a,50b], T. Guillemin[117], S. Guindon[2], U. Gul[53], C. Gumpert[44], J. Guo[33e], S. Gupta[120], P. Gutierrez[113], N.G. Gutierrez Ortiz[53], C. Gutschow[44], C. Guyot[136], C. Gwenlan[120], C.B. Gwilliam[74], A. Haas[110], C. Haber[15], H.K. Hadavand[8], N. Haddad[135e], P. Haefner[21], S. Hageböck[21], Z. Hajduk[39], H. Hakobyan[177], M. Haleem[42], J. Haley[114], D. Hall[120], G. Halladjian[90], G.D. Hallewell[85], K. Hamacher[175], P. Hamal[115], K. Hamano[169], M. Hamer[54], A. Hamilton[145a], G.N. Hamity[145c], P.G. Hamnett[42], L. Han[33b], K. Hanagaki[118], K. Hanawa[155], M. Hance[15], P. Hanke[58a], R. Hanna[136], J.B. Hansen[36], J.D. Hansen[36], M.C. Hansen[21], P.H. Hansen[36], K. Hara[160], A.S. Hard[173], T. Harenberg[175], F. Hariri[117], S. Harkusha[92], R.D. Harrington[46], P.F. Harrison[170], F. Hartjes[107], M. Hasegawa[67], S. Hasegawa[103], Y. Hasegawa[140], A. Hasib[113], S. Hassani[136], S. Haug[17], R. Hauser[90], L. Hauswald[44], M. Havranek[127], C.M. Hawkes[18], R.J. Hawkings[30], A.D. Hawkins[81], T. Hayashi[160], D. Hayden[90], C.P. Hays[120], J.M. Hays[76], H.S. Hayward[74], S.J. Haywood[131], S.J. Head[18], T. Heck[83], V. Hedberg[81], L. Heelan[8], S. Heim[122], T. Heim[175], B. Heinemann[15], L. Heinrich[110], J. Hejbal[127], L. Helary[22], S. Hellman[146a,146b], D. Hellmich[21], C. Helsens[30], J. Henderson[120], R.C.W. Henderson[72], Y. Heng[173], C. Hengler[42], A. Henrichs[176], A.M. Henriques Correia[30], S. Henrot-Versille[117], G.H. Herbert[16], Y. Hernández Jiménez[167], R. Herrberg-Schubert[16], G. Herten[48], R. Hertenberger[100], L. Hervas[30], G.G. Hesketh[78], N.P. Hessey[107], J.W. Hetherly[40], R. Hickling[76], E. Higón-Rodriguez[167], E. Hill[169], J.C. Hill[28], K.H. Hiller[42], S.J. Hillier[18], I. Hinchliffe[15], E. Hines[122], R.R. Hinman[15], M. Hirose[157], D. Hirschbuehl[175], J. Hobbs[148], N. Hod[107], M.C. Hodgkinson[139], P. Hodgson[139], A. Hoecker[30], M.R. Hoeferkamp[105], F. Hoenig[100], M. Hohlfeld[83], D. Hohn[21], T.R. Holmes[15], M. Homann[43], T.M. Hong[125], L. Hooft van Huysduynen[110], W.H. Hopkins[116], Y. Horii[103], A.J. Horton[142], J-Y. Hostachy[55], S. Hou[151], A. Hoummada[135a], J. Howard[120], J. Howarth[42], M. Hrabovsky[115], I. Hristova[16], J. Hrivnac[117], T. Hryn'ova[5], A. Hrynevich[93], C. Hsu[145c], P.J. Hsu[151,p], S.-C. Hsu[138], D. Hu[35], Q. Hu[33b], X. Hu[89], Y. Huang[42], Z. Hubacek[30], F. Hubaut[85],

JHEP08(2015)105

F. Huegging[21], T.B. Huffman[120], E.W. Hughes[35], G. Hughes[72], M. Huhtinen[30], T.A. Hülsing[83], N. Huseynov[65,b], J. Huston[90], J. Huth[57], G. Iacobucci[49], G. Iakovidis[25], I. Ibragimov[141], L. Iconomidou-Fayard[117], E. Ideal[176], Z. Idrissi[135e], P. Iengo[30], O. Igonkina[107], T. Iizawa[171], Y. Ikegami[66], K. Ikematsu[141], M. Ikeno[66], Y. Ilchenko[31,q], D. Iliadis[154], N. Ilic[143], Y. Inamaru[67], T. Ince[101], P. Ioannou[9], M. Iodice[134a], K. Iordanidou[35], V. Ippolito[57], A. Irles Quiles[167], C. Isaksson[166], M. Ishino[68], M. Ishitsuka[157], R. Ishmukhametov[111], C. Issever[120], S. Istin[19a], J.M. Iturbe Ponce[84], R. Iuppa[133a,133b], J. Ivarsson[81], W. Iwanski[39], H. Iwasaki[66], J.M. Izen[41], V. Izzo[104a], S. Jabbar[3], B. Jackson[122], M. Jackson[74], P. Jackson[1], M.R. Jaekel[30], V. Jain[2], K. Jakobs[48], S. Jakobsen[30], T. Jakoubek[127], J. Jakubek[128], D.O. Jamin[151], D.K. Jana[79], E. Jansen[78], R.W. Jansky[62], J. Janssen[21], M. Janus[170], G. Jarlskog[81], N. Javadov[65,b], T. Javůrek[48], L. Jeanty[15], J. Jejelava[51a,r], G.-Y. Jeng[150], D. Jennens[88], P. Jenni[48,s], J. Jentzsch[43], C. Jeske[170], S. Jézéquel[5], H. Ji[173], J. Jia[148], Y. Jiang[33b], S. Jiggins[78], J. Jimenez Pena[167], S. Jin[33a], A. Jinaru[26a], O. Jinnouchi[157], M.D. Joergensen[36], P. Johansson[139], K.A. Johns[7], K. Jon-And[146a,146b], G. Jones[170], R.W.L. Jones[72], T.J. Jones[74], J. Jongmanns[58a], P.M. Jorge[126a,126b], K.D. Joshi[84], J. Jovicevic[159a], X. Ju[173], C.A. Jung[43], P. Jussel[62], A. Juste Rozas[12,o], M. Kaci[167], A. Kaczmarska[39], M. Kado[117], H. Kagan[111], M. Kagan[143], S.J. Kahn[85], E. Kajomovitz[45], C.W. Kalderon[120], S. Kama[40], A. Kamenshchikov[130], N. Kanaya[155], M. Kaneda[30], S. Kaneti[28], V.A. Kantserov[98], J. Kanzaki[66], B. Kaplan[110], A. Kapliy[31], D. Kar[53], K. Karakostas[10], A. Karamaoun[3], N. Karastathis[10,107], M.J. Kareem[54], M. Karnevskiy[83], S.N. Karpov[65], Z.M. Karpova[65], K. Karthik[110], V. Kartvelishvili[72], A.N. Karyukhin[130], L. Kashif[173], R.D. Kass[111], A. Kastanas[14], Y. Kataoka[155], A. Katre[49], J. Katzy[42], K. Kawagoe[70], T. Kawamoto[155], G. Kawamura[54], S. Kazama[155], V.F. Kazanin[109,c], M.Y. Kazarinov[65], R. Keeler[169], R. Kehoe[40], J.S. Keller[42], J.J. Kempster[77], H. Keoshkerian[84], O. Kepka[127], B.P. Kerševan[75], S. Kersten[175], R.A. Keyes[87], F. Khalil-zada[11], H. Khandanyan[146a,146b], A. Khanov[114], A.G. Kharlamov[109,c], T.J. Khoo[28], V. Khovanskiy[97], E. Khramov[65], J. Khubua[51b,t], H.Y. Kim[8], H. Kim[146a,146b], S.H. Kim[160], Y. Kim[31], N. Kimura[154], O.M. Kind[16], B.T. King[74], M. King[167], R.S.B. King[120], S.B. King[168], J. Kirk[131], A.E. Kiryunin[101], T. Kishimoto[67], D. Kisielewska[38a], F. Kiss[48], K. Kiuchi[160], O. Kivernyk[136], E. Kladiva[144b], M.H. Klein[35], M. Klein[74], U. Klein[74], K. Kleinknecht[83], P. Klimek[146a,146b], A. Klimentov[25], R. Klingenberg[43], J.A. Klinger[84], T. Klioutchnikova[30], E.-E. Kluge[58a], P. Kluit[107], S. Kluth[101], E. Kneringer[62], E.B.F.G. Knoops[85], A. Knue[53], A. Kobayashi[155], D. Kobayashi[157], T. Kobayashi[155], M. Kobel[44], M. Kocian[143], P. Kodys[129], T. Koffas[29], E. Koffeman[107], L.A. Kogan[120], S. Kohlmann[175], Z. Kohout[128], T. Kohriki[66], T. Koi[143], H. Kolanoski[16], I. Koletsou[5], A.A. Komar[96,*], Y. Komori[155], T. Kondo[66], N. Kondrashova[42], K. Köneke[48], A.C. König[106], S. König[83], T. Kono[66,u], R. Konoplich[110,v], N. Konstantinidis[78], R. Kopeliansky[152], S. Koperny[38a], L. Köpke[83], A.K. Kopp[48], K. Korcyl[39], K. Kordas[154], A. Korn[78], A.A. Korol[109,c], I. Korolkov[12], E.V. Korolkova[139], O. Kortner[101], S. Kortner[101], T. Kosek[129], V.V. Kostyukhin[21], V.M. Kotov[65], A. Kotwal[45], A. Kourkoumeli-Charalampidi[154], C. Kourkoumelis[9], V. Kouskoura[25], A. Koutsman[159a], R. Kowalewski[169], T.Z. Kowalski[38a], W. Kozanecki[136], A.S. Kozhin[130], V.A. Kramarenko[99], G. Kramberger[75], D. Krasnopevtsev[98], M.W. Krasny[80], A. Krasznahorkay[30], J.K. Kraus[21], A. Kravchenko[25], S. Kreiss[110], M. Kretz[58c], J. Kretzschmar[74], K. Kreutzfeldt[52], P. Krieger[158], K. Krizka[31], K. Kroeninger[43], H. Kroha[101], J. Kroll[122], J. Kroseberg[21], J. Krstic[13], U. Kruchonak[65], H. Krüger[21], N. Krumnack[64], Z.V. Krumshteyn[65], A. Kruse[173], M.C. Kruse[45], M. Kruskal[22], T. Kubota[88], H. Kucuk[78], S. Kuday[4c], S. Kuehn[48], A. Kugel[58c], F. Kuger[174], A. Kuhl[137], T. Kuhl[42], V. Kukhtin[65], Y. Kulchitsky[92], S. Kuleshov[32b], M. Kuna[132a,132b], T. Kunigo[68], A. Kupco[127], H. Kurashige[67], Y.A. Kurochkin[92], R. Kurumida[67], V. Kus[127], E.S. Kuwertz[169], M. Kuze[157], J. Kvita[115], T. Kwan[169], D. Kyriazopoulos[139], A. La Rosa[49], J.L. La Rosa Navarro[24d], L. La Rotonda[37a,37b],

JHEP08(2015)105

C. Lacasta[167], F. Lacava[132a,132b], J. Lacey[29], H. Lacker[16], D. Lacour[80], V.R. Lacuesta[167], E. Ladygin[65], R. Lafaye[5], B. Laforge[80], T. Lagouri[176], S. Lai[48], L. Lambourne[78], S. Lammers[61], C.L. Lampen[7], W. Lampl[7], E. Lançon[136], U. Landgraf[48], M.P.J. Landon[76], V.S. Lang[58a], J.C. Lange[12], A.J. Lankford[163], F. Lanni[25], K. Lantzsch[30], S. Laplace[80], C. Lapoire[30], J.F. Laporte[136], T. Lari[91a], F. Lasagni Manghi[20a,20b], M. Lassnig[30], P. Laurelli[47], W. Lavrijsen[15], A.T. Law[137], P. Laycock[74], T. Lazovich[57], O. Le Dortz[80], E. Le Guirriec[85], E. Le Menedeu[12], M. LeBlanc[169], T. LeCompte[6], F. Ledroit-Guillon[55], C.A. Lee[145b], S.C. Lee[151], L. Lee[1], G. Lefebvre[80], M. Lefebvre[169], F. Legger[100], C. Leggett[15], A. Lehan[74], G. Lehmann Miotto[30], X. Lei[7], W.A. Leight[29], A. Leisos[154,w], A.G. Leister[176], M.A.L. Leite[24d], R. Leitner[129], D. Lellouch[172], B. Lemmer[54], K.J.C. Leney[78], T. Lenz[21], B. Lenzi[30], R. Leone[7], S. Leone[124a,124b], C. Leonidopoulos[46], S. Leontsinis[10], C. Leroy[95], C.G. Lester[28], M. Levchenko[123], J. Levêque[5], D. Levin[89], L.J. Levinson[172], M. Levy[18], A. Lewis[120], A.M. Leyko[21], M. Leyton[41], B. Li[33b,x], H. Li[148], H.L. Li[31], L. Li[45], L. Li[33e], S. Li[45], Y. Li[33c,y], Z. Liang[137], H. Liao[34], B. Liberti[133a], A. Liblong[158], P. Lichard[30], K. Lie[165], J. Liebal[21], W. Liebig[14], C. Limbach[21], A. Limosani[150], S.C. Lin[151,z], T.H. Lin[83], F. Linde[107], B.E. Lindquist[148], J.T. Linnemann[90], E. Lipeles[122], A. Lipniacka[14], M. Lisovyi[58b], T.M. Liss[165], D. Lissauer[25], A. Lister[168], A.M. Litke[137], B. Liu[151,aa], D. Liu[151], J. Liu[85], J.B. Liu[33b], K. Liu[85], L. Liu[165], M. Liu[45], M. Liu[33b], Y. Liu[33b], M. Livan[121a,121b], A. Lleres[55], J. Llorente Merino[82], S.L. Lloyd[76], F. Lo Sterzo[151], E. Lobodzinska[42], P. Loch[7], W.S. Lockman[137], F.K. Loebinger[84], A.E. Loevschall-Jensen[36], A. Loginov[176], T. Lohse[16], K. Lohwasser[42], M. Lokajicek[127], B.A. Long[22], J.D. Long[89], R.E. Long[72], K.A. Looper[111], L. Lopes[126a], D. Lopez Mateos[57], B. Lopez Paredes[139], I. Lopez Paz[12], J. Lorenz[100], N. Lorenzo Martinez[61], M. Losada[162], P. Loscutoff[15], P.J. Lösel[100], X. Lou[33a], A. Lounis[117], J. Love[6], P.A. Love[72], N. Lu[89], H.J. Lubatti[138], C. Luci[132a,132b], A. Lucotte[55], F. Luehring[61], W. Lukas[62], L. Luminari[132a], O. Lundberg[146a,146b], B. Lund-Jensen[147], D. Lynn[25], R. Lysak[127], E. Lytken[81], H. Ma[25], L.L. Ma[33d], G. Maccarrone[47], A. Macchiolo[101], C.M. Macdonald[139], J. Machado Miguens[122,126b], D. Macina[30], D. Madaffari[85], R. Madar[34], H.J. Maddocks[72], W.F. Mader[44], A. Madsen[166], S. Maeland[14], T. Maeno[25], A. Maevskiy[99], E. Magradze[54], K. Mahboubi[48], J. Mahlstedt[107], C. Maiani[136], C. Maidantchik[24a], A.A. Maier[101], T. Maier[100], A. Maio[126a,126b,126d], S. Majewski[116], Y. Makida[66], N. Makovec[117], B. Malaescu[80], Pa. Malecki[39], V.P. Maleev[123], F. Malek[55], U. Mallik[63], D. Malon[6], C. Malone[143], S. Maltezos[10], V.M. Malyshev[109], S. Malyukov[30], J. Mamuzic[42], G. Mancini[47], B. Mandelli[30], L. Mandelli[91a], I. Mandić[75], R. Mandrysch[63], J. Maneira[126a,126b], A. Manfredini[101], L. Manhaes de Andrade Filho[24b], J. Manjarres Ramos[159b], A. Mann[100], P.M. Manning[137], A. Manousakis-Katsikakis[9], B. Mansoulie[136], R. Mantifel[87], M. Mantoani[54], L. Mapelli[30], L. March[145c], G. Marchiori[80], M. Marcisovsky[127], C.P. Marino[169], M. Marjanovic[13], F. Marroquim[24a], S.P. Marsden[84], Z. Marshall[15], L.F. Marti[17], S. Marti-Garcia[167], B. Martin[90], T.A. Martin[170], V.J. Martin[46], B. Martin dit Latour[14], M. Martinez[12,o], S. Martin-Haugh[131], V.S. Martoiu[26a], A.C. Martyniuk[78], M. Marx[138], F. Marzano[132a], A. Marzin[30], L. Masetti[83], T. Mashimo[155], R. Mashinistov[96], J. Masik[84], A.L. Maslennikov[109,c], I. Massa[20a,20b], L. Massa[20a,20b], N. Massol[5], P. Mastrandrea[148], A. Mastroberardino[37a,37b], T. Masubuchi[155], P. Mättig[175], J. Mattmann[83], J. Maurer[26a], S.J. Maxfield[74], D.A. Maximov[109,c], R. Mazini[151], S.M. Mazza[91a,91b], L. Mazzaferro[133a,133b], G. Mc Goldrick[158], S.P. Mc Kee[89], A. McCarn[89], R.L. McCarthy[148], T.G. McCarthy[29], N.A. McCubbin[131], K.W. McFarlane[56,*], J.A. Mcfayden[78], G. Mchedlidze[54], S.J. McMahon[131], R.A. McPherson[169,k], M. Medinnis[42], S. Meehan[145a], S. Mehlhase[100], A. Mehta[74], K. Meier[58a], C. Meineck[100], B. Meirose[41], B.R. Mellado Garcia[145c], F. Meloni[17], A. Mengarelli[20a,20b], S. Menke[101], E. Meoni[161], K.M. Mercurio[57], S. Mergelmeyer[21], P. Mermod[49], L. Merola[104a,104b], C. Meroni[91a], F.S. Merritt[31], A. Messina[132a,132b], J. Metcalfe[25], A.S. Mete[163], C. Meyer[83], C. Meyer[122], J-P. Meyer[136], J. Meyer[107], R.P. Middleton[131],

JHEP08(2015)105

S. Miglioranzi[164a,164c], L. Mijović[21], G. Mikenberg[172], M. Mikestikova[127], M. Mikuž[75], M. Milesi[88], A. Milic[30], D.W. Miller[31], C. Mills[46], A. Milov[172], D.A. Milstead[146a,146b], A.A. Minaenko[130], Y. Minami[155], I.A. Minashvili[65], A.I. Mincer[110], B. Mindur[38a], M. Mineev[65], Y. Ming[173], L.M. Mir[12], T. Mitani[171], J. Mitrevski[100], V.A. Mitsou[167], A. Miucci[49], P.S. Miyagawa[139], J.U. Mjörnmark[81], T. Moa[146a,146b], K. Mochizuki[85], S. Mohapatra[35], W. Mohr[48], S. Molander[146a,146b], R. Moles-Valls[167], K. Mönig[42], C. Monini[55], J. Monk[36], E. Monnier[85], J. Montejo Berlingen[12], F. Monticelli[71], S. Monzani[132a,132b], R.W. Moore[3], N. Morange[117], D. Moreno[162], M. Moreno Llácer[54], P. Morettini[50a], M. Morgenstern[44], M. Morii[57], M. Morinaga[155], V. Morisbak[119], S. Moritz[83], A.K. Morley[147], G. Mornacchi[30], J.D. Morris[76], S.S. Mortensen[36], A. Morton[53], L. Morvaj[103], M. Mosidze[51b], J. Moss[111], K. Motohashi[157], R. Mount[143], E. Mountricha[25], S.V. Mouraviev[96,*], E.J.W. Moyse[86], S. Muanza[85], R.D. Mudd[18], F. Mueller[101], J. Mueller[125], K. Mueller[21], R.S.P. Mueller[100], T. Mueller[28], D. Muenstermann[49], P. Mullen[53], Y. Munwes[153], J.A. Murillo Quijada[18], W.J. Murray[170,131], H. Musheghyan[54], E. Musto[152], A.G. Myagkov[130,ab], M. Myska[128], O. Nackenhorst[54], J. Nadal[54], K. Nagai[120], R. Nagai[157], Y. Nagai[85], K. Nagano[66], A. Nagarkar[111], Y. Nagasaka[59], K. Nagata[160], M. Nagel[101], E. Nagy[85], A.M. Nairz[30], Y. Nakahama[30], K. Nakamura[66], T. Nakamura[155], I. Nakano[112], H. Namasivayam[41], R.F. Naranjo Garcia[42], R. Narayan[31], T. Naumann[42], G. Navarro[162], R. Nayyar[7], H.A. Neal[89], P.Yu. Nechaeva[96], T.J. Neep[84], P.D. Nef[143], A. Negri[121a,121b], M. Negrini[20a], S. Nektarijevic[106], C. Nellist[117], A. Nelson[163], S. Nemecek[127], P. Nemethy[110], A.A. Nepomuceno[24a], M. Nessi[30,ac], M.S. Neubauer[165], M. Neumann[175], R.M. Neves[110], P. Nevski[25], P.R. Newman[18], D.H. Nguyen[6], R.B. Nickerson[120], R. Nicolaidou[136], B. Nicquevert[30], J. Nielsen[137], N. Nikiforou[35], A. Nikiforov[16], V. Nikolaenko[130,ab], I. Nikolic-Audit[80], K. Nikolopoulos[18], J.K. Nilsen[119], P. Nilsson[25], Y. Ninomiya[155], A. Nisati[132a], R. Nisius[101], T. Nobe[157], M. Nomachi[118], I. Nomidis[29], T. Nooney[76], S. Norberg[113], M. Nordberg[30], O. Novgorodova[44], S. Nowak[101], M. Nozaki[66], L. Nozka[115], K. Ntekas[10], G. Nunes Hanninger[88], T. Nunnemann[100], E. Nurse[78], F. Nuti[88], B.J. O'Brien[46], F. O'grady[7], D.C. O'Neil[142], V. O'Shea[53], F.G. Oakham[29,d], H. Oberlack[101], T. Obermann[21], J. Ocariz[80], A. Ochi[67], I. Ochoa[78], J.P. Ochoa-Ricoux[32a], S. Oda[70], S. Odaka[66], H. Ogren[61], A. Oh[84], S.H. Oh[45], C.C. Ohm[15], H. Ohman[166], H. Oide[30], W. Okamura[118], H. Okawa[160], Y. Okumura[31], T. Okuyama[155], A. Olariu[26a], S.A. Olivares Pino[46], D. Oliveira Damazio[25], E. Oliver Garcia[167], A. Olszewski[39], J. Olszowska[39], A. Onofre[126a,126e], P.U.E. Onyisi[31,q], C.J. Oram[159a], M.J. Oreglia[31], Y. Oren[153], D. Orestano[134a,134b], N. Orlando[154], C. Oropeza Barrera[53], R.S. Orr[158], B. Osculati[50a,50b], R. Ospanov[84], G. Otero y Garzon[27], H. Otono[70], M. Ouchrif[135d], E.A. Ouellette[169], F. Ould-Saada[119], A. Ouraou[136], K.P. Oussoren[107], Q. Ouyang[33a], A. Ovcharova[15], M. Owen[53], R.E. Owen[18], V.E. Ozcan[19a], N. Ozturk[8], K. Pachal[142], A. Pacheco Pages[12], C. Padilla Aranda[12], M. Pagáčová[48], S. Pagan Griso[15], E. Paganis[139], C. Pahl[101], F. Paige[25], P. Pais[86], K. Pajchel[119], G. Palacino[159b], S. Palestini[30], M. Palka[38b], D. Pallin[34], A. Palma[126a,126b], Y.B. Pan[173], E. Panagiotopoulou[10], C.E. Pandini[80], J.G. Panduro Vazquez[77], P. Pani[146a,146b], S. Panitkin[25], D. Pantea[26a], L. Paolozzi[49], Th.D. Papadopoulou[10], K. Papageorgiou[154], A. Paramonov[6], D. Paredes Hernandez[154], M.A. Parker[28], K.A. Parker[139], F. Parodi[50a,50b], J.A. Parsons[35], U. Parzefall[48], E. Pasqualucci[132a], S. Passaggio[50a], F. Pastore[134a,134b,*], Fr. Pastore[77], G. Pásztor[29], S. Pataraia[175], N.D. Patel[150], J.R. Pater[84], T. Pauly[30], J. Pearce[169], B. Pearson[113], L.E. Pedersen[36], M. Pedersen[119], S. Pedraza Lopez[167], R. Pedro[126a,126b], S.V. Peleganchuk[109,c], D. Pelikan[166], H. Peng[33b], B. Penning[31], J. Penwell[61], D.V. Perepelitsa[25], E. Perez Codina[159a], M.T. Pérez García-Estañ[167], L. Perini[91a,91b], H. Pernegger[30], S. Perrella[104a,104b], R. Peschke[42], V.D. Peshekhonov[65], K. Peters[30], R.F.Y. Peters[84], B.A. Petersen[30], T.C. Petersen[36], E. Petit[42], A. Petridis[146a,146b], C. Petridou[154], E. Petrolo[132a], F. Petrucci[134a,134b], N.E. Pettersson[157],

JHEP08(2015)105

R. Pezoa[32b], P.W. Phillips[131], G. Piacquadio[143], E. Pianori[170], A. Picazio[49], E. Piccaro[76], M. Piccinini[20a,20b], M.A. Pickering[120], R. Piegaia[27], D.T. Pignotti[111], J.E. Pilcher[31], A.D. Pilkington[84], J. Pina[126a,126b,126d], M. Pinamonti[164a,164c,ad], J.L. Pinfold[3], A. Pingel[36], B. Pinto[126a], S. Pires[80], M. Pitt[172], C. Pizio[91a,91b], L. Plazak[144a], M.-A. Pleier[25], V. Pleskot[129], E. Plotnikova[65], P. Plucinski[146a,146b], D. Pluth[64], R. Poettgen[83], L. Poggioli[117], D. Pohl[21], G. Polesello[121a], A. Policicchio[37a,37b], R. Polifka[158], A. Polini[20a], C.S. Pollard[53], V. Polychronakos[25], K. Pommès[30], L. Pontecorvo[132a], B.G. Pope[90], G.A. Popeneciu[26b], D.S. Popovic[13], A. Poppleton[30], S. Pospisil[128], K. Potamianos[15], I.N. Potrap[65], C.J. Potter[149], C.T. Potter[116], G. Poulard[30], J. Poveda[30], V. Pozdnyakov[65], P. Pralavorio[85], A. Pranko[15], S. Prasad[30], S. Prell[64], D. Price[84], L.E. Price[6], M. Primavera[73a], S. Prince[87], M. Proissl[46], K. Prokofiev[60c], F. Prokoshin[32b], E. Protopapadaki[136], S. Protopopescu[25], J. Proudfoot[6], M. Przybycien[38a], E. Ptacek[116], D. Puddu[134a,134b], E. Pueschel[86], D. Puldon[148], M. Purohit[25,ae], P. Puzo[117], J. Qian[89], G. Qin[53], Y. Qin[84], A. Quadt[54], D.R. Quarrie[15], W.B. Quayle[164a,164b], M. Queitsch-Maitland[84], D. Quilty[53], S. Raddum[119], V. Radeka[25], V. Radescu[42], S.K. Radhakrishnan[148], P. Radloff[116], P. Rados[88], F. Ragusa[91a,91b], G. Rahal[178], S. Rajagopalan[25], M. Rammensee[30], C. Rangel-Smith[166], F. Rauscher[100], S. Rave[83], T. Ravenscroft[53], M. Raymond[30], A.L. Read[119], N.P. Readioff[74], D.M. Rebuzzi[121a,121b], A. Redelbach[174], G. Redlinger[25], R. Reece[137], K. Reeves[41], L. Rehnisch[16], H. Reisin[27], M. Relich[163], C. Rembser[30], H. Ren[33a], A. Renaud[117], M. Rescigno[132a], S. Resconi[91a], O.L. Rezanova[109,c], P. Reznicek[129], R. Rezvani[95], R. Richter[101], S. Richter[78], E. Richter-Was[38b], O. Ricken[21], M. Ridel[80], P. Rieck[16], C.J. Riegel[175], J. Rieger[54], M. Rijssenbeek[148], A. Rimoldi[121a,121b], L. Rinaldi[20a], B. Ristić[49], E. Ritsch[62], I. Riu[12], F. Rizatdinova[114], E. Rizvi[76], S.H. Robertson[87,k], A. Robichaud-Veronneau[87], D. Robinson[28], J.E.M. Robinson[84], A. Robson[53], C. Roda[124a,124b], S. Roe[30], O. Røhne[119], S. Rolli[161], A. Romaniouk[98], M. Romano[20a,20b], S.M. Romano Saez[34], E. Romero Adam[167], N. Rompotis[138], M. Ronzani[48], L. Roos[80], E. Ros[167], S. Rosati[132a], K. Rosbach[48], P. Rose[137], P.L. Rosendahl[14], O. Rosenthal[141], V. Rossetti[146a,146b], E. Rossi[104a,104b], L.P. Rossi[50a], R. Rosten[138], M. Rotaru[26a], I. Roth[172], J. Rothberg[138], D. Rousseau[117], C.R. Royon[136], A. Rozanov[85], Y. Rozen[152], X. Ruan[145c], F. Rubbo[143], I. Rubinskiy[42], V.I. Rud[99], C. Rudolph[44], M.S. Rudolph[158], F. Rühr[48], A. Ruiz-Martinez[30], Z. Rurikova[48], N.A. Rusakovich[65], A. Ruschke[100], H.L. Russell[138], J.P. Rutherfoord[7], N. Ruthmann[48], Y.F. Ryabov[123], M. Rybar[165], G. Rybkin[117], N.C. Ryder[120], A.F. Saavedra[150], G. Sabato[107], S. Sacerdoti[27], A. Saddique[3], H.F-W. Sadrozinski[137], R. Sadykov[65], F. Safai Tehrani[132a], M. Saimpert[136], H. Sakamoto[155], Y. Sakurai[171], G. Salamanna[134a,134b], A. Salamon[133a], M. Saleem[113], D. Salek[107], P.H. Sales De Bruin[138], D. Salihagic[101], A. Salnikov[143], J. Salt[167], D. Salvatore[37a,37b], F. Salvatore[149], A. Salvucci[106], A. Salzburger[30], D. Sampsonidis[154], A. Sanchez[104a,104b], J. Sánchez[167], V. Sanchez Martinez[167], H. Sandaker[14], R.L. Sandbach[76], H.G. Sander[83], M.P. Sanders[100], M. Sandhoff[175], C. Sandoval[162], R. Sandstroem[101], D.P.C. Sankey[131], M. Sannino[50a,50b], A. Sansoni[47], C. Santoni[34], R. Santonico[133a,133b], H. Santos[126a], I. Santoyo Castillo[149], K. Sapp[125], A. Sapronov[65], J.G. Saraiva[126a,126d], B. Sarrazin[21], O. Sasaki[66], Y. Sasaki[155], K. Sato[160], G. Sauvage[5,*], E. Sauvan[5], G. Savage[77], P. Savard[158,d], C. Sawyer[120], L. Sawyer[79,n], J. Saxon[31], C. Sbarra[20a], A. Sbrizzi[20a,20b], T. Scanlon[78], D.A. Scannicchio[163], M. Scarcella[150], V. Scarfone[37a,37b], J. Schaarschmidt[172], P. Schacht[101], D. Schaefer[30], R. Schaefer[42], J. Schaeffer[83], S. Schaepe[21], S. Schaetzel[58b], U. Schäfer[83], A.C. Schaffer[117], D. Schaile[100], R.D. Schamberger[148], V. Scharf[58a], V.A. Schegelsky[123], D. Scheirich[129], M. Schernau[163], C. Schiavi[50a,50b], C. Schillo[48], M. Schioppa[37a,37b], S. Schlenker[30], E. Schmidt[48], K. Schmieden[30], C. Schmitt[83], S. Schmitt[58b], S. Schmitt[42], B. Schneider[159a], Y.J. Schnellbach[74], U. Schnoor[44], L. Schoeffel[136], A. Schoening[58b], B.D. Schoenrock[90], E. Schopf[21], A.L.S. Schorlemmer[54], M. Schott[83], D. Schouten[159a],

JHEP08(2015)105

J. Schovancova[8], S. Schramm[158], M. Schreyer[174], C. Schroeder[83], N. Schuh[83], M.J. Schultens[21], H.-C. Schultz-Coulon[58a], H. Schulz[16], M. Schumacher[48], B.A. Schumm[137], Ph. Schune[136], C. Schwanenberger[84], A. Schwartzman[143], T.A. Schwarz[89], Ph. Schwegler[101], H. Schweiger[84], Ph. Schwemling[136], R. Schwienhorst[90], J. Schwindling[136], T. Schwindt[21], M. Schwoerer[5], F.G. Sciacca[17], E. Scifo[117], G. Sciolla[23], F. Scuri[124a,124b], F. Scutti[21], J. Searcy[89], G. Sedov[42], E. Sedykh[123], P. Seema[21], S.C. Seidel[105], A. Seiden[137], F. Seifert[128], J.M. Seixas[24a], G. Sekhniaidze[104a], K. Sekhon[89], S.J. Sekula[40], K.E. Selbach[46], D.M. Seliverstov[123,*], N. Semprini-Cesari[20a,20b], C. Serfon[30], L. Serin[117], L. Serkin[164a,164b], T. Serre[85], M. Sessa[134a,134b], R. Seuster[159a], H. Severini[113], T. Sfiligoj[75], F. Sforza[101], A. Sfyrla[30], E. Shabalina[54], M. Shamim[116], L.Y. Shan[33a], R. Shang[165], J.T. Shank[22], M. Shapiro[15], P.B. Shatalov[97], K. Shaw[164a,164b], S.M. Shaw[84], A. Shcherbakova[146a,146b], C.Y. Shehu[149], P. Sherwood[78], L. Shi[151,af], S. Shimizu[67], C.O. Shimmin[163], M. Shimojima[102], M. Shiyakova[65], A. Shmeleva[96], D. Shoaleh Saadi[95], M.J. Shochet[31], S. Shojaii[91a,91b], S. Shrestha[111], E. Shulga[98], M.A. Shupe[7], S. Shushkevich[42], P. Sicho[127], O. Sidiropoulou[174], D. Sidorov[114], A. Sidoti[20a,20b], F. Siegert[44], Dj. Sijacki[13], J. Silva[126a,126d], Y. Silver[153], S.B. Silverstein[146a], V. Simak[128], O. Simard[5], Lj. Simic[13], S. Simion[117], E. Simioni[83], B. Simmons[78], D. Simon[34], R. Simoniello[91a,91b], P. Sinervo[158], N.B. Sinev[116], G. Siragusa[174], A.N. Sisakyan[65,*], S.Yu. Sivoklokov[99], J. Sjölin[146a,146b], T.B. Sjursen[14], M.B. Skinner[72], H.P. Skottowe[57], P. Skubic[113], M. Slater[18], T. Slavicek[128], M. Slawinska[107], K. Sliwa[161], V. Smakhtin[172], B.H. Smart[46], L. Smestad[14], S.Yu. Smirnov[98], Y. Smirnov[98], L.N. Smirnova[99,ag], O. Smirnova[81], M.N.K. Smith[35], R.W. Smith[35], M. Smizanska[72], K. Smolek[128], A.A. Snesarev[96], G. Snidero[76], S. Snyder[25], R. Sobie[169,k], F. Socher[44], A. Soffer[153], D.A. Soh[151,af], C.A. Solans[30], M. Solar[128], J. Solc[128], E.Yu. Soldatov[98], U. Soldevila[167], A.A. Solodkov[130], A. Soloshenko[65], O.V. Solovyanov[130], V. Solovyev[123], P. Sommer[48], H.Y. Song[33b], N. Soni[1], A. Sood[15], A. Sopczak[128], B. Sopko[128], V. Sopko[128], V. Sorin[12], D. Sosa[58b], M. Sosebee[8], C.L. Sotiropoulou[124a,124b], R. Soualah[164a,164c], P. Soueid[95], A.M. Soukharev[109,c], D. South[42], B.C. Sowden[77], S. Spagnolo[73a,73b], M. Spalla[124a,124b], F. Spanò[77], W.R. Spearman[57], F. Spettel[101], R. Spighi[20a], G. Spigo[30], L.A. Spiller[88], M. Spousta[129], T. Spreitzer[158], R.D. St. Denis[53,*], S. Staerz[44], J. Stahlman[122], R. Stamen[58a], S. Stamm[16], E. Stanecka[39], C. Stanescu[134a], M. Stanescu-Bellu[42], M.M. Stanitzki[42], S. Stapnes[119], E.A. Starchenko[130], J. Stark[55], P. Staroba[127], P. Starovoitov[42], R. Staszewski[39], P. Stavina[144a,*], P. Steinberg[25], B. Stelzer[142], H.J. Stelzer[30], O. Stelzer-Chilton[159a], H. Stenzel[52], S. Stern[101], G.A. Stewart[53], J.A. Stillings[21], M.C. Stockton[87], M. Stoebe[87], G. Stoicea[26a], P. Stolte[54], S. Stonjek[101], A.R. Stradling[8], A. Straessner[44], M.E. Stramaglia[17], J. Strandberg[147], S. Strandberg[146a,146b], A. Strandlie[119], E. Strauss[143], M. Strauss[113], P. Strizenec[144b], R. Ströhmer[174], D.M. Strom[116], R. Stroynowski[40], A. Strubig[106], S.A. Stucci[17], B. Stugu[14], N.A. Styles[42], D. Su[143], J. Su[125], R. Subramaniam[79], A. Succurro[12], Y. Sugaya[118], C. Suhr[108], M. Suk[128], V.V. Sulin[96], S. Sultansoy[4d], T. Sumida[68], S. Sun[57], X. Sun[33a], J.E. Sundermann[48], K. Suruliz[149], G. Susinno[37a,37b], M.R. Sutton[149], S. Suzuki[66], Y. Suzuki[66], M. Svatos[127], S. Swedish[168], M. Swiatlowski[143], I. Sykora[144a], T. Sykora[129], D. Ta[90], C. Taccini[134a,134b], K. Tackmann[42], J. Taenzer[158], A. Taffard[163], R. Tafirout[159a], N. Taiblum[153], H. Takai[25], R. Takashima[69], H. Takeda[67], T. Takeshita[140], Y. Takubo[66], M. Talby[85], A.A. Talyshev[109,c], J.Y.C. Tam[174], K.G. Tan[88], J. Tanaka[155], R. Tanaka[117], S. Tanaka[66], B.B. Tannenwald[111], N. Tannoury[21], S. Tapprogge[83], S. Tarem[152], F. Tarrade[29], G.F. Tartarelli[91a], P. Tas[129], M. Tasevsky[127], T. Tashiro[68], E. Tassi[37a,37b], A. Tavares Delgado[126a,126b], Y. Tayalati[135d], F.E. Taylor[94], G.N. Taylor[88], W. Taylor[159b], F.A. Teischinger[30], M. Teixeira Dias Castanheira[76], P. Teixeira-Dias[77], K.K. Temming[48], H. Ten Kate[30], P.K. Teng[151], J.J. Teoh[118], F. Tepel[175], S. Terada[66], K. Terashi[155], J. Terron[82], S. Terzo[101], M. Testa[47], R.J. Teuscher[158,k],

JHEP08(2015)105

J. Therhaag[21], T. Theveneaux-Pelzer[34], J.P. Thomas[18], J. Thomas-Wilsker[77], E.N. Thompson[35], P.D. Thompson[18], R.J. Thompson[84], A.S. Thompson[53], L.A. Thomsen[176], E. Thomson[122], M. Thomson[28], R.P. Thun[89,*], M.J. Tibbetts[15], R.E. Ticse Torres[85], V.O. Tikhomirov[96,ah], Yu.A. Tikhonov[109,c], S. Timoshenko[98], E. Tiouchichine[85], P. Tipton[176], S. Tisserant[85], T. Todorov[5,*], S. Todorova-Nova[129], J. Tojo[70], S. Tokár[144a], K. Tokushuku[66], K. Tollefson[90], E. Tolley[57], L. Tomlinson[84], M. Tomoto[103], L. Tompkins[143,ai], K. Toms[105], E. Torrence[116], H. Torres[142], E. Torró Pastor[167], J. Toth[85,aj], F. Touchard[85], D.R. Tovey[139], T. Trefzger[174], L. Tremblet[30], A. Tricoli[30], I.M. Trigger[159a], S. Trincaz-Duvoid[80], M.F. Tripiana[12], W. Trischuk[158], B. Trocmé[55], C. Troncon[91a], M. Trottier-McDonald[15], M. Trovatelli[134a,134b], P. True[90], L. Truong[164a,164c], M. Trzebinski[39], A. Trzupek[39], C. Tsarouchas[30], J.C-L. Tseng[120], P.V. Tsiareshka[92], D. Tsionou[154], G. Tsipolitis[10], N. Tsirintanis[9], S. Tsiskaridze[12], V. Tsiskaridze[48], E.G. Tskhadadze[51a], I.I. Tsukerman[97], V. Tsulaia[15], S. Tsuno[66], D. Tsybychev[148], A. Tudorache[26a], V. Tudorache[26a], A.N. Tuna[122], S.A. Tupputi[20a,20b], S. Turchikhin[99,ag], D. Turecek[128], R. Turra[91a,91b], A.J. Turvey[40], P.M. Tuts[35], A. Tykhonov[49], M. Tylmad[146a,146b], M. Tyndel[131], I. Ueda[155], R. Ueno[29], M. Ughetto[146a,146b], M. Ugland[14], M. Uhlenbrock[21], F. Ukegawa[160], G. Unal[30], A. Undrus[25], G. Unel[163], F.C. Ungaro[48], Y. Unno[66], C. Unverdorben[100], J. Urban[144b], P. Urquijo[88], P. Urrejola[83], G. Usai[8], A. Usanova[62], L. Vacavant[85], V. Vacek[128], B. Vachon[87], C. Valderanis[83], N. Valencic[107], S. Valentinetti[20a,20b], A. Valero[167], L. Valery[12], S. Valkar[129], E. Valladolid Gallego[167], S. Vallecorsa[49], J.A. Valls Ferrer[167], W. Van Den Wollenberg[107], P.C. Van Der Deijl[107], R. van der Geer[107], H. van der Graaf[107], R. Van Der Leeuw[107], N. van Eldik[152], P. van Gemmeren[6], J. Van Nieuwkoop[142], I. van Vulpen[107], M.C. van Woerden[30], M. Vanadia[132a,132b], W. Vandelli[30], R. Vanguri[122], A. Vaniachine[6], F. Vannucci[80], G. Vardanyan[177], R. Vari[132a], E.W. Varnes[7], T. Varol[40], D. Varouchas[80], A. Vartapetian[8], K.E. Varvell[150], F. Vazeille[34], T. Vazquez Schroeder[87], J. Veatch[7], L.M. Veloce[158], F. Veloso[126a,126c], T. Velz[21], S. Veneziano[132a], A. Ventura[73a,73b], D. Ventura[86], M. Venturi[169], N. Venturi[158], A. Venturini[23], V. Vercesi[121a], M. Verducci[132a,132b], W. Verkerke[107], J.C. Vermeulen[107], A. Vest[44], M.C. Vetterli[142,d], O. Viazlo[81], I. Vichou[165], T. Vickey[139], O.E. Vickey Boeriu[139], G.H.A. Viehhauser[120], S. Viel[15], R. Vigne[30], M. Villa[20a,20b], M. Villaplana Perez[91a,91b], E. Vilucchi[47], M.G. Vincter[29], V.B. Vinogradov[65], I. Vivarelli[149], F. Vives Vaque[3], S. Vlachos[10], D. Vladoiu[100], M. Vlasak[128], M. Vogel[32a], P. Vokac[128], G. Volpi[124a,124b], M. Volpi[88], H. von der Schmitt[101], H. von Radziewski[48], E. von Toerne[21], V. Vorobel[129], K. Vorobev[98], M. Vos[167], R. Voss[30], J.H. Vossebeld[74], N. Vranjes[13], M. Vranjes Milosavljevic[13], V. Vrba[127], M. Vreeswijk[107], R. Vuillermet[30], I. Vukotic[31], Z. Vykydal[128], P. Wagner[21], W. Wagner[175], H. Wahlberg[71], S. Wahrmund[44], J. Wakabayashi[103], J. Walder[72], R. Walker[100], W. Walkowiak[141], C. Wang[33c], F. Wang[173], H. Wang[15], H. Wang[40], J. Wang[42], J. Wang[33a], K. Wang[87], R. Wang[6], S.M. Wang[151], T. Wang[21], X. Wang[176], C. Wanotayaroj[116], A. Warburton[87], C.P. Ward[28], D.R. Wardrope[78], M. Warsinsky[48], A. Washbrook[46], C. Wasicki[42], P.M. Watkins[18], A.T. Watson[18], I.J. Watson[150], M.F. Watson[18], G. Watts[138], S. Watts[84], B.M. Waugh[78], S. Webb[84], M.S. Weber[17], S.W. Weber[174], J.S. Webster[31], A.R. Weidberg[120], B. Weinert[61], J. Weingarten[54], C. Weiser[48], H. Weits[107], P.S. Wells[30], T. Wenaus[25], T. Wengler[30], S. Wenig[30], N. Wermes[21], M. Werner[48], P. Werner[30], M. Wessels[58a], J. Wetter[161], K. Whalen[29], A.M. Wharton[72], A. White[8], M.J. White[1], R. White[32b], S. White[124a,124b], D. Whiteson[163], F.J. Wickens[131], W. Wiedenmann[173], M. Wielers[131], P. Wienemann[21], C. Wiglesworth[36], L.A.M. Wiik-Fuchs[21], A. Wildauer[101], H.G. Wilkens[30], H.H. Williams[122], S. Williams[107], C. Willis[90], S. Willocq[86], A. Wilson[89], J.A. Wilson[18], I. Wingerter-Seez[5], F. Winklmeier[116], B.T. Winter[21], M. Wittgen[143], J. Wittkowski[100], S.J. Wollstadt[83], M.W. Wolter[39], H. Wolters[126a,126c], B.K. Wosiek[39], J. Wotschack[30], M.J. Woudstra[84], K.W. Wozniak[39], M. Wu[55],

JHEP08(2015)105

M. Wu[31], S.L. Wu[173], X. Wu[49], Y. Wu[89], T.R. Wyatt[84], B.M. Wynne[46], S. Xella[36], D. Xu[33a], L. Xu[33b,ak], B. Yabsley[150], S. Yacoob[145b,al], R. Yakabe[67], M. Yamada[66], Y. Yamaguchi[118], A. Yamamoto[66], S. Yamamoto[155], T. Yamanaka[155], K. Yamauchi[103], Y. Yamazaki[67], Z. Yan[22], H. Yang[33e], H. Yang[173], Y. Yang[151], L. Yao[33a], W-M. Yao[15], Y. Yasu[66], E. Yatsenko[5], K.H. Yau Wong[21], J. Ye[40], S. Ye[25], I. Yeletskikh[65], A.L. Yen[57], E. Yildirim[42], K. Yorita[171], R. Yoshida[6], K. Yoshihara[122], C. Young[143], C.J.S. Young[30], S. Youssef[22], D.R. Yu[15], J. Yu[8], J.M. Yu[89], J. Yu[114], L. Yuan[67], A. Yurkewicz[108], I. Yusuff[28,am], B. Zabinski[39], R. Zaidan[63], A.M. Zaitsev[130,ab], J. Zalieckas[14], A. Zaman[148], S. Zambito[57], L. Zanello[132a,132b], D. Zanzi[88], C. Zeitnitz[175], M. Zeman[128], A. Zemla[38a], K. Zengel[23], O. Zenin[130], T. Ženiš[144a], D. Zerwas[117], D. Zhang[89], F. Zhang[173], J. Zhang[6], L. Zhang[48], R. Zhang[33b], X. Zhang[33d], Z. Zhang[117], X. Zhao[40], Y. Zhao[33d,117], Z. Zhao[33b], A. Zhemchugov[65], J. Zhong[120], B. Zhou[89], C. Zhou[45], L. Zhou[35], L. Zhou[40], N. Zhou[163], C.G. Zhu[33d], H. Zhu[33a], J. Zhu[89], Y. Zhu[33b], X. Zhuang[33a], K. Zhukov[96], A. Zibell[174], D. Zieminska[61], N.I. Zimine[65], C. Zimmermann[83], S. Zimmermann[48], Z. Zinonos[54], M. Zinser[83], M. Ziolkowski[141], L. Živković[13], G. Zobernig[173], A. Zoccoli[20a,20b], M. zur Nedden[16], G. Zurzolo[104a,104b], L. Zwalinski[30].

[1] *Department of Physics, University of Adelaide, Adelaide, Australia*
[2] *Physics Department, SUNY Albany, Albany NY, United States of America*
[3] *Department of Physics, University of Alberta, Edmonton AB, Canada*
[4] [(a)] *Department of Physics, Ankara University, Ankara;* [(c)] *Istanbul Aydin University, Istanbul;* [(d)] *Division of Physics, TOBB University of Economics and Technology, Ankara, Turkey*
[5] *LAPP, CNRS/IN2P3 and Université Savoie Mont Blanc, Annecy-le-Vieux, France*
[6] *High Energy Physics Division, Argonne National Laboratory, Argonne IL, United States of America*
[7] *Department of Physics, University of Arizona, Tucson AZ, United States of America*
[8] *Department of Physics, The University of Texas at Arlington, Arlington TX, United States of America*
[9] *Physics Department, University of Athens, Athens, Greece*
[10] *Physics Department, National Technical University of Athens, Zografou, Greece*
[11] *Institute of Physics, Azerbaijan Academy of Sciences, Baku, Azerbaijan*
[12] *Institut de Física d'Altes Energies and Departament de Física de la Universitat Autònoma de Barcelona, Barcelona, Spain*
[13] *Institute of Physics, University of Belgrade, Belgrade, Serbia*
[14] *Department for Physics and Technology, University of Bergen, Bergen, Norway*
[15] *Physics Division, Lawrence Berkeley National Laboratory and University of California, Berkeley CA, United States of America*
[16] *Department of Physics, Humboldt University, Berlin, Germany*
[17] *Albert Einstein Center for Fundamental Physics and Laboratory for High Energy Physics, University of Bern, Bern, Switzerland*
[18] *School of Physics and Astronomy, University of Birmingham, Birmingham, United Kingdom*
[19] [(a)] *Department of Physics, Bogazici University, Istanbul;* [(b)] *Department of Physics, Dogus University, Istanbul;* [(c)] *Department of Physics Engineering, Gaziantep University, Gaziantep, Turkey*
[20] [(a)] *INFN Sezione di Bologna;* [(b)] *Dipartimento di Fisica e Astronomia, Università di Bologna, Bologna, Italy*
[21] *Physikalisches Institut, University of Bonn, Bonn, Germany*
[22] *Department of Physics, Boston University, Boston MA, United States of America*
[23] *Department of Physics, Brandeis University, Waltham MA, United States of America*
[24] [(a)] *Universidade Federal do Rio De Janeiro COPPE/EE/IF, Rio de Janeiro;* [(b)] *Electrical Circuits Department, Federal University of Juiz de Fora (UFJF), Juiz de Fora;* [(c)] *Federal University of Sao Joao del Rei (UFSJ), Sao Joao del Rei;* [(d)] *Instituto de Fisica, Universidade de Sao Paulo, Sao Paulo, Brazil*

JHEP08(2015)105

[25] Physics Department, Brookhaven National Laboratory, Upton NY, United States of America
[26] [(a)] National Institute of Physics and Nuclear Engineering, Bucharest; [(b)] National Institute for Research and Development of Isotopic and Molecular Technologies, Physics Department, Cluj Napoca; [(c)] University Politehnica Bucharest, Bucharest; [(d)] West University in Timisoara, Timisoara, Romania
[27] Departamento de Física, Universidad de Buenos Aires, Buenos Aires, Argentina
[28] Cavendish Laboratory, University of Cambridge, Cambridge, United Kingdom
[29] Department of Physics, Carleton University, Ottawa ON, Canada
[30] CERN, Geneva, Switzerland
[31] Enrico Fermi Institute, University of Chicago, Chicago IL, United States of America
[32] [(a)] Departamento de Física, Pontificia Universidad Católica de Chile, Santiago; [(b)] Departamento de Física, Universidad Técnica Federico Santa María, Valparaíso, Chile
[33] [(a)] Institute of High Energy Physics, Chinese Academy of Sciences, Beijing; [(b)] Department of Modern Physics, University of Science and Technology of China, Anhui; [(c)] Department of Physics, Nanjing University, Jiangsu; [(d)] School of Physics, Shandong University, Shandong; [(e)] Department of Physics and Astronomy, Shanghai Key Laboratory for Particle Physics and Cosmology, Shanghai Jiao Tong University, Shanghai; [(f)] Physics Department, Tsinghua University, Beijing 100084, China
[34] Laboratoire de Physique Corpusculaire, Clermont Université and Université Blaise Pascal and CNRS/IN2P3, Clermont-Ferrand, France
[35] Nevis Laboratory, Columbia University, Irvington NY, United States of America
[36] Niels Bohr Institute, University of Copenhagen, Kobenhavn, Denmark
[37] [(a)] INFN Gruppo Collegato di Cosenza, Laboratori Nazionali di Frascati; [(b)] Dipartimento di Fisica, Università della Calabria, Rende, Italy
[38] [(a)] AGH University of Science and Technology, Faculty of Physics and Applied Computer Science, Krakow; [(b)] Marian Smoluchowski Institute of Physics, Jagiellonian University, Krakow, Poland
[39] Institute of Nuclear Physics Polish Academy of Sciences, Krakow, Poland
[40] Physics Department, Southern Methodist University, Dallas TX, United States of America
[41] Physics Department, University of Texas at Dallas, Richardson TX, United States of America
[42] DESY, Hamburg and Zeuthen, Germany
[43] Institut für Experimentelle Physik IV, Technische Universität Dortmund, Dortmund, Germany
[44] Institut für Kern- und Teilchenphysik, Technische Universität Dresden, Dresden, Germany
[45] Department of Physics, Duke University, Durham NC, United States of America
[46] SUPA - School of Physics and Astronomy, University of Edinburgh, Edinburgh, United Kingdom
[47] INFN Laboratori Nazionali di Frascati, Frascati, Italy
[48] Fakultät für Mathematik und Physik, Albert-Ludwigs-Universität, Freiburg, Germany
[49] Section de Physique, Université de Genève, Geneva, Switzerland
[50] [(a)] INFN Sezione di Genova; [(b)] Dipartimento di Fisica, Università di Genova, Genova, Italy
[51] [(a)] E. Andronikashvili Institute of Physics, Iv. Javakhishvili Tbilisi State University, Tbilisi; [(b)] High Energy Physics Institute, Tbilisi State University, Tbilisi, Georgia
[52] II Physikalisches Institut, Justus-Liebig-Universität Giessen, Giessen, Germany
[53] SUPA - School of Physics and Astronomy, University of Glasgow, Glasgow, United Kingdom
[54] II Physikalisches Institut, Georg-August-Universität, Göttingen, Germany
[55] Laboratoire de Physique Subatomique et de Cosmologie, Université Grenoble-Alpes, CNRS/IN2P3, Grenoble, France
[56] Department of Physics, Hampton University, Hampton VA, United States of America
[57] Laboratory for Particle Physics and Cosmology, Harvard University, Cambridge MA, United States of America
[58] [(a)] Kirchhoff-Institut für Physik, Ruprecht-Karls-Universität Heidelberg, Heidelberg; [(b)] Physikalisches Institut, Ruprecht-Karls-Universität Heidelberg, Heidelberg; [(c)] ZITI Institut für technische Informatik, Ruprecht-Karls-Universität Heidelberg, Mannheim, Germany
[59] Faculty of Applied Information Science, Hiroshima Institute of Technology, Hiroshima, Japan

JHEP08(2015)105

[60] [(a)] Department of Physics, The Chinese University of Hong Kong, Shatin, N.T., Hong Kong; [(b)] Department of Physics, The University of Hong Kong, Hong Kong; [(c)] Department of Physics, The Hong Kong University of Science and Technology, Clear Water Bay, Kowloon, Hong Kong, China
[61] Department of Physics, Indiana University, Bloomington IN, United States of America
[62] Institut für Astro- und Teilchenphysik, Leopold-Franzens-Universität, Innsbruck, Austria
[63] University of Iowa, Iowa City IA, United States of America
[64] Department of Physics and Astronomy, Iowa State University, Ames IA, United States of America
[65] Joint Institute for Nuclear Research, JINR Dubna, Dubna, Russia
[66] KEK, High Energy Accelerator Research Organization, Tsukuba, Japan
[67] Graduate School of Science, Kobe University, Kobe, Japan
[68] Faculty of Science, Kyoto University, Kyoto, Japan
[69] Kyoto University of Education, Kyoto, Japan
[70] Department of Physics, Kyushu University, Fukuoka, Japan
[71] Instituto de Física La Plata, Universidad Nacional de La Plata and CONICET, La Plata, Argentina
[72] Physics Department, Lancaster University, Lancaster, United Kingdom
[73] [(a)] INFN Sezione di Lecce; [(b)] Dipartimento di Matematica e Fisica, Università del Salento, Lecce, Italy
[74] Oliver Lodge Laboratory, University of Liverpool, Liverpool, United Kingdom
[75] Department of Physics, Jožef Stefan Institute and University of Ljubljana, Ljubljana, Slovenia
[76] School of Physics and Astronomy, Queen Mary University of London, London, United Kingdom
[77] Department of Physics, Royal Holloway University of London, Surrey, United Kingdom
[78] Department of Physics and Astronomy, University College London, London, United Kingdom
[79] Louisiana Tech University, Ruston LA, United States of America
[80] Laboratoire de Physique Nucléaire et de Hautes Energies, UPMC and Université Paris-Diderot and CNRS/IN2P3, Paris, France
[81] Fysiska institutionen, Lunds universitet, Lund, Sweden
[82] Departamento de Fisica Teorica C-15, Universidad Autonoma de Madrid, Madrid, Spain
[83] Institut für Physik, Universität Mainz, Mainz, Germany
[84] School of Physics and Astronomy, University of Manchester, Manchester, United Kingdom
[85] CPPM, Aix-Marseille Université and CNRS/IN2P3, Marseille, France
[86] Department of Physics, University of Massachusetts, Amherst MA, United States of America
[87] Department of Physics, McGill University, Montreal QC, Canada
[88] School of Physics, University of Melbourne, Victoria, Australia
[89] Department of Physics, The University of Michigan, Ann Arbor MI, United States of America
[90] Department of Physics and Astronomy, Michigan State University, East Lansing MI, United States of America
[91] [(a)] INFN Sezione di Milano; [(b)] Dipartimento di Fisica, Università di Milano, Milano, Italy
[92] B.I. Stepanov Institute of Physics, National Academy of Sciences of Belarus, Minsk, Republic of Belarus
[93] National Scientific and Educational Centre for Particle and High Energy Physics, Minsk, Republic of Belarus
[94] Department of Physics, Massachusetts Institute of Technology, Cambridge MA, United States of America
[95] Group of Particle Physics, University of Montreal, Montreal QC, Canada
[96] P.N. Lebedev Institute of Physics, Academy of Sciences, Moscow, Russia
[97] Institute for Theoretical and Experimental Physics (ITEP), Moscow, Russia
[98] National Research Nuclear University MEPhI, Moscow, Russia
[99] D.V. Skobeltsyn Institute of Nuclear Physics, M.V. Lomonosov Moscow State University, Moscow, Russia
[100] Fakultät für Physik, Ludwig-Maximilians-Universität München, München, Germany
[101] Max-Planck-Institut für Physik (Werner-Heisenberg-Institut), München, Germany
[102] Nagasaki Institute of Applied Science, Nagasaki, Japan

JHEP08(2015)105

[103] Graduate School of Science and Kobayashi-Maskawa Institute, Nagoya University, Nagoya, Japan
[104] [(a)] INFN Sezione di Napoli; [(b)] Dipartimento di Fisica, Università di Napoli, Napoli, Italy
[105] Department of Physics and Astronomy, University of New Mexico, Albuquerque NM, United States of America
[106] Institute for Mathematics, Astrophysics and Particle Physics, Radboud University Nijmegen/Nikhef, Nijmegen, Netherlands
[107] Nikhef National Institute for Subatomic Physics and University of Amsterdam, Amsterdam, Netherlands
[108] Department of Physics, Northern Illinois University, DeKalb IL, United States of America
[109] Budker Institute of Nuclear Physics, SB RAS, Novosibirsk, Russia
[110] Department of Physics, New York University, New York NY, United States of America
[111] Ohio State University, Columbus OH, United States of America
[112] Faculty of Science, Okayama University, Okayama, Japan
[113] Homer L. Dodge Department of Physics and Astronomy, University of Oklahoma, Norman OK, United States of America
[114] Department of Physics, Oklahoma State University, Stillwater OK, United States of America
[115] Palacký University, RCPTM, Olomouc, Czech Republic
[116] Center for High Energy Physics, University of Oregon, Eugene OR, United States of America
[117] LAL, Université Paris-Sud and CNRS/IN2P3, Orsay, France
[118] Graduate School of Science, Osaka University, Osaka, Japan
[119] Department of Physics, University of Oslo, Oslo, Norway
[120] Department of Physics, Oxford University, Oxford, United Kingdom
[121] [(a)] INFN Sezione di Pavia; [(b)] Dipartimento di Fisica, Università di Pavia, Pavia, Italy
[122] Department of Physics, University of Pennsylvania, Philadelphia PA, United States of America
[123] National Research Centre 'Kurchatov Institute' B.P.Konstantinov Petersburg Nuclear Physics Institute, St. Petersburg, Russia
[124] [(a)] INFN Sezione di Pisa; [(b)] Dipartimento di Fisica E. Fermi, Università di Pisa, Pisa, Italy
[125] Department of Physics and Astronomy, University of Pittsburgh, Pittsburgh PA, United States of America
[126] [(a)] Laboratório de Instrumentação e Física Experimental de Partículas - LIP, Lisboa; [(b)] Faculdade de Ciências, Universidade de Lisboa, Lisboa; [(c)] Department of Physics, University of Coimbra, Coimbra; [(d)] Centro de Física Nuclear da Universidade de Lisboa, Lisboa; [(e)] Departamento de Fisica, Universidade do Minho, Braga; [(f)] Departamento de Fisica Teorica y del Cosmos and CAFPE, Universidad de Granada, Granada (Spain); [(g)] Dep Fisica and CEFITEC of Faculdade de Ciencias e Tecnologia, Universidade Nova de Lisboa, Caparica, Portugal
[127] Institute of Physics, Academy of Sciences of the Czech Republic, Praha, Czech Republic
[128] Czech Technical University in Prague, Praha, Czech Republic
[129] Faculty of Mathematics and Physics, Charles University in Prague, Praha, Czech Republic
[130] State Research Center Institute for High Energy Physics, Protvino, Russia
[131] Particle Physics Department, Rutherford Appleton Laboratory, Didcot, United Kingdom
[132] [(a)] INFN Sezione di Roma; [(b)] Dipartimento di Fisica, Sapienza Università di Roma, Roma, Italy
[133] [(a)] INFN Sezione di Roma Tor Vergata; [(b)] Dipartimento di Fisica, Università di Roma Tor Vergata, Roma, Italy
[134] [(a)] INFN Sezione di Roma Tre; [(b)] Dipartimento di Matematica e Fisica, Università Roma Tre, Roma, Italy
[135] [(a)] Faculté des Sciences Ain Chock, Réseau Universitaire de Physique des Hautes Energies - Université Hassan II, Casablanca; [(b)] Centre National de l'Energie des Sciences Techniques Nucleaires, Rabat; [(c)] Faculté des Sciences Semlalia, Université Cadi Ayyad, LPHEA-Marrakech; [(d)] Faculté des Sciences, Université Mohamed Premier and LPTPM, Oujda; [(e)] Faculté des sciences, Université Mohammed V-Agdal, Rabat, Morocco
[136] DSM/IRFU (Institut de Recherches sur les Lois Fondamentales de l'Univers), CEA Saclay (Commissariat à l'Energie Atomique et aux Energies Alternatives), Gif-sur-Yvette, France

JHEP08(2015)105

[137] Santa Cruz Institute for Particle Physics, University of California Santa Cruz, Santa Cruz CA, United States of America
[138] Department of Physics, University of Washington, Seattle WA, United States of America
[139] Department of Physics and Astronomy, University of Sheffield, Sheffield, United Kingdom
[140] Department of Physics, Shinshu University, Nagano, Japan
[141] Fachbereich Physik, Universität Siegen, Siegen, Germany
[142] Department of Physics, Simon Fraser University, Burnaby BC, Canada
[143] SLAC National Accelerator Laboratory, Stanford CA, United States of America
[144] [(a)] Faculty of Mathematics, Physics & Informatics, Comenius University, Bratislava; [(b)] Department of Subnuclear Physics, Institute of Experimental Physics of the Slovak Academy of Sciences, Kosice, Slovak Republic
[145] [(a)] Department of Physics, University of Cape Town, Cape Town; [(b)] Department of Physics, University of Johannesburg, Johannesburg; [(c)] School of Physics, University of the Witwatersrand, Johannesburg, South Africa
[146] [(a)] Department of Physics, Stockholm University; [(b)] The Oskar Klein Centre, Stockholm, Sweden
[147] Physics Department, Royal Institute of Technology, Stockholm, Sweden
[148] Departments of Physics & Astronomy and Chemistry, Stony Brook University, Stony Brook NY, United States of America
[149] Department of Physics and Astronomy, University of Sussex, Brighton, United Kingdom
[150] School of Physics, University of Sydney, Sydney, Australia
[151] Institute of Physics, Academia Sinica, Taipei, Taiwan
[152] Department of Physics, Technion: Israel Institute of Technology, Haifa, Israel
[153] Raymond and Beverly Sackler School of Physics and Astronomy, Tel Aviv University, Tel Aviv, Israel
[154] Department of Physics, Aristotle University of Thessaloniki, Thessaloniki, Greece
[155] International Center for Elementary Particle Physics and Department of Physics, The University of Tokyo, Tokyo, Japan
[156] Graduate School of Science and Technology, Tokyo Metropolitan University, Tokyo, Japan
[157] Department of Physics, Tokyo Institute of Technology, Tokyo, Japan
[158] Department of Physics, University of Toronto, Toronto ON, Canada
[159] [(a)] TRIUMF, Vancouver BC; [(b)] Department of Physics and Astronomy, York University, Toronto ON, Canada
[160] Faculty of Pure and Applied Sciences, University of Tsukuba, Tsukuba, Japan
[161] Department of Physics and Astronomy, Tufts University, Medford MA, United States of America
[162] Centro de Investigaciones, Universidad Antonio Narino, Bogota, Colombia
[163] Department of Physics and Astronomy, University of California Irvine, Irvine CA, United States of America
[164] [(a)] INFN Gruppo Collegato di Udine, Sezione di Trieste, Udine; [(b)] ICTP, Trieste; [(c)] Dipartimento di Chimica, Fisica e Ambiente, Università di Udine, Udine, Italy
[165] Department of Physics, University of Illinois, Urbana IL, United States of America
[166] Department of Physics and Astronomy, University of Uppsala, Uppsala, Sweden
[167] Instituto de Física Corpuscular (IFIC) and Departamento de Física Atómica, Molecular y Nuclear and Departamento de Ingeniería Electrónica and Instituto de Microelectrónica de Barcelona (IMB-CNM), University of Valencia and CSIC, Valencia, Spain
[168] Department of Physics, University of British Columbia, Vancouver BC, Canada
[169] Department of Physics and Astronomy, University of Victoria, Victoria BC, Canada
[170] Department of Physics, University of Warwick, Coventry, United Kingdom
[171] Waseda University, Tokyo, Japan
[172] Department of Particle Physics, The Weizmann Institute of Science, Rehovot, Israel
[173] Department of Physics, University of Wisconsin, Madison WI, United States of America
[174] Fakultät für Physik und Astronomie, Julius-Maximilians-Universität, Würzburg, Germany
[175] Fachbereich C Physik, Bergische Universität Wuppertal, Wuppertal, Germany

JHEP08(2015)105

[176] Department of Physics, Yale University, New Haven CT, United States of America
[177] Yerevan Physics Institute, Yerevan, Armenia
[178] Centre de Calcul de l'Institut National de Physique Nucléaire et de Physique des Particules (IN2P3), Villeurbanne, France
[a] Also at Department of Physics, King's College London, London, United Kingdom
[b] Also at Institute of Physics, Azerbaijan Academy of Sciences, Baku, Azerbaijan
[c] Also at Novosibirsk State University, Novosibirsk, Russia
[d] Also at TRIUMF, Vancouver BC, Canada
[e] Also at Department of Physics, California State University, Fresno CA, United States of America
[f] Also at Department of Physics, University of Fribourg, Fribourg, Switzerland
[g] Also at Departamento de Fisica e Astronomia, Faculdade de Ciencias, Universidade do Porto, Portugal
[h] Also at Tomsk State University, Tomsk, Russia
[i] Also at CPPM, Aix-Marseille Université and CNRS/IN2P3, Marseille, France
[j] Also at Universita di Napoli Parthenope, Napoli, Italy
[k] Also at Institute of Particle Physics (IPP), Canada
[l] Also at Particle Physics Department, Rutherford Appleton Laboratory, Didcot, United Kingdom
[m] Also at Department of Physics, St. Petersburg State Polytechnical University, St. Petersburg, Russia
[n] Also at Louisiana Tech University, Ruston LA, United States of America
[o] Also at Institucio Catalana de Recerca i Estudis Avancats, ICREA, Barcelona, Spain
[p] Also at Department of Physics, National Tsing Hua University, Taiwan
[q] Also at Department of Physics, The University of Texas at Austin, Austin TX, United States of America
[r] Also at Institute of Theoretical Physics, Ilia State University, Tbilisi, Georgia
[s] Also at CERN, Geneva, Switzerland
[t] Also at Georgian Technical University (GTU),Tbilisi, Georgia
[u] Also at Ochadai Academic Production, Ochanomizu University, Tokyo, Japan
[v] Also at Manhattan College, New York NY, United States of America
[w] Also at Hellenic Open University, Patras, Greece
[x] Also at Institute of Physics, Academia Sinica, Taipei, Taiwan
[y] Also at LAL, Université Paris-Sud and CNRS/IN2P3, Orsay, France
[z] Also at Academia Sinica Grid Computing, Institute of Physics, Academia Sinica, Taipei, Taiwan
[aa] Also at School of Physics, Shandong University, Shandong, China
[ab] Also at Moscow Institute of Physics and Technology State University, Dolgoprudny, Russia
[ac] Also at Section de Physique, Université de Genève, Geneva, Switzerland
[ad] Also at International School for Advanced Studies (SISSA), Trieste, Italy
[ae] Also at Department of Physics and Astronomy, University of South Carolina, Columbia SC, United States of America
[af] Also at School of Physics and Engineering, Sun Yat-sen University, Guangzhou, China
[ag] Also at Faculty of Physics, M.V.Lomonosov Moscow State University, Moscow, Russia
[ah] Also at National Research Nuclear University MEPhI, Moscow, Russia
[ai] Also at Department of Physics, Stanford University, Stanford CA, United States of America
[aj] Also at Institute for Particle and Nuclear Physics, Wigner Research Centre for Physics, Budapest, Hungary
[ak] Also at Department of Physics, The University of Michigan, Ann Arbor MI, United States of America
[al] Also at Discipline of Physics, University of KwaZulu-Natal, Durban, South Africa
[am] Also at University of Malaya, Department of Physics, Kuala Lumpur, Malaysia
[*] Deceased

JHEP08(2015)105